

Copyright  
by  
Ha Thu Le  
2010

**The Dissertation Committee for Ha Thu Le Certifies that this is the approved  
version of the following dissertation:**

**INCREASING WIND POWER PENETRATION  
AND VOLTAGE STABILITY LIMITS  
USING ENERGY STORAGE SYSTEMS**

**Committee:**

---

Surya Santoso, Supervisor

---

Aristotle Arapostathis

---

Robert Bishop

---

Mircea Driga

---

W. Mack Grady

**INCREASING WIND POWER PENETRATION  
AND VOLTAGE STABILITY LIMITS  
USING ENERGY STORAGE SYSTEMS**

**by**

**Ha Thu Le, BSEE, MEEE**

**Dissertation**

Presented to the Faculty of the Graduate School of  
The University of Texas at Austin  
in Partial Fulfillment  
of the Requirements  
for the Degree of

**Doctor of Philosophy**

**The University of Texas at Austin**

**May 2010**

**Dedicated to my beloved parents, husband & son Wing**

## **Acknowledgements**

I wish to thank my Dissertation Committee members, Prof. Surya Santoso, Prof. W. Mack Grady, Prof. Mircea Driga, Prof. Robert Bishop, and Prof. Aristotle Arapostathis for serving on the Committee. I sincerely thank Prof. Santoso, my supervisor, for his guidance and support during my study and research at UT-Austin. He was a big critic of my work sometimes, but he also commented it very thoroughly. He always encouraged me to try achieving the highest possible research quality. I am grateful to Prof. Grady for lending a helping hand every time I needed it. He is my first advisor at the university. I thank Prof. Driga, Prof. Bishop and Prof. Arapostathis for sparing their time, and for their support to myself. Prof. Driga understands the difficulties that graduate students like me are coping with on a daily basis and tried to help. Prof. Bishop shared with me his experience in research. He even spent time to introduce me and some friends to a Vietnamese restaurant in Austin, helping us adjust to the new environment. Prof. Arapostathis is always encouraging. My emails sent to him were replied on the same day or the next. I thank the Vietnam Education Foundation for funding my study for three years. Also, I am grateful to the National Science Foundation for funding my dissertation wind project for two years. I appreciate the assistance of my former professors, Prof. Tom Downs, Prof. Tapan Saha and Prof. Zhao Dong from the University of Queensland. Lastly but most importantly, I am grateful to my family. Wherever I am, my parents follow my every step. They try their best to provide me with everything I want. My sister Huong is my best friend and my brother Hoc is an enthusiastic helper. I would not have gone this far without my husband Thang. He is my constant supporter, inspirer and research team-mate. Every time the research stalled, my husband and my little son gave me the energy to continue. My considerate Wing already understands when mom is busy with work and let me go without crying. Wing is very familiar with the engineering building since his dad drove him there to pick mom up many days and nights. He too is busy with study where he learns to talk and count from 1 to 10. My hard work is worthwhile because I do it for all the wonderful people.

**INCREASING WIND POWER PENETRATION  
AND VOLTAGE STABILITY LIMITS  
USING ENERGY STORAGE SYSTEMS**

Publication No. \_\_\_\_\_

Ha Thu Le, Ph.D.

The University of Texas at Austin, 2010

Supervisor: Surya Santoso

**Abstract**

The research is motivated by the need to address two major challenges in wind power integration: how to mitigate wind power fluctuation and how to ensure stability of the farm and host grid. It is envisaged that wind farm power output fluctuation can be reduced by using a specific type of buffer, such as an energy storage system (ESS), to absorb its negative impact. The proposed solution, therefore, employs ESS to solve the problems. The key research findings include a new technique for calculating the desired power output profile, an ESS charge-discharge scheme, a novel direct-calculation (optimization-based) method for determining ESS optimal rating, and an ESS operation scheme for improving wind farm transient stability. Analysis with 14 wind farms and a compressed-air energy storage system (CAES) shows that the charge-discharge scheme and the desired output calculation technique are appropriate for ESS operation. The optimal ESSs for the 14 wind farms perform four or less switching operations daily (73.2%–85.5% of the 365 days) while regulating the farms output variation. On average, the ESSs carry out 2.5 to 3.1 switching operations per day. By using the direct-calculation method, an optimal ESS rating can be found for any wind farm with a high degree of accuracy. The method has a considerable advantage over traditional

differential-based methods because it does not require knowledge of the analytical form of the objective function. For ESSs optimal rating, the improvement in wind energy integration is between 1.7% and 8%. In addition, a net increase in grid steady-state voltage stability of 8.3%–18.3% is achieved by 13 of the 14 evaluated ESSs. For improving wind farm transient stability, the proposed ESS operation scheme is effective. It exploits the use of a synchronous-machine-based ESS as a synchronous condenser to dynamically supply a wind farm with reactive power during faults. Analysis with an ESS and a 60-MW wind farm consisting of stall-regulated wind turbines shows that the ESS increases the farm critical clearing time (CCT) by 1 cycle for worst-case bolted three-phase-to-ground faults. For bolted single-phase-to-ground faults, the CCT is improved by 23.1%–52.2%.

## Table of Contents

Abstract .....	vi
List of Tables .....	xii
List of Figures .....	xiii
Chapter 1 Introduction.....	1
1.1 Research motivation: Wind power strong growth and voltage stability problems.....	1
1.1.1 Wind power capacity, growth rate, and penetration level.....	1
1.1.2 Voltage stability problems related to wind power integration .....	3
1.2 Research objectives .....	5
1.2.1 Proposed solution to wind farm voltage stability problems.....	5
1.2.2 Research objectives.....	6
1.3 Research approach.....	6
1.4 Research tools: Power systems, wind farm data, and software for computation.....	7
1.5 Research contribution and presentation.....	8
Chapter 2 Modeling of stall-regulated wind turbine for wind power studies.....	11
2.1 Characteristics of wind energy conversion systems .....	11
2.1.1 Wind turbine components [38] .....	11
2.1.2 Electrical generators and power electronics [13, 39, 40].....	13
2.1.3 Wind turbine types and dynamic features [13, 39-41].....	13
2.2 Modeling of stall-regulated wind turbine .....	16
2.2.1 Aerodynamic block.....	16
2.2.2 Mechanical block.....	19
2.2.3 Electrical block .....	23
2.2.4 Control block .....	26
2.3 Validation of stall-regulated wind turbine model.....	26
2.3.1 Solution for wind turbine equations.....	26
2.3.2 Numerical integration of wind turbine differential equations.....	27
2.3.3 Performance of stall-regulated wind turbine model.....	29

2.4	Development of wind farm model .....	39
2.5	Chapter concluding remarks .....	40
Chapter 3	Analysis of voltage stability, optimal wind power penetration limits and benefit of energy storage systems .....	41
3.1	Introduction .....	41
3.2	Analytical voltage stability solution and software validation.....	42
3.2.1	Description of a 6-bus power system and wind farm.....	42
3.2.2	Criteria for evaluating system voltage stability condition .....	44
3.2.3	Calculation of system V-Q self sensitivity and eigenvalues.....	45
3.2.4	Comparison of analytical and Neplan-based results .....	51
3.3	Case study 1: Analysis of wind farm impacts on 6-bus power system.....	52
3.4	Case study 2: Determination of maximum-possible wind power penetration levels .....	55
3.5	Case study 3: Application of an energy storage system for improving wind power integration and voltage stability .....	57
3.6	Chapter concluding remarks .....	63
Chapter 4	Development and analysis of an ESS-based application for regulating wind farm power output variation.....	64
4.1	Introduction .....	64
4.2	Problem analysis and solution .....	65
4.2.1	Problem analysis .....	65
4.2.2	Solution – Steps for implementing ESS-based application .....	67
4.3	Formulation of a case study .....	68
4.3.1	Description of 27-bus power system and wind farm .....	68
4.3.2	Technique for determining desired output profile .....	68
4.3.3	Development of ESS charge-discharge scheme.....	71
4.3.4	Techniques for quantifying ESS efficacy .....	73
4.4	Case study results and analyses .....	77
4.4.1	ESS effect on wind power integration .....	77
4.4.2	ESS effect on grid voltage stability .....	79
4.4.3	ESS effect on load-demand mismatch reduction .....	80
4.5	Chapter concluding remarks .....	84

Chapter 5 Determination of ESS optimal rating and impacts on wind power integration and voltage stability.....	86
5.1 Introduction .....	86
5.2 Analytical solution: Problem analysis, formulation, and solution.....	88
5.2.1 Problem analysis and formulation .....	88
5.2.2 Problem solution .....	90
5.3 Formulation of a case study.....	91
5.3.1 Calculating revenue from discharged energy.....	92
5.3.2 Calculating revenue from other benefits.....	94
5.3.3 Calculating ESS annual financial requirement .....	95
5.3.4 Wind farm, system demand, and CAES data.....	96
5.4 Case study results and analyses .....	97
5.4.1 ESS optimal rating versus wind farm rating .....	97
5.4.2 Revenue, cost and profit versus ESS optimal rating.....	100
5.4.3 Revenue component.....	101
5.4.4 Relation between ESS discharge duration and profit.....	103
5.4.5 ESS switching behavior .....	104
5.4.6 Increase in wind energy integration versus ESS optimal rating .....	107
5.4.7 Voltage stability improvement versus ESS optimal rating .....	109
5.4.8 Existence and uniqueness of solution to ESS-sizing problem .....	111
5.5 Chapter concluding remarks .....	111
Chapter 6 Improving wind farm transient stability using synchronous-machine based ESS .....	114
6.1 Introduction .....	114
6.2 Proposed scheme background.....	115
6.3 Modeling of wind turbines and power system components .....	116
6.3.1 Modeling of stall-controlled wind turbine .....	116
6.3.2 Modeling of DFIG .....	116
6.3.3 Validation of stall-regulated wind turbine and DFIG models.....	117
6.3.4 Modeling of power system components .....	118
6.4 Experiment with stall-regulated wind turbine .....	120
6.4.1 Wind farm voltage recovery after a remote fault.....	120
6.4.2 Critical clearing time for wind farm .....	122
6.4.3 Voltage sag at the wind farm terminals under nearby faults.....	124

6.5 Experiment with DFIG .....	125
6.5.1 Wind farm voltage recovery after a remote fault.....	126
6.5.2 Voltage sag at the wind farm terminals under nearby faults.....	127
6.6 Chapter concluding remarks .....	128
Chapter 7 Conclusion and future work.....	130
7.1 Research summary.....	130
7.2 Future work.....	134
Appendix A1 Publication record.....	136
Appendix A2 Power system, wind turbine, and ESS data.....	137
Appendix A3 One-line diagram of 27-bus grid with peak-load power flow.....	140
Appendix A4 Validation of Matpower optimal power flow solution.....	141
References .....	146
Vita .....	152

## List of Tables

Table 3.1 Wind farm real power output profile.....	44
Table 3.2 Selected analytical and software-based V-Q self-sensitivities .....	51
Table 3.3 Selected analytical and software-based eigenvalues .....	51
Table 3.4 System eigenvalues for four selected variants.....	54
Table 3.5 System eigenvalues for different wind power injection levels.....	56
Table 3.6 Calculation of power charge-discharge profile for ESS.....	60
Table 4.1 Generator limits and cost data [53, 59, 60] .....	71
Table 4.2 Correlation coefficient and reduction in demand-mismatch .....	83
Table 5.1 Data summary for 14 wind farms.....	96
Table 5.2 CAES cost data and other information [65, 66] .....	97
Table 5.3 ESS optimal ratings for 14 wind farms .....	98
Table 5.4 Cost and return rate for 14 ESS projects .....	101
Table 5.5 ESS switching operation for 365 days.....	105
Table 5.6 Increase in wind energy integration by ESS.....	107
Table 5.7 Net increase in voltage stability by ESS.....	109
Table 6.1 Critical clearing time for 60-MW wind farm.....	123
Table 6.2 Magnitude of voltage at wind farm terminal.....	124
Table 6.3 Magnitude of voltage at wind farm terminal (DFIG).....	127
Table A2.1 Stall-regulated wind turbine data [33, 47].....	137
Table A2.2 DFIG data [30, 82-84].....	137
Table A2.3 5-bus power system data .....	138
Table A2.4 Synchronous-machine-based ESS data .....	139
Table A4.1 Data for 6-bus power system generators .....	142
Table A4.2 Analytical OPF solution versus Matpower OPF solution.....	145

## List of Figures

Fig. 1.1 World wind power cumulative capacity for 2003-2007 [1-3].....	1
Fig. 1.2 US cumulative wind power capacity for 2003-2009 [3, 6].....	2
Fig. 2.1 Nacelle of Vestas V90 3-MW wind turbine [13].....	12
Fig. 2.2 Typical wind turbine configurations [13].....	15
Fig. 2.3. Block diagram of a wind turbine.....	16
Fig. 2.4 Wind rotor power coefficient for selected pitch angles .....	18
Fig. 2.5 Rotational system with a disk [44].....	19
Fig. 2.6 Rotational system with a gear train in the middle [44] .....	20
Fig. 2.7 Modeling of wind turbine system drive train .....	21
Fig. 2.8 Solution for wind turbine equations in block diagram form .....	27
Fig. 2.9 Wind turbine grid connection scheme.....	30
Fig. 2.10 Power curve by analytical calculation and PSCAD simulation .....	31
Fig. 2.11 Torque variation – analytical (upper) and PSCAD (lower) .....	32
Fig. 2.12 Angular speed variation–analytical (upper) and PSCAD (lower).....	33
Fig. 2.13 Real and reactive power output – analytical (upper) and PSCAD (lower) .....	34
Fig. 2.14 Critical speed for analytical model (upper) and PSCAD (lower) .....	36
Fig. 2.15 Runaway speed for analytical model (upper) and PSCAD (lower) .....	38
Fig. 2.16. Power curve of two 15-MW wind farm models.....	40
Fig. 3.1 Schematic diagram of the 6-bus power system with 140-MW wind farm.....	43
Fig. 3.2 Equivalent circuit representation of the 6-bus power system.....	45
Fig. 3.3 System real power losses under various wind power generation levels.....	52
Fig. 3.4 Selected V-Q curves calculated at Bus 5 .....	53
Fig. 3.5 Amount of integrated wind power versus Q-reserve margin .....	55
Fig. 3.6 Uncontrolled wind farm output and target power profile for 8 hours .....	59

Fig. 3.7 Change in Q-reserve margin with and without ESS .....	61
Fig. 3.8 Change in system smallest eigenvalue with and without ESS .....	61
Fig. 4.1 Scenario of using ESS for regulating wind farm output variability .....	66
Fig. 4.2 Diagram for ESS charge-discharge scheme .....	72
Fig. 4.3 Discharged wind energy versus ESS rating .....	78
Fig. 4.4 Voltage stability net improvement vs. ESS rating .....	80
Fig. 4.5 Regulated wind farm output for a winter day (Feb 05, 2005).....	81
Fig. 4.6 Regulated wind farm output for a summer day (Jul 24, 2005).....	82
Fig. 4.7 Correlation between regulated 183-MW wind farm output and grid demand ....	83
Fig. 5.1 ESS optimal power and energy rating for wind farms 1–7 .....	98
Fig. 5.2 ESS optimal power and energy rating for wind farms 8–14 .....	99
Fig. 5.3 Revenue, cost and profit for wind farms 1–7 .....	100
Fig. 5.4 Revenue, cost and profit for wind farms 8–14 .....	100
Fig. 5.5 Revenue component for wind farms 1–7 .....	102
Fig. 5.6 Revenue component for wind farms 8–14 .....	102
Fig. 5.7 ESS discharge duration versus profit for wind farms 1–7 .....	103
Fig. 5.8 ESS discharge duration versus profit for wind farms 8–14 .....	103
Fig. 5.9 ESS switching operation for one day .....	104
Fig. 5.10 ESS switching behavior for wind farms 1–7 .....	106
Fig. 5.11 ESS switching behavior for wind farms 8–14 .....	106
Fig. 5.12 Increase in wind energy integration for wind farms 1–7 .....	108
Fig. 5.13 Increase in wind energy integration for wind farms 8–14 .....	108
Fig. 5.14 Net increase in voltage stability for wind farms 1–7 .....	110
Fig. 5.15 Net increase in voltage stability for wind farms 8–14 .....	110
Fig. 6.1 Power curves of stall-regulated wind turbine and DFIG.....	117

Fig. 6.2 Schematic diagram of 5-bus power system with 60-MW wind farm.....	118
Fig. 6.3 Wind farm voltage profile under 30-cycle remote 3P2G fault.....	121
Fig. 6.4 ESS and SVC reactive output .....	122
Fig. 6.5 Critical clearing time under bolted 1P2G fault .....	123
Fig. 6.6 Voltage sag duration under 4-cyc 3P2G and 26-cyc 1P2G faults .....	125
Fig. 6.7 Voltage profile at the wind farm terminal under 30-cyc 3P2G fault.....	126
Fig. 6.8 SVC and ESS reactive output (3P2G fault with DFIG).....	127
Fig. 6.9 Voltage sag duration under 4-cyc 3P2G and 26-cyc 1P2G faults (DFIG).....	128
Fig. A4.1 Schematic diagram of 6-bus power system.....	141

# Chapter 1

## Introduction

This chapter first reviews the development of the wind power industry in the United States and around the world. It discusses the research motivation by summarizing voltage stability issues precipitated by intermittent and variable wind power. The research objectives are subsequently defined, and followed by a discussion of the computational tools and a synopsis of key technical contributions.

### 1.1 RESEARCH MOTIVATION: WIND POWER STRONG GROWTH AND VOLTAGE STABILITY PROBLEMS

#### 1.1.1 Wind power capacity, growth rate, and penetration level

The continued fast and strong development of wind power is a great encouragement for the industry and renewable energy advocates. Between 2003 and 2008, the worldwide wind power grows at the average rate of 24.4%. By the end of 2008, the total installed wind capacity is over 120,000 MW, a 219-percent increase compared to the 2003-capacity (Fig. 1.1) [1-3].

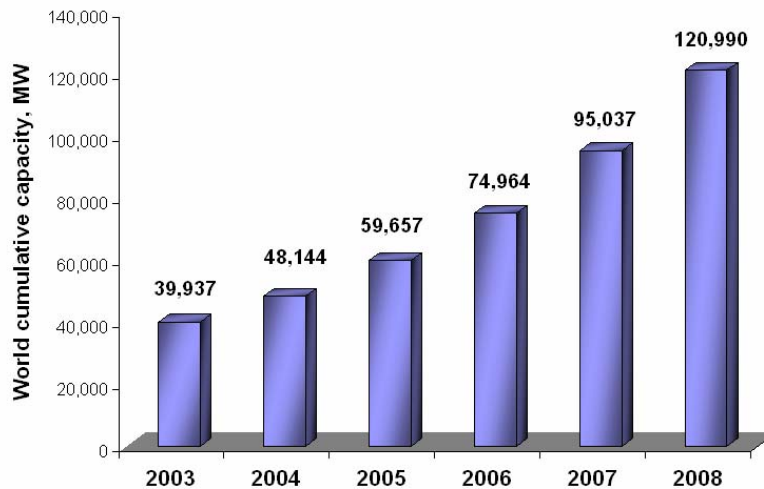


Fig. 1.1 World wind power cumulative capacity for 2003-2007 [1-3]

By the end of 2008, the United States becomes the leading country of wind power with over 25,000 MW installed capacity (Fig. 1.2). The four countries that follow are Germany (23,093 MW), Spain (16,754 MW), China (12,210 MW) and India (9,645 MW) [2, 4].

The U.S. wind industry has been very active during the past few years. It added 9,922 MW of wind generation in 2009, raising the total installed capacity to 35,159 MW (Fig. 1.2). This is a 39.3-percent increase compared to that of 2008 (25,237 MW). As of December 2009, Texas leads the country with 8,797-MW installed capacity, followed by Iowa (3,053 MW), California (2,787 MW), Minnesota (1,805 MW), and Oregon (1,659 MW) [3, 5]

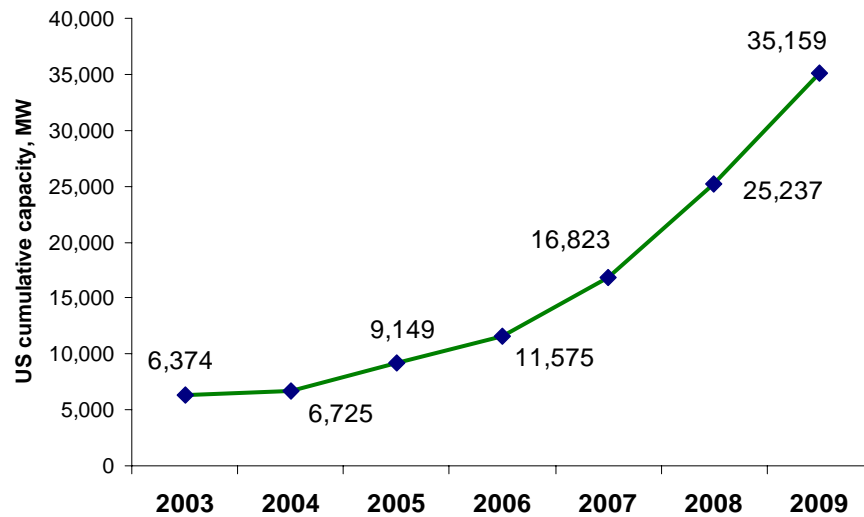


Fig. 1.2 US cumulative wind power capacity for 2003-2009 [3, 6]

By the end of 2007, the wind power penetration level is 3.7% for the whole European Union (i.e. the enlarged EU-27). The penetration level reaches 21% in Denmark, 7% in Germany and 12% in Spain [1]. In 2008, wind farms supply 1.25% of the U.S. electricity demand. Minnesota and Iowa are at the nation top with the penetration level of 7.48% and 7.1%, respectively [3].

Wind power is expected to continue its strong growth in the coming years. Assuming a moderate-market growth, the Global Wind Energy Council estimated that the world wind capacity will reach 1,129,000 MW in 2030. In other words, in 2030 the installed wind power capacity will be over 19 times of that in 2005. Therefore, wind power penetration level is expected to rise rapidly in many countries. For example, a study carried out by the German Energy Agency (DENA) in 2005 concludes that, by 2015, there would be 36,000 MW of wind capacity installed on the country land and offshore. This amount of wind capacity would supply around 14% of German electricity demand [4, 7].

A study by the U.S Department of Energy (DOE) estimated that the U.S. wind generators could supply 20% of the country electricity demand by 2030. California and Hawaii are the most

ambitious states with the goal (called Renewable Portfolio Standard, or RPS) to have 33% (California RPS 2020) and 40% (Hawaii RPS 2030) of the total electricity from wind. About 23 other states have the RPS-goal of generating 15-25% of their electricity from wind by the year 2020 or 2025. Texas RPS requires that the state have 5,880 MW of generation from renewable sources (mainly wind) by 2015. However, Texas already reached this goal with 8,797 MW of wind generation capacity in 2009. The state current peak load (December 2009) is approximately 77,218 MW. At full output, the wind farms would supply 11.4% of the state demand. With around 660-MW ongoing wind projects, more wind farms are expected to go online in Texas in a short time [3, 8-10]. In short, huge amount of wind power is expected to integrate into the power grid worldwide in the coming years.

### **1.1.2 Voltage stability problems related to wind power integration**

The following section summarizes prior work reported in the literature on how wind farms can adversely impact the grid voltage stability. It helps clarify the need to carry out this dissertation research.

Based on [11], voltage stability is defined as “the ability of a power system to maintain steady acceptable voltages at all buses in the system under normal operating conditions and after subjected to a disturbance”.

Voltage stability may be divided into two categories: large-disturbance (transient) voltage stability and small-disturbance (steady-state) voltage stability. Large-disturbance voltage stability involves a system ability to control voltages after being subjected to large disturbances such as faults, loss of load or loss of generation. This is the dynamic performance of the system over a period of time. Large-disturbance voltage stability can be studied using dynamic (time-domain) simulations. Small-disturbance voltage stability is concerned with a system ability to control voltages following small disturbances, such as gradual changes in load. This type of voltage stability can be examined using steady-state techniques which linearize the system dynamic equations at a given operating point [11].

Wind farms unique characteristics potentially harmful to grid voltage stability are as follows [12, 13]:

***Variability of power output:*** As wind speed varies, the power production of each wind turbine in a wind farm changes, resulting in the wind farm fluctuating power output.

***Intermittency and load mismatch:*** Since the power production of a wind farm depends on the availability of wind, the wind power profile tends to mismatch the grid load demand and cannot be dispatched at the time of needs in general.

***High demand for reactive power:*** Since most wind turbines employ induction machines, they require reactive power to provide excitation.

Based on utility records, wind farms could cause the following voltage problems to power systems [12-14]:

- Voltage fluctuation at the point of connection;
- Voltage drop (sag) or rise;
- Voltage asymmetry and flicker;
- Voltage collapse.

Examples of voltage problems caused by wind farms are described below.

In Hawaii's Big Island, wind farms have been causing annoyance to the island 150-MW grid controllers. At wind gusts, the rate of change in the power output of, say, a 20-MW wind farm, could be over 2 MW in just two seconds. The surge in power is so fast that the island oil-fired generators could not catch up by reducing their outputs in time to balance the supply and demand. This power imbalance, even momentary, can alter voltage and frequency on the network, putting equipment at risk and causing lights to flicker [15].

In Denmark, to prepare for integrating three 150-MW offshore wind farms during the period 2002-2008, a study was performed in 1999 to evaluate the impacts of the wind farms on the East Danish power system. The study found that, due to the reactive characteristics of their wind turbines, the wind farms could have severe negative impacts on the system voltage stability and power loss. A three-phase fault anywhere on the 132-kV network would cause voltage collapse, unless appropriate actions are taken. In addition, the network average annual power loss increased by 32% compared to the power loss without the three wind farms [14].

In Germany, stability and network congestion concerns related to wind power have been raised and discussed intensively by the power industry. Wind power integration already causes overloads in some parts of the country 110-kV networks, especially in the upper North Germany close to Danish border. As a result, at times the network operators have to resort to Wind Generation Management, i.e., reducing the wind power flow into the system. Dynamic characteristics of wind turbines in relation to system voltage stability raised great concerns and Germany now has strict requirements (grid codes) for wind turbines regarding this issue [16, 17].

Other studies also found that wind power has different impacts on power systems voltage stability, which could be a limiting factor that affects the amount of wind power being channeled into both distribution and transmission systems [18-24].

Supply-demand imbalance and power shortage due to wind farms are very serious concerns of power systems operators. At times when wind is weak, the output from wind farms can be very low, causing severe permanent or momentary power shortages in power grids. Severe power shortages can occur due to tripping of massive wind capacity after a system short-circuit, or due to safety shut-down of numerous wind farms at above-rating wind speeds. The systems spinning reserves may also be affected by wind farms. All the situations could lead to profound voltage stability and frequency problems, which could eventually cause power systems to collapse.

It is clear that ensuring voltage stability is a crucial task in wind power integration. As wind capacity increases rapidly around the world, wind farms impacts on host-systems voltage stability will be increasingly intensified. In addition, in the today deregulated electricity market, power networks are operated for maximum economic benefits, resulting in transmission congestion problems. Both situations make power systems more vulnerable to voltage instability. Therefore, to integrate an increasing amount of wind power into power networks, the voltage stability problems caused by wind farms must be dealt with in an appropriate manner.

## **1.2 RESEARCH OBJECTIVES**

### **1.2.1 Proposed solution to wind farm voltage stability problems**

The discussion presented in Section 1.1.2 suggests that, to solve the voltage stability problems, the adverse impacts of wind farms (output variability, intermittency, and high demand for reactive power) must be controlled, mitigated and/or minimized.

The wind power output fluctuation can be reduced by using a specific type of buffer, such as an energy storage systems (ESS), to absorb the negative impact. The energy storage system can be used to store unwanted wind power from time to time and appropriately re-dispatch it later. The ESS can also be used to stabilize wind farm by dynamic reactive power supply during faults. It is proposed, therefore, to use energy storage systems to solve the wind-farm-related problems.

Energy storage systems of various technologies are used around the world. Examples of ESSs are pumped-hydroelectric energy storage (PHES), compressed-air energy storage (CAES), batteries, flywheels, superconducting magnetic energy storage (SMES), and supercapacitors. They are used or being considered for a variety of purposes. Some examples are: power back-up systems to serve industrial facilities and emergency purposes, medium-voltage UPS (Uninterrupted Power Supply) systems to mitigate power quality problems, ESSs for grid reactive power support, spinning reserve, power system stabilizer, transmission system stability, and

voltage regulation. Utilizing ESSs for renewable energy management is considered the next potential application of the systems. Thanks to recent advances in storage technology, today ESSs can store megawatts-hour of energy [25-28]. This is a significant advantage for wind energy management, which generally requires large-scale storage. Therefore, using ESSs to improve wind power integration and grid voltage stability is a potentially effective solution.

### **1.2.2 Research objectives**

The overall research goal is to *“Increase both wind power penetration and voltage stability limits using energy storage systems”*. The term “wind power penetration” is defined as the amount of wind power channeled into the grid. The term “voltage stability” includes two types; steady-state (small-disturbance) voltage stability and transient (large-disturbance) stability.

Specifically, the research aims to design an application, based on an energy storage system, to regulate the output from a wind farm in order to meet the overall research goal. Conceptually, the design consists of a wind farm and an ESS, defined as an “aggregate system”. The system may also include several wind farms and one ESS. The expanded research objectives are:

- (i) To develop a wind turbine model suitable for voltage stability studies.
- (ii) To define a framework for the ESS-based application by specifying the sequence (steps) to be followed when designing an ESS for use with a wind farm.
- (iii) To develop a unique method for estimating the optimal ESS rating, a technique for determining a reference power profile, and an ESS charge-discharge scheme, based on the farm rating and other characteristics such as capacity factor and power output profile.
- (iv) To use the wind turbine model, the ESS-application framework, and the optimal-sizing method to construct a unique strategy for the operation of an ESS which meets the overall research goal of increasing wind power integration and grid voltage stability.

### **1.3 RESEARCH APPROACH**

The wind-farm related problems are solved using current engineering theories and quantitative validation. The overall research is broken down into a set of sub-problems which are solved one step at a time. For each sub-problem, an analytical solution or procedure is developed based on power system voltage stability criteria, optimization, and general science. The solution or procedure is then quantitatively validated or tested using realistic power systems and wind farm data.

The specific approach for each objective is as follows.

- (i) **Objective 1:** In developing a wind turbine model, wind turbine, electric machine, and modeling theories are used. The wind turbine model is connected to a power system and comprehensively tested to ensure accuracy. The validation criteria are wind turbine power generation behavior and torque-speed characteristics under normal and fault conditions.
- (ii) **Objective 2:** In defining the framework for an ESS-based application, existing knowledge of power system operations and wind farms are utilized together with engineering design concepts. The framework efficacy is evaluated using the case study of a 183 MW wind farm connected to 27-bus power system. The evaluation criteria include voltage stability, ESS impact on wind power integration, and the ability of an ESS to reduce mismatch between wind farm output and grid demand.
- (iii) **Objective 3:** For the development of a reference power profile (desired output profile), an ESS charge-discharge scheme, and a new method of determining ESS optimal rating, optimization theory is applied. The aim of this stage is to increase wind power integration and grid steady-state voltage stability. The outcomes are validated using both technical and economic criteria, and a large data set. The data set includes 14 wind farms with diverse characteristics, a wide range of ESS ratings (0.5–165 MW and 0.5–8 hours) and 27-bus grid realistic load conditions. The ESS technology under consideration is compressed-air energy storage (CAES).
- (iv) **Objective 4:** A new ESS operation scheme for increasing wind farm transient stability is proposed. The scheme efficacy is assessed using a case study with a 60 MW wind farm, a 5-bus power system, and two types of popular wind turbines (stall-regulated and DFIG). The stability criteria for evaluation are critical clearing time, voltage recovery, and voltage sag.

Four computation and simulation packages are used for all of the studies. They are PSCAD/EMTDC [29], Matlab [30], Neplan [31], and Matpower [32]. Software results are either validated by analytical calculation or cross-checked with a comparable package to ensure accuracy. All codes used for computation are written in Matlab.

#### **1.4 RESEARCH TOOLS: POWER SYSTEMS, WIND FARM DATA, AND SOFTWARE FOR COMPUTATION**

Two power systems are used for research analyses, namely, a 27-bus power system and a 6-bus power system. The 27-bus system is a real-world regional transmission network of a large

power utility. The 6-bus power system is derived based on the 27-bus system. Depending on the requirements of a specific study, either the 6-bus or 27-bus system is appropriately used.

Wind farm data set includes the data from 15 real-world wind power plants. Of the 15 plants, a 183-MW wind farm is utilized for the study in Chapter 4. The remaining 14 wind farms are used for the study in Chapter 5. A 60-MW wind farm, custom-designed for analysis in Chapter 6, uses real-world stall-regulated wind turbine data and a Matlab built-in model of doubly-fed induction-generator based wind turbine (DFIG).

As said before, four computation and simulation packages are used for all studies. They are PSCAD/EMTDC, Matlab, Neplan, and Matpower. PSCAD, Matlab and Neplan are popular computation and power system simulation packages. Matpower is a publicly available Matlab-based program that performs power flow and optimal power flow calculations. To ensure accuracy, all results produced by simulation packages are verified either by analytical calculation or cross-checked using a comparable package. All codes used for calculation are written in Matlab.

The 6-bus power system and wind turbine data are provided in Appendix A2. The 27-bus one-line diagram with peak-load power flow is provided in Appendix A3.

## **1.5 RESEARCH CONTRIBUTION AND PRESENTATION**

The dissertation is organized in seven chapters, beginning with the introduction (Chapter 1) and ending with the conclusion (Chapter 7). Five other chapters (Chapter 2–6), the core of the research, present developed analytical solutions or procedures, along with the corresponding quantitative validation. The key results are as follows.

- (i) Objective 1 is met with the development of a stall-regulated wind turbine model which is one of the most popular types of wind turbines in use today. Detailed testing shows that the developed model is accurate. Given that dynamic wind turbine models are in a developmental stage, this model contributes to the area of wind turbine modeling. The work is presented in Chapter 2 and partially published in [33].
- (ii) The solution method of using energy storage systems for solving the wind-farm related problems is analyzed and validated via a pilot study. The study establishes voltage stability criteria, determines critical wind power penetration levels, and investigates ESS benefits in relation to voltage stability and wind power integration. An analytical calculation is done to demonstrate utilized solution methods of voltage stability and verify Neplan, the simulation package used for the study. The results

show that the proposed ESS-based solution method is effective. Without the ESS, the system smallest eigenvalue (i.e. the voltage stability limit) is reduced by 26.09% from time to time. With the ESS, a steady power level of 60 MW to the grid is maintained for the observed 8-hour period. The 26.09-percent reduction in stability is eliminated and the stability limit is brought close to that of the original system (operation without the wind farm). This forms a basis for implementing the method in a realistic and practical manner (Objectives 2–4). The work is presented in Chapter 3 and published in [34].

- (iii) Objective 2 and part of Objective 3 are met with the proposal of a framework for designing an ESS-based application. The framework includes the sequence (steps) for designing the application, a new technique for calculating the desired power output profile, a charge-discharge scheme for ESS, and a unique optimization-based (direct-calculation) method for determining an optimal ESS rating. The technique for calculating the desired power profile uses optimal power flow to determine the best output profile achievable by the aggregate system for the benefit of the grid. The term “benefit” is defined as “minimizing the total cost of grid generated power”. Regulating the wind farm output according to the desired profile causes the farm to behave like a dispatch-able source while taking into account the cost of system generation. This technique, to the best knowledge of the author, has never been proposed and, therefore, is a completely new approach. The charge-discharge scheme directs the ESS to store unwanted wind power and re-dispatch it as needed. Analysis with 14 wind farms shows that the developed charge-discharge scheme and the desired output calculation technique are appropriate for ESS operation. While regulating output variation from the 14 wind farms, the optimal ESSs perform four or less switching operations daily for 73.2%–85.5% of 365 days. On average, the ESSs carry out 2.5–3.1 switching operations per day. Analysis with the 183-MW wind farm shows that the evaluated ESS can increase the grid steady-state voltage stability, measured using smallest eigenvalue, by a net amount of 2.7%–22.3%, compared to the case where the farm output variability is completely unregulated. For ESS rating of 1–183 MW and 0.5–8 hours, the increase in wind energy integration is between 0.1% and 32.9%. The mismatch between the wind farm output and the grid load-demand is reduced by 0.1%–77.7%. The work is reported in Chapter 4 and 5 and part of the results is published in [35].

- (iv) With respect to Objective 3, a unique method for determining an optimal ESS rating is developed. It is based on the formulation of a cost-based objective function, discretization of this function, and an exhaustive search of the function values to determine the optimal ESS rating. Using this method, an optimal ESS rating can be calculated for any wind farm with a high degree of accuracy. Analysis with a compressed-air energy storage system (CAES) and 14 wind farms shows a significant trend. For wind farms with ratings of 91.5–210 MW and a capacity factor of 33% or better, the ESS optimal power rating is between 9% and 14% of the farm nameplate capacity. The optimal ESS energy rating is 4–4.5 hours. Using the same cost and benefit values, this finding is recommended for the empirical estimation of an CAES rating for similar wind farms. The result is based on the ESS operating under the developed charge-discharge scheme and being able to discharge 100% of accumulated energy. The analysis with the 14 wind farms shows that, for optimal ESSs rating, the overall enhancement in wind energy integration is between 1.7% and 8%. In addition, a net increase in steady-state voltage stability of 8.3%–18.3% is achieved for the 27-bus grid by 13 of the 14 evaluated ESSs. The work is presented in Chapter 5 and partially published in [36].
- (v) The final Objective 4 is met by the proposal of a novel operation scheme for ESS to improve wind farm transient stability. The scheme exploits the use of a synchronous-machine-based ESS as a synchronous condenser to dynamically supply a wind farm with reactive power during faults. Analysis with an ESS and the 60-MW wind farm consisting of stall-regulated wind turbines shows that the ESS increases the farm critical clearing time (CCT) by 1 cycle for worst-case bolted three-phase-to-ground faults. For bolted single-phase-to-ground faults, the CCT is improved by 23.1%–52.2%. The ESS helps mitigate the voltage sag severity and reduce the post-fault voltage recovery duration by up to 54.5%. In most of the situations investigated, the performance of the ESS is better than that for a static var compensator (SVC) of comparable capacitive rating. This leads to a new technique for operating a synchronous-machine-based ESS so as to increase its efficiency and value. The work is reported in Chapter 6 and published in [37].

## Chapter 2

### Modeling of stall-regulated wind turbine for wind power studies

Wind turbines models are indispensable for any wind power study. However, unlike conventional synchronous electrical generators, “standard” or “off-the-shelf” wind turbine models are not readily available in most, if not all, simulation software. Therefore, the research starts with modeling of a basic model of wind turbine for use in subsequent analyses. The goal is to develop the most basic yet comprehensive time-domain wind turbine model upon which more sophisticated models can be developed. The wind turbine model presented in this chapter is a stall-regulated (or fixed-speed) wind turbine model. Stall-regulated wind turbine is one of the most popular wind turbines in practice. Modeling of other wind turbine types, such as variable-speed pitch-controlled or doubly-fed wind turbines (DFIG) can be done based on a stall-regulated wind turbine model. To achieve the mentioned goal, the model component-blocks are modeled separately so as to make it easy to expand the model or customize it to suite an arbitrary wind power study. An aggregate wind turbine model, or wind farm, is also developed. This is followed by case studies to validate the models and demonstrate how the models can be used to study wind turbine operation and wind power integration issues.

**Publication:** Part of the work reported in this Chapter has been published in *Renewable Energy* journal vol. 32, No 14, pp. 2436-2452, 2006 with the title "Fundamental time-domain wind turbine models for wind power studies" [33].

#### 2.1 CHARACTERISTICS OF WIND ENERGY CONVERSION SYSTEMS

##### 2.1.1 Wind turbine components [38]

A horizontal axis wind turbine, the most popular wind energy conversion system, consists of the following main components: the turbine rotor with two or three blades, the power train, the nacelle structure, the tower, the ground equipment station. Figure 2.1 shows a wind turbine nacelle and housed components.

*Turbine rotor:* The main component of the rotor is its blades fastened to a central hub. The two general types of rotor hubs are rigid and teetered. Medium and large-scale wind turbine rotors often contain a mechanism for adjusting blade pitch, which is the angle between the blade chord line and the plane of rotation. This pitch-change mechanism, which may control the angle

of the entire blade (full-span pitch control) or only that of an outboard section (partial-span pitch control), provides a means of controlling starting torque, peak power, and stopping torque. Pitch-change mechanisms are high-quality mechanical devices with strong actuators and computerized control. The rotor blades are made of high-density wood or glass fiber and epoxy composites.

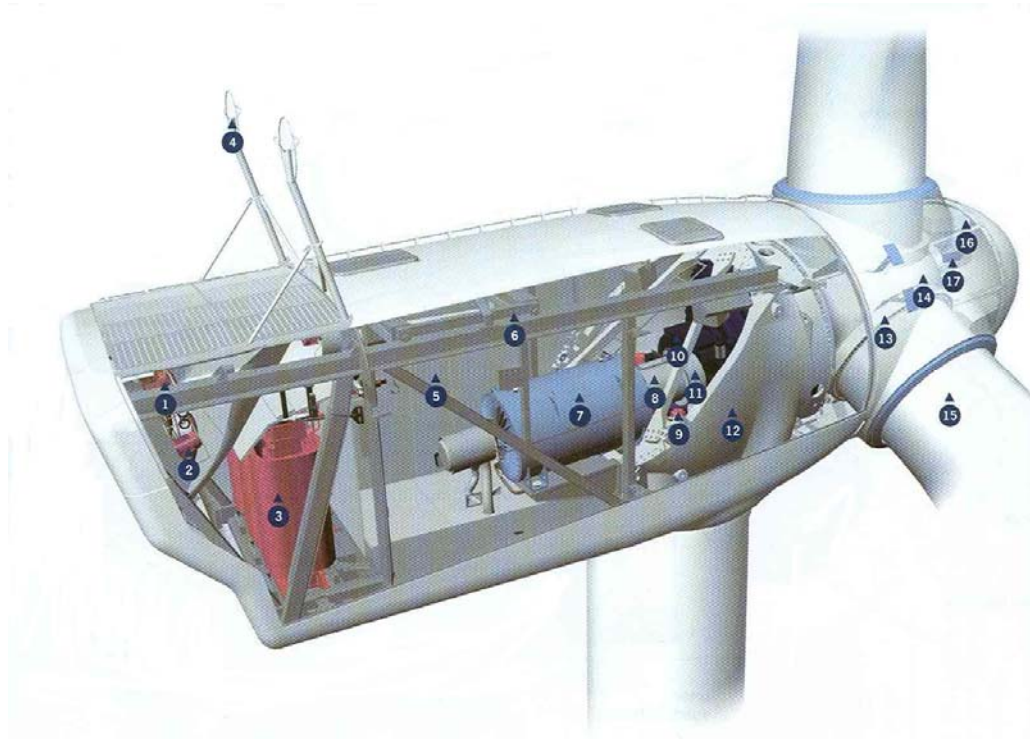


Fig. 2.1 Nacelle of Vestas V90 3-MW wind turbine [13]

**Note:** 1. Oil cooler 2. Generator cooler 3. Transformer 4. Ultrasonic wind sensor 5. VMP-Top controller with converter 6. Service crane 7. Generator 8. Composite disc coupling 9. Yaw gear 10. Gearbox 11. Parking brake 12. Machine foundation 13. Blade bearing 14. Blade hub 15. Blade 16. Pitch cylinder 17. Hub controller

*Power train:* The power train consists of a series of mechanical and electrical components needed to convert the mechanical energy power received from the rotor hub to electric power. A typical wind turbine power train consists of a turbine shaft assembly, a speed-increasing gearbox, a generator drive shaft, a rotor brake, an electrical generator, and auxiliary equipment for control, lubrication, and cooling functions.

*Nacelle structure:* The nacelle structure is the primary load path from the turbine shaft to the tower on which the turbine shaft bearings, the power train components, and the yaw drive mechanism are mounted. The yaw drive mechanism enables the nacelle to turn so as to keep the rotor shaft properly aligned with the wind.

*Tower:* The tower raises the rotor and power train to the specified hub elevation, the distance from the ground to the center of the swept area. The tower structure can be a steel or reinforced-concrete shell, or a steel truss which is usually supported on a massive spread foundation of reinforced concrete or a smaller foundation tied down by rock anchors.

*Ground equipment station:* The ground equipment station consists of components which are necessary for interfacing the wind turbine with a power system. Typical components in the ground equipment station are transformers, circuit breakers, power converters (for variable-speed wind turbines), a ground control unit, and data recording devices. Some or all of these components may be located within the base section of the tower.

### **2.1.2 Electrical generators and power electronics [13, 39, 40]**

DC generators, synchronous and asynchronous generators are used in wind turbines. They include squirrel cage induction generator (SCIG), wound-rotor induction generator (WRIG), permanent magnet synchronous generator (PMSG), and wound-rotor synchronous generator (WRSG). The most commonly-used generators are induction machines (SCIG and WRIG).

Power electronics used for wind power applications include soft-starters (and capacitor banks), rectifiers, inverters, and frequency converters (or power converters). Depending on the design, frequency converters can be divided into Direct Frequency Converters and Indirect Frequency Converters.

Wind turbines can be of fixed-speed or variable-speed types. Variable-speed wind turbines are connected to power grids with fixed frequency of 50 or 60 Hz using power converters. Variable-speed small wind turbines with DC or AC generators are generally implemented with one of the following types of converters: AC-DC, DC-AC, AC-AC, or AC-DC-AC. Large turbines usually use direct AC to AC frequency converters, or DC link converters.

### **2.1.3 Wind turbine types and dynamic features [13, 39-41]**

Variable-speed wind turbines are becoming more and more popular than fixed or constant-speed wind turbines. The major advantage of variable-speed wind turbines over constant-speed wind turbines is their capability to capture wind energy. Variable-speed wind turbines can collect on average up to 10% more power annually. Other theory and field experience show that variable-speed operation yields 20% to 30% more energy than the fixed speed operation.

As mentioned above, wind turbines are of two major types, fixed-speed and variable-speed. Each of these types may be divided into smaller categories depending on their speed-

control schemes, or the use of power electronics. Therefore, wind turbines may be classified into four typical types below. Figure 2.2 shows the typical configurations for the four types of wind turbines.

- Type A: fixed-speed
- Type B: limited variable-speed
- Type C: variable-speed with partial-scale frequency converter
- Type D: variable-speed with full-scale frequency converter

**Type A:** A wind turbine of this type uses a squirrel case induction generator (SCIG) which is directly connected to the power system via a transformer. Since the electrical generator consumes reactive power, this configuration uses a capacitor bank for reactive power compensation. The speed control schemes can be stall control, pitch control, or active stall control.

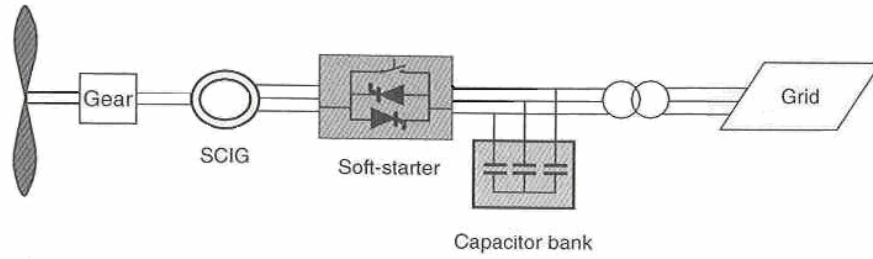
**Type B:** This configuration uses a wound rotor induction generator (WRIG) in association with a variable generator rotor resistance and pitch control. The allowable speed range is 0–10% above the synchronous speed.

**Type C:** This configuration is called doubly-fed induction generator (DFIG) concept. It is a limited variable-speed wind turbine with a wound rotor induction generator, partial-scale frequency converter, and pitch control. The frequency converter performs the reactive power compensation and enables a smoother grid connection. The typical speed ranges from –40% to +30% of synchronous speed.

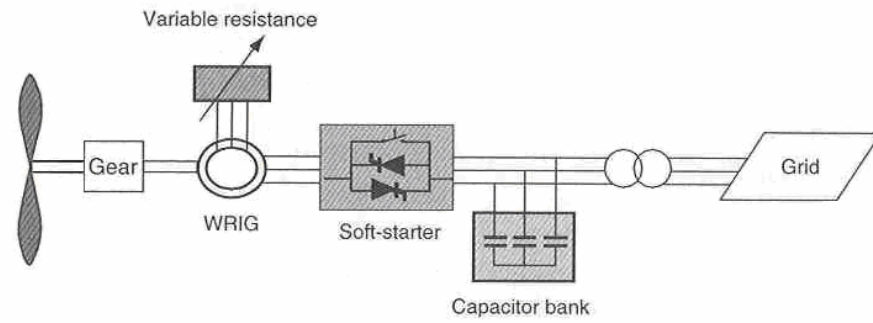
**Type D:** This is a variable-speed, pitch-controlled wind turbine that uses a generator connected to the grid via a full-scale frequency converter. Reactive power compensation is carried out by the converter and smoother grid connection is possible. The electrical generator may be a wound rotor induction generator (WRIG), a permanent magnet synchronous generator (PMSG), or, typically, a direct driven synchronous generator.

Fixed-speed wind turbines (Type A) had been very popular until the year 2000. An internet survey (page 65 of [13]) conducted for thirteen world largest wind turbine suppliers shows that fixed-speed wind turbines represent 40.8% and 39% of market share in 1999 and 2000, respectively. From 2001, variable-speed wind turbines with partial-scale frequency converters (Type C, or DFIG) have become more common. Turbines of this type account for 46.8% of all sold turbines in 2002 while the share for fixed-speed turbines is reduced to 27.8%.

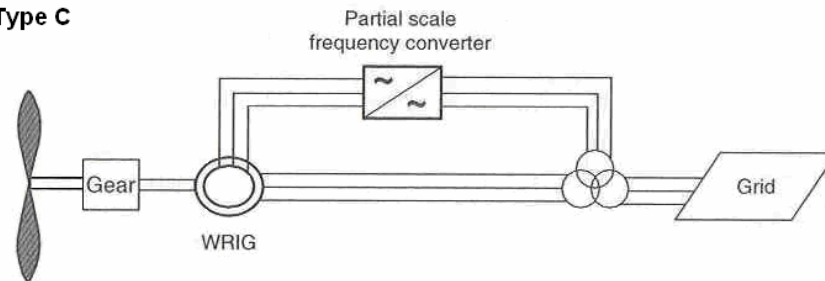
**Type A**



**Type B**



**Type C**



**Type D**

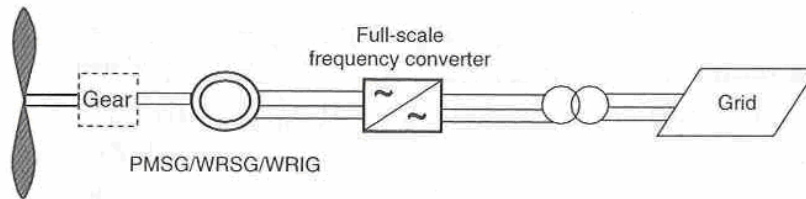


Fig. 2.2 Typical wind turbine configurations [13]

**Note:** SCIG=squirrel cage induction generators, WRIG=wound-rotor induction generators, PMSG=permanent magnet synchronous generators, and WRSG=wound-rotor synchronous generators. The most commonly-used generators are induction machines (SCIG and WRIG). There may or may not be a gearbox for Type D.

## 2.2 MODELING OF STALL-REGULATED WIND TURBINE

Based on the characteristics of wind turbines described in Section 2.1, the primary components of a wind turbine for modelling purposes are the following (Fig. 2.3):

- (i) *Aerodynamic block*: The wind rotor (i.e. the prime mover)
- (ii) *Mechanical block*: The shaft and gearbox unit (i.e. the drive train and a speed changer)
- (iii) *Electrical block*: Electric generator (e.g. SCIG, WRIG)
- (iv) *Control block*: Pitch-angle control system, power control etc.

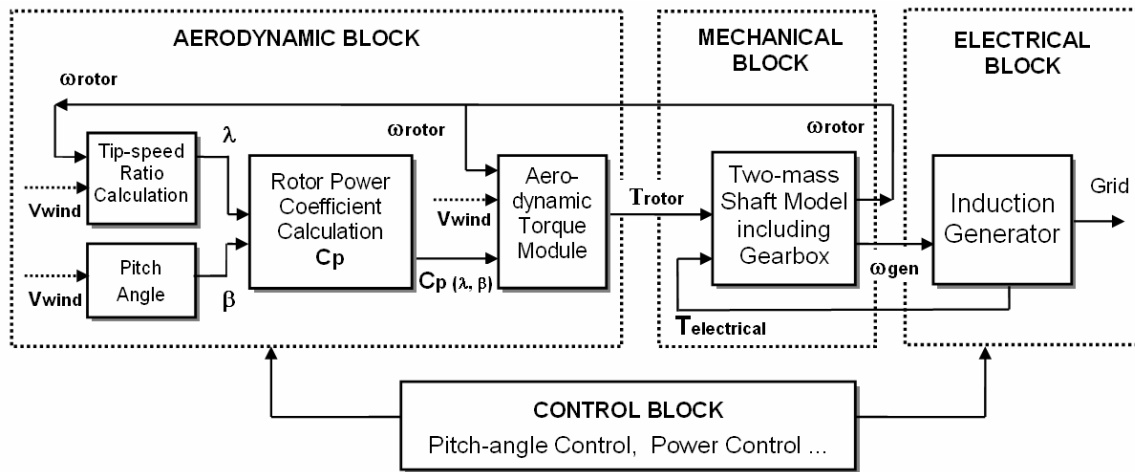


Fig. 2.3. Block diagram of a wind turbine

The modeling of aerodynamic block, the shaft and the electrical generator is presented in detail the following sections.

### 2.2.1 Aerodynamic block

The aerodynamic block consists of five modules: wind speed, tip-speed ratio calculation, pitch-angle determination, rotor power coefficient (or  $C_p$  calculation), and aerodynamic torque.

#### 1) Wind speed input

Wind speed varies according to the local heating and atmospheric condition. Therefore, a wind speed module is needed to provide an input signal representing a desired or actual wind speed. The wind speed range is bounded between the cut-in and cut-out speeds (5 and 25 m/s, respectively). The input signal can be set to any value in the speed range during the simulation run-time. It can also be in the form of time-series data of an actual wind speed measurement.

## 2) Tip-speed ratio calculation

The tip-speed ratio, denoted by  $\lambda$ , is the ratio of the blade-tip linear speed to the wind speed. The tip-speed ratio together with the blade pitch angle  $\beta$ , determines the efficiency of the rotor,  $C_P$ . It can be calculated as follows [38, 39, 42]:

$$\lambda = \frac{\text{Bladetip speed}}{\text{Wind speed}} = \frac{\omega_T R_T}{v_{wind}} \quad (2.1)$$

where

$\omega_T$  = wind rotor angular speed [rad/s];

$R_T$  = wind rotor radius [m];

$v_{wind}$  = wind speed [m/s].

## 3) Pitch-angle determination

The rotor power coefficient  $C_P$ , defined in the next subsection, varies with the tip-speed ratio  $\lambda$  for a given wind speed.  $C_P$  is maximum for a particular tip-speed ratio  $\lambda$ . Thus, to keep  $C_P$  maximum for all wind speeds, the angular speed of the rotor must be adjusted such that its corresponding  $\lambda$  yields a maximum  $C_P$ . The rotor speed can be adjusted by varying the blade pitch angle  $\beta$ . This is essentially the principle behind variable-speed wind turbines [39]. For a fixed-speed stall-regulated wind turbine, the pitch angle is fixed. The pitch-angle control module can be expanded for modelling of variable-speed wind turbines.

## 4) $C_P$ calculation

The rotor power coefficient is a measure of the rotor power efficiency and is defined as follows [42].

$$C_P = \frac{\text{Rotor power}}{\text{Power in the wind}} = \frac{P_{rotor}}{P_{wind}} \quad (2.2)$$

As mentioned above, the rotor power coefficient  $C_P$  is a function of the tip speed ratio,  $\lambda$ , and the blade pitch angle,  $\beta$ . To obtain the optimal  $C_P$  curve for a particular wind turbine, constant  $\lambda$  must be maintained at all times for all wind speeds. Variable-speed wind turbines are equipped with a pitch-change mechanism to adjust the blade tip speed so they have a better power coefficient profile. In case of direct-connect wind turbines, the electrical generator speed is fixed by the grid. In turn, the rotor speed is also fixed since it is directly connected to the generator via a gearbox. This means that the blade tip speed is practically unchanged. Therefore, as the wind speed increases, the  $C_P$  of a direct-connect fixed-speed wind turbine will increase at first, then decreases after the rated power is reached.

The rotor power coefficient  $C_P$  can be determined as a function of the tip-speed ratio,  $\lambda$ , and the blade pitch angle,  $\beta$ . In this research,  $C_P$  is reproduced using actual data by piece-wise linear interpolation technique. The plot of  $C_P$  for selected  $\beta$  is shown in Fig 2.4.

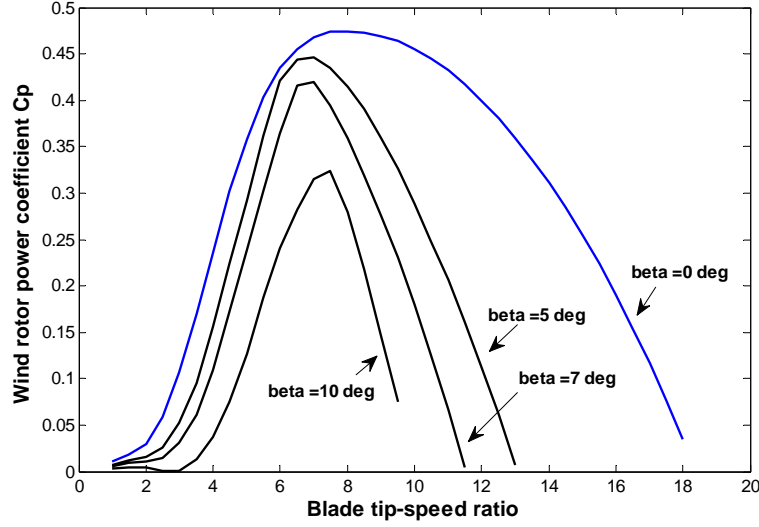


Fig. 2.4 Wind rotor power coefficient for selected pitch angles

The rotor power coefficient  $C_P$  can be estimated using the following polynomial functions for pitch angle of  $0^0$ ,  $3^0$ ,  $5^0$ , and  $7^0$  in the stated order. This approach has lower accuracy compared to the piece-wise linear interpolation technique, which reproduces the  $C_P$  measured data very closely.

$$C_{p_0} = 0.13605 - 0.05306\lambda + 0.01545\lambda^2 + 0.00147\lambda^3 - 0.00022\lambda^4 - 0.000009\lambda^5$$

$$C_{p_3} = 0.10936 - 0.05829\lambda + 0.01678\lambda^2 + 0.00174\lambda^3 - 0.00026\lambda^4 - 0.00001\lambda^5$$

$$C_{p_5} = 0.00872 - 0.05847\lambda + 0.01666\lambda^2 + 0.00185\lambda^3 - 0.00028\lambda^4 - 0.00001\lambda^5$$

$$C_{p_7} = 0.06065 - 0.05669\lambda + 0.01599\lambda^2 + 0.00191\lambda^3 - 0.00029\lambda^4 - 0.00001\lambda^5$$

### 5) Aerodynamic torque module

The aerodynamic torque developed on the rotor blades is determined based on [42, 43] as follows.

$$P_{wind} = (1/2) \rho v_{wind}^3 \pi R_{rotor}^2 \quad (2.3)$$

This is the dynamic power from the wind available at the rotor blades. However, a non-ideal rotor can capture only part of this power, as defined by the rotor power coefficient  $C_P$ ,

$$P_{rotor} = (1/2)C_p \rho v_{wind}^3 \pi R_{rotor}^2 \quad (2.4)$$

The aerodynamic torque  $T_T$  produced by the wind rotor blades is

$$T_T = \frac{(1/2)C_p \rho v_{wind}^3 \pi R_T^2}{\omega_T} \quad (2.5)$$

In the above equations,  $\rho$  is the standard air density (i.e. 1.225 kg/m<sup>3</sup>).

## 2.2.2 Mechanical block

The mechanical block, or the wind turbine rotor-generator drive train, consists of the wind turbine shaft, generator shaft and a gearbox. The wind turbine generator shaft and the gearbox are modelled using a two-mass inertia representation as follows.

### 1) Theoretical background

Consider a rotational system [44] shown in Fig. 2.5a, which consists of a disk with a moment of inertia  $J$  mounted on a shaft fixed at one end. The viscous friction coefficient (damping) between the two surfaces is  $D$  and the shaft torsional spring constant (stiffness) is  $K$ .

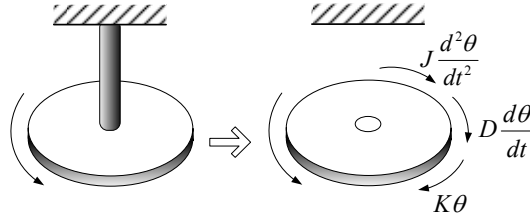


Fig. 2.5 Rotational system with a disk [44]

The torque about the axis of the shaft can be written from the free-body diagram, shown in Fig. 2.5b, as follows.

$$\Gamma(t) = J \frac{d^2 \theta(t)}{dt^2} + D \frac{d \theta(t)}{dt} + K \theta(t) \quad (2.6)$$

Next, consider a rotational system shown in Fig. 2.6a which consists of two systems similar to the one above. The difference is that the two systems are linked with a gear train.  $\Gamma$  is the external torque applied to the disk of System 1 (the time-dependent notation  $t$  is omitted for clarity).  $\Gamma_1$ ,  $\Gamma_2$  are transmitted torques.  $N_1$ ,  $N_2$  are the numbers of teeth of Gear 1 and Gear 2.  $J_1$ ,  $J_2$ ,  $D_1$ ,  $D_2$ ,  $K_1$ ,  $K_2$  are the moments of inertia, damping, and stiffness of System 1 and System 2, respectively.

Applying (2.6) to the system in Fig. 2.6a, the torque equation on the side of Gear 1 is

$$\Gamma = J_1 \frac{d^2\theta_1}{dt} + D_1 \frac{d\theta_1}{dt} + K_1\theta_1 + \Gamma_1 \quad (2.7)$$

The torque equation on the side of Gear 2 is

$$\Gamma_2 = J_2 \frac{d^2\theta_2}{dt} + D_2 \frac{d\theta_2}{dt} + K_2\theta_2 \quad (2.8)$$

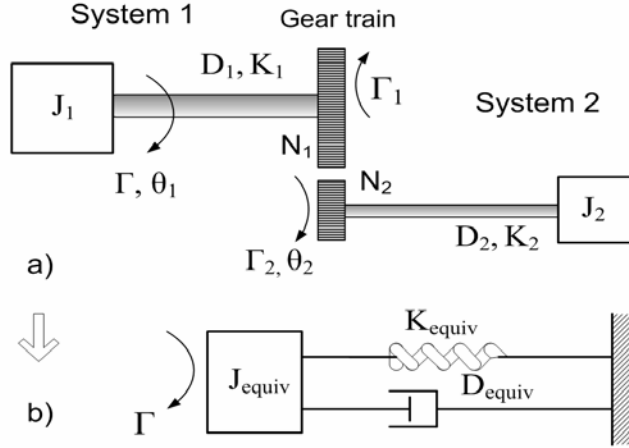


Fig. 2.6 Rotational system with a gear train in the middle [44]

Knowing that  $\Gamma_1 = (N_1/N_2)\Gamma_2$  and  $\theta_2 = (N_1/N_2)\theta_1$  [44]-[45], the quantities on Gear 2 can be referred to the Gear 1 side.

$$\Gamma_1 = \left(\frac{N_1}{N_2}\right) \left[ J_2 \frac{d^2\theta_2}{dt} + D_2 \frac{d\theta_2}{dt} + K_2\theta_2 \right] \quad (2.9)$$

$$\Gamma_1 = \left(\frac{N_1}{N_2}\right) \left[ J_2 \left(\frac{N_1}{N_2}\right) \frac{d^2\theta_1}{dt} + D_2 \left(\frac{N_1}{N_2}\right) \frac{d\theta_1}{dt} + K_2 \left(\frac{N_1}{N_2}\right) \theta_1 \right] \quad (2.10)$$

$$\Gamma_1 = J_{refl} \frac{d^2\theta_1}{dt} + D_{refl} \frac{d\theta_1}{dt} + K_{refl} \theta_1 \quad (2.11)$$

where  $J_{refl}$ ,  $D_{refl}$ , and  $K_{refl}$  are the respective quantities reflected to the Gear 1 side. Substituting (2.11) into (2.7) and rearranging, we obtain the expression for the applied torque. The system in Fig. 2.6a is reduced to the equivalent system in Fig. 2.6b with the gear train eliminated.

$$\Gamma = J_{equiv} \frac{d^2\theta_1}{dt} + D_{equiv} \frac{d\theta_1}{dt} + K_{equiv} \theta_1 \quad (2.12)$$

where

$$\begin{aligned}
J_{equiv} &= J_1 + J_2(N_1 / N_2)^2 = J_1 + J_{refl} \\
D_{equiv} &= D_1 + D_2(N_1 / N_2)^2 = D_1 + D_{refl} \\
K_{equiv} &= K_1 + K_2(N_1 / N_2)^2 = K_1 + K_{refl}
\end{aligned}
\tag{2.13}$$

## 2) Wind turbine drive-train modeling

By visual inspection, it is clear that the basic wind turbine configuration shown in Fig. 2.7a is analogous to that in Fig. 2.6a. Therefore, the wind turbine system can be modelled using the same approach. The difference is that the quantities on the left side of the gearbox are reflected to the right (generator) side. In this way the gearbox is eliminated and a two-mass representation of the wind turbine system results (Fig. 2.7b). Since the moment of inertia of the gearbox is very small compared with the moment of inertia of the wind turbine rotor and its damping and stiffness are considered negligible, it can be ignored.

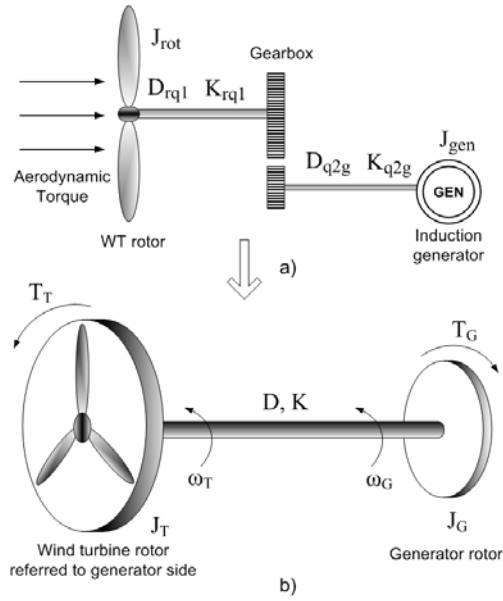


Fig. 2.7 Modeling of wind turbine system drive train

Torque equations describing the mechanical behavior of the wind turbine system can now be written based on the two-mass model. Note that the aerodynamic torque from the wind turbine rotor is counteracted by the electromechanical torque from the direct-connect electrical generator. Torque equations with all rotor-side quantities referred to the generator frame are as follows:

$$\begin{aligned}
J_T \ddot{\theta}_T + D(\omega_T - \omega_r) + K(\theta_T - \theta_r) &= T_T \\
J_G \ddot{\theta}_r + D(\omega_r - \omega_T) + K(\theta_r - \theta_T) &= T_G
\end{aligned}
\tag{2.14}$$

where

- $J_T, J_G$  = moments of inertia of wind rotor and generator rotor [kgmm];
- $T_T, T_G$  = aerodynamic torque and generator electromagnetic torque [Nm];
- $w_T, w_r$  = wind rotor speed and generator speed [rad/s];
- $\theta_T, \theta_r$  = angular position of wind rotor and generator rotor [rad];
- $D, K$  = equivalent damping and stiffness [Nms/rad], [Nm/rad].

For computer simulation, speeds and torques of the turbine rotor and the generator are determined for each simulation time step by solving the above two equations using a state-space approach. The state-space equations are:

$$\begin{aligned} \frac{d}{dt}(\theta_T - \theta_r) &= \omega_T - \omega_r \\ \dot{\omega}_T &= (1/J_T)[T_T - D(\omega_T - \omega_r) - K(\theta_T - \theta_r)] \\ \dot{\omega}_r &= (1/J_G)[D(\omega_T - \omega_r) + K(\theta_T - \theta_r) + T_G] \end{aligned} \quad (2.15)$$

Note that the electromagnetic torque is positive when the induction generator speed is less than the synchronous speed (i.e. in motor mode) and is negative when the generator speed is greater than the synchronous speed (i.e. in generator mode).

Assume that the generator shaft (high-speed shaft) is completely stiff [46] and using a 1.5-MW wind turbine data, the equivalent quantities for the wind turbine model are determined with reference to (2.13). The generator mechanical angular speed and rated torque are also calculated as follows:

$$J_T = \frac{J_{rot}}{GR^2} = \frac{4915797.5}{70^2} = 995.8 \text{ kgmm}$$

$$D = D_{q2g} + D_{rq1}(1/GR)^2 = 30.3 \text{ Nms/rad}$$

$$K = K_{rq1}(1/GR)^2 = 19720 \text{ Nm/rad}$$

$$\omega_n = \omega_{mech} = \frac{2\pi \times 60}{p} = 125.6637 \text{ rad/s}$$

$$T_{gen\_rated} = \frac{P_{mech}}{\omega_n} = \frac{1.5 \times 10^6}{125.6637} = 11937 \text{ Nm}$$

The complete data for the 1.5-MW wind turbine and the electrical generator are provided in Appendix A2.

### 2.2.3 Electrical block

The main component of the electrical block is an induction generator. For the purpose of modelling a fixed speed wind turbine, a squirrel cage induction machine is sufficient. However, a wound rotor induction machine is required for modeling a variable speed wind turbine of type C (i.e. DFIG). Modeling of squirrel cage induction generator is based on the theory of symmetrical induction machines in [47].

The machine basic equations (i.e. voltage, torque) are first expressed in terms of machine variables (flux linkages, resistances, inductances). Then, the equations are transformed to an arbitrary reference frame using the methods developed by Park, Stanley, Kron and Brereton [47]. Expressing the machine basic equations in arbitrary reference frame eliminates the labor of transforming the equations individually each time one changes the reference frame. Three most frequently used reference frames are the stationary reference frame, the reference frame fixed on the rotor and the synchronously rotating reference frame. The machine equations can be expressed in any of these reference frames by assigning the speed appropriate to the reference frame of interest [47]. The transformation is commonly known as abc-to-qd0 transformation where “abc” refers to 3-phase variables. The modeling of the induction generator in this study follows the theory closely because of the generality and flexibility offered by the use of the arbitrary reference frame. Modeling of asynchronous machines is basic so only key equations are presented here. For detailed modeling, refer to [47].

Applying the abc-to-qd0 transformation, the machine basic equations can be expressed in terms of qd0-variables in the arbitrary reference frame. The flux linkage per second  $\Psi_{qd0}$ , derived from the machine voltage equations with currents eliminated, are calculated as [47]

$$\dot{\Psi}_{qs} = \omega_b \left[ v_{qs} - \frac{\omega}{\omega_b} \Psi_{ds} + \frac{r_s}{X_{ls}} (\Psi_{mq} - \Psi_{qs}) \right] \quad (2.16)$$

$$\dot{\Psi}_{ds} = \omega_b \left[ v_{ds} + \frac{\omega}{\omega_b} \Psi_{qs} + \frac{r_s}{X_{ls}} (\Psi_{md} - \Psi_{ds}) \right] \quad (2.17)$$

$$\dot{\Psi}_{0s} = \omega_b \left[ v_{0s} - \frac{r_s}{X_{ls}} \Psi_{0s} \right] \quad (2.18)$$

$$\dot{\Psi}_{qr} = \omega_b \left[ v_{qr} - \left( \frac{\omega - \omega_r}{\omega_b} \right) \Psi_{dr} + \frac{r_r}{X_{lr}} (\Psi_{mq} - \Psi_{qr}) \right] \quad (2.19)$$

$$\dot{\Psi}_{dr} = \omega_b \left[ v_{dr} + \left( \frac{\omega - \omega_r}{\omega_b} \right) \Psi_{qr} + \frac{r_r}{X_{lr}} (\Psi_{md} - \Psi_{dr}) \right] \quad (2.20)$$

$$\dot{\psi}_{0r} = \omega_b \left[ v_{0r} - \frac{r_r}{X_{lr}} \psi_{0r} \right] \quad (2.21)$$

The subscripts “*q*”, “*d*”, “*0*” denote quadrature-, direct-, and zero-quantities. The subscripts “*s*” and “*r*” denote stator and rotor quantities, respectively. The qd0-voltage (i.e. the voltage applied to the machine stator) is *v* with the appropriate subscript ( “*qs*”, “*ds*” etc). In the  $\Psi_{qd0}$  equations

$$\begin{aligned} \psi_{mq} &= X_{aq} \left[ \frac{\psi_{qs}}{X_{ls}} + \frac{\psi_{qr}}{X_{lr}} \right] \\ \psi_{md} &= X_{ad} \left[ \frac{\psi_{ds}}{X_{ls}} + \frac{\psi_{dr}}{X_{lr}} \right] \\ X_{aq} &= X_{ad} = \left[ \frac{1}{X_M} + \frac{1}{X_{ls}} + \frac{1}{X_{lr}} \right]^{-1} \end{aligned}$$

The qd0-currents are computed as

$$i_{qs} = \frac{1}{X_{ls}} (\psi_{qs} - \psi_{mq}) \quad (2.22)$$

$$i_{ds} = \frac{1}{X_{ls}} (\psi_{ds} - \psi_{md}) \quad (2.23)$$

$$i_{0s} = \frac{1}{X_{ls}} \psi_{0s} \quad (2.24)$$

$$i_{qr} = \frac{1}{X_{lr}} (\psi_{qr} - \psi_{mq}) \quad (2.25)$$

$$i_{dr} = \frac{1}{X_{lr}} (\psi_{dr} - \psi_{md}) \quad (2.26)$$

$$i_{0r} = \frac{1}{X_{lr}} \psi_{0r} \quad (2.27)$$

where

$r_s$  = stator resistance [ohm];

$X_{ls}$  = stator leakage reactance [ohm];

$X_M$  = magnetizing reactance [ohm];

$r_r$  = rotor resistance referred to stator side [ohm];

$X_{lr}$  = rotor leakage reactance referred to stator side [ohm];

$\omega_b$  = base electrical velocity [rad/s];

$\omega$  = reference-frame arbitrary velocity [rad/s].

The electromagnetic torque equation is

$$T_G = \left(\frac{3}{2}\right) \left(\frac{Poles}{2}\right) \frac{X_M}{D \omega_b} (\psi_{qs} \psi_{dr} - \psi_{qr} \psi_{ds}) \quad (2.28)$$

where  $D = (X_{ls} + X_M)(X_{lr} + X_M) - X_M^2$  ;

$Poles$  = number of poles.

For balanced conditions, only the qd-quantities are present while the zero-quantities are not present in the equations for flux linkages per second and currents. Though, the zero-quantities are included in the induction machine model for completeness. They are also useful in case unbalanced conditions need to be considered.

Under balanced conditions, the 3-phase real power  $P$  and the 3-phase reactive power  $Q$  are computed as [47] [11]

$$\begin{aligned} P &= (3/2) (v_{qs} i_{qs} + v_{ds} i_{ds}) \\ Q &= (3/2) (v_{qs} i_{ds} - v_{ds} i_{qs}) \end{aligned} \quad (2.29)$$

In this study, the synchronously rotating reference frame is used for the induction machine model i.e.  $\omega_b = \omega$  (377 rad/s for a 60-Hz power system). The use of the synchronous reference frame is very convenient when incorporating the machine dynamic characteristics for studying transient stability of large power systems. This reference frame is also frequently used to analyze balanced conditions [47] which are present or can be assumed for many grids. The type of induction machine of consideration is the widely-used squirrel-cage machine. Under qd0-transformation with synchronous reference frame,  $v_{ds} = 0$  [47]. The interesting result is that the real and reactive power are decoupled and the equations (2.29) become

$$\begin{aligned} P &= (3/2) v_{qs} i_{qs} \\ Q &= (3/2) v_{qs} i_{ds} \end{aligned} \quad (2.30)$$

**Conversion to per unit system:** All the machine quantities so far are in MKS units. It is straightforward to convert the quantities to per unit by dividing the MKS-values by their respective base values. The only note is that while the base voltage for the abc-variables is the rms phase voltage  $V_{B(abc)}$ , the base voltage for the qd0-variables is the peak value  $V_{B(qd0)} = \sqrt{2} V_{B(abc)}$  [47]. It is easy to show that the base current for the qd0-variables is  $I_{B(qd0)} = \sqrt{2} I_{B(abc)}$ , where  $I_{B(abc)}$  is the base current for abc-variables.

#### 2.2.4 Control block

For a direct-connect fixed-speed wind turbine system, pitch-angle control and power control are not required. One can develop this block for different purposes such as modelling variable-speed wind turbine systems or controlling a reactive compensation device to meet the wind turbine reactive power demand using techniques presented in other technical papers, such as [48-50].

### 2.3 VALIDATION OF STALL-REGULATED WIND TURBINE MODEL

#### 2.3.1 Solution for wind turbine equations

As shown in Section 2.2, the wind turbine model consists of three major blocks, namely the aerodynamic block, the shaft, and the induction generator. Each of these blocks is represented by the respective equations, which must be solved simultaneously to obtain the wind turbine dynamic characteristics (i.e. torque, speed, power etc.).

For the aerodynamic block and the shaft, the aerodynamic torque is calculated using (2.5) for a specific wind speed. The wind rotor speed and the corresponding generator rotor speed are obtained by solving (2.15), which represents the dynamic interaction between the wind rotor and the generator. The driving aerodynamic torque and the resulting generator speed are the inputs for solving the generator equations.

For the induction generator, with knowledge of the voltages applied to the stator terminals, the other unknown quantities (i.e. current, torque, power etc.) can be obtained by first solving (2.16) through (2.21) for flux linkages per second. Then, the currents are calculated using (2.22) through (2.27). The electromagnetic torque and the 3-phase power are computed using (2.28) and (2.30), respectively. The block diagram for solving the wind turbine equations is shown in Fig. 2.8, where  $K_s$  and  $K_r$  are qd0-transformation matrices.

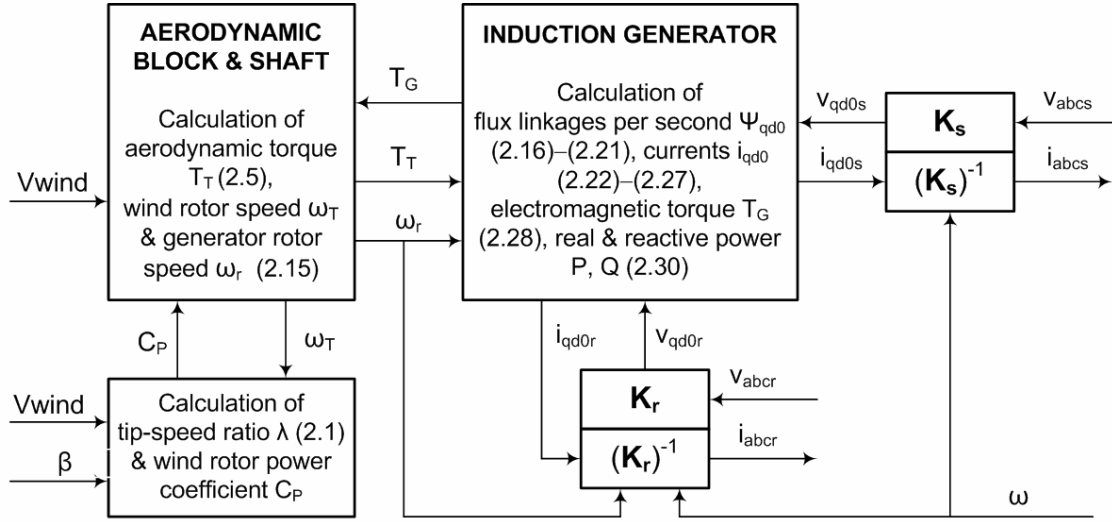


Fig. 2.8 Solution for wind turbine equations in block diagram form

## 2.3.2 Numerical integration of wind turbine differential equations

### 2.3.2.1 Numerical integration methods

The two numerical integration methods used to solve the wind turbine equations are the standard Euler method and the second-order Runge-Kutta (R-K) method. The short description of the methods is presented below. For details, see Chapter 13 of [11].

Consider the first-order differential equations [11]

$$\frac{d\mathbf{x}}{dt} = \mathbf{f}(\mathbf{x}, t) \quad (2.31)$$

where  $\mathbf{x}$  is the state vector of  $n$  dependent variables and  $t$  is time. We are interested in solving for  $\mathbf{x}$  as a function of  $t$ , knowing the initial values of the variables  $\mathbf{x}_0$  and  $t_0$ .

The standard Euler method approximates the curve of true solution using tangents, or the first two terms of the Taylor series. At  $\mathbf{x} = \mathbf{x}_0$  and  $t = t_0$

$$\left. \frac{d\mathbf{x}}{dt} \right|_{\mathbf{x}=\mathbf{x}_0} = \mathbf{f}(\mathbf{x}_0, t_0) \Rightarrow \Delta\mathbf{x} = \mathbf{f}(\mathbf{x}_0, t_0) \cdot \Delta t = \left. \frac{d\mathbf{x}}{dt} \right|_{\mathbf{x}=\mathbf{x}_0} \cdot \Delta t \quad (2.32)$$

The value of  $\mathbf{x}$  at  $t_1 = t_0 + \Delta t$  is calculated as

$$\mathbf{x}_1 = \mathbf{x}_0 + \Delta\mathbf{x} = \mathbf{x}_0 + \mathbf{f}(\mathbf{x}_0, t_0) \cdot \Delta t \quad (2.33)$$

where  $\Delta t$  is the time step. We can continue this way to solve for the solution by computing all the following  $\mathbf{x}$ . The update formula for the  $(n+1)^{st}$  steps is

$$\mathbf{x}_{n+1} = \mathbf{x}_n + \mathbf{f}(\mathbf{x}_n, t_n) \cdot \Delta t \quad (2.34)$$

The Runge-Kutta methods also base on the Taylor series, but compute higher derivatives by several evaluations of the first derivative. The second-order Runge-Kutta method solves (2.30) as follows. At  $t_1 = t_0 + \Delta t$  the value of  $\mathbf{x}$  is given by

$$\begin{aligned} \mathbf{x}_1 &= \mathbf{x}_0 + \Delta \mathbf{x} = \mathbf{x}_0 + \frac{\mathbf{k}_1 + \mathbf{k}_2}{2} \\ \mathbf{k}_1 &= \mathbf{f}(\mathbf{x}_0, t_0) \Delta t \\ \mathbf{k}_2 &= \mathbf{f}(\mathbf{x}_0 + \mathbf{k}_1, t_0 + \Delta t) \Delta t \end{aligned} \quad (2.35)$$

The general formula for the  $(n+1)^{st}$  step is

$$\begin{aligned} \mathbf{x}_{n+1} &= \mathbf{x}_n + \frac{\mathbf{k}_1 + \mathbf{k}_2}{2} \\ \mathbf{k}_1 &= \mathbf{f}(\mathbf{x}_n, t_n) \Delta t \\ \mathbf{k}_2 &= \mathbf{f}(\mathbf{x}_n + \mathbf{k}_1, t_n + \Delta t) \Delta t \end{aligned} \quad (2.36)$$

### 2.3.2.2 Numerical integration of wind turbine equations

The standard Euler and the second-order Runge-Kutta methods are known as explicit methods. They are straightforward and easy to implement. However, they have a significant limitation of being numerically unstable unless a sufficiently small time step is used [11]. Therefore, to ensure numerical stability, this study solution uses a conservatively small time step of 0.0001.

Referring to Section 2.2 with the emphasis on Fig. 2.8, the most important sets of differential equations to be solved are the set of equations describing the shaft dynamics (2.15) and the set of equations for flux linkages per second (2.16–2.21). For brevity, the first step of solution for flux linkages per second is presented below. The second-order Runge-Kutta method is used for calculation.

The 3-phase balanced abc-voltages applied to the induction generator stator (generator rated voltage is 690 V, see Appendix A2) are

$$v_{as} = \sqrt{2}(398.37) \cos(377t)$$

$$v_{bs} = \sqrt{2}(398.37) \cos(377t - \frac{2\pi}{3})$$

$$v_{cs} = \sqrt{2}(398.37) \cos(377t + \frac{2\pi}{3})$$

The abc-voltages are transformed into the qd0-voltages using the qd0-transformation technique. The initial value for flux linkages per second at  $t_0 = 0$  is

$$\Psi_0 = \Psi_{qd0}(0) = [\psi_{qs} \ \psi_{ds} \ \psi_{0s} \ \psi_{qr} \ \psi_{dr} \ \psi_{0r}]^T = \mathbf{0}$$

Applying (2.35), at  $t_1 = t_0 + \Delta t$  ( $\Delta t = 0.0001$ ), flux linkages per second are given by

$$\Psi_1 = \Psi_0 + \frac{\mathbf{k}_1 + \mathbf{k}_2}{2}$$

where the notation “qd0” is dropped for clarity. The  $\mathbf{k}_1$  and  $\mathbf{k}_2$  are computed using (2.35) and the  $\Psi_{qd0}$  equations (2.16–2.21) to give

$$\mathbf{k}_1 = \begin{bmatrix} 21.239025 \\ 0 \\ 0 \\ 0 \\ 0 \\ 0 \end{bmatrix} \quad \mathbf{k}_2 = \begin{bmatrix} 21.187563 \\ 0.800692 \\ 0 \\ 0.038913 \\ 0 \\ 0 \end{bmatrix}$$

The flux linkages per second is

$$\Psi_1 = \mathbf{0} + \frac{\mathbf{k}_1 + \mathbf{k}_2}{2} = \begin{bmatrix} 21.213294 \\ 0.400346 \\ 0 \\ 0.019457 \\ 0 \\ 0 \end{bmatrix}$$

The wind turbine equations are solved using Matlab and the entire solution implementation is available in Matlab codes.

### 2.3.3 Performance of stall-regulated wind turbine model

*Scenario:* The developed wind turbine model (called analytical model) is solved numerically using Matlab as described in Section 2.3.2. Then, the same model is built using the time-domain package PSCAD/EMTDC. The validity of the wind turbine model is verified by

comparing its major dynamic characteristics (i.e. torque, speed and power output etc.) with the respective results by PSCAD, and the power output data of a 1.5-MW real-world variable-speed wind turbine. The wind turbine model data are provided in Appendix A2.

The wind turbine grid-connection scheme is shown in Fig 2.9. The developed wind turbine is connected via a transformer to a very strong grid, modeled as an infinity bus. Its simulated characteristics are recorded for comparison with the results by the Matlab calculation. The transformer is 10-MVA 690V/34.5kV delta-wye-grounded with the leakage reactance of 7%. Since the generator terminal voltages, real power output and reactive power consumption may be different for different grid strengths, connecting the wind turbine to the infinity bus helps eliminate the possible discrepancies. Also, this connection scheme is a conventional model for transient stability studies and will be used later to validate the transient stability performance of the wind turbine model.

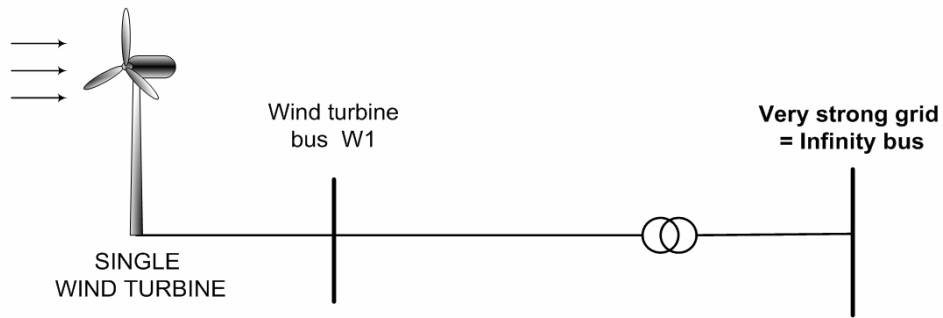


Fig. 2.9 Wind turbine grid connection scheme

**Initialization of wind turbine model:** The wind turbine is started immediately in generator mode where the generator and the wind rotor are assumed to be running at the synchronous speed (i.e. 125.6637 rad/s) at time  $t = 0$ . This setting essentially excludes the wind rotor and the induction generator starting transients, which are not of interest in this analysis. The aerodynamic torque is set to zero for the first 0.01 second for PSCAD simulation. Then, the torque assumes the quantity computed in (2.5). The pitch angle  $\beta$  is fixed at 4.8 degrees to achieve the rated real power of 1.5 MW at the rated wind speed of 15 m/s.

### 2.3.3.1 Power curve

The real power output versus wind speed curve (i.e. the power curve) of the 1.5-MW analytical wind turbine model is obtained by calculating the power output for each wind speed, which is varied from the cut-in to the cut-out speed in 1-m/s increment. The obtained analytical

result is shown in Fig. 2.10 where it is compared with those by PSCAD and a real-world variable-speed 1.5-MW wind turbine.

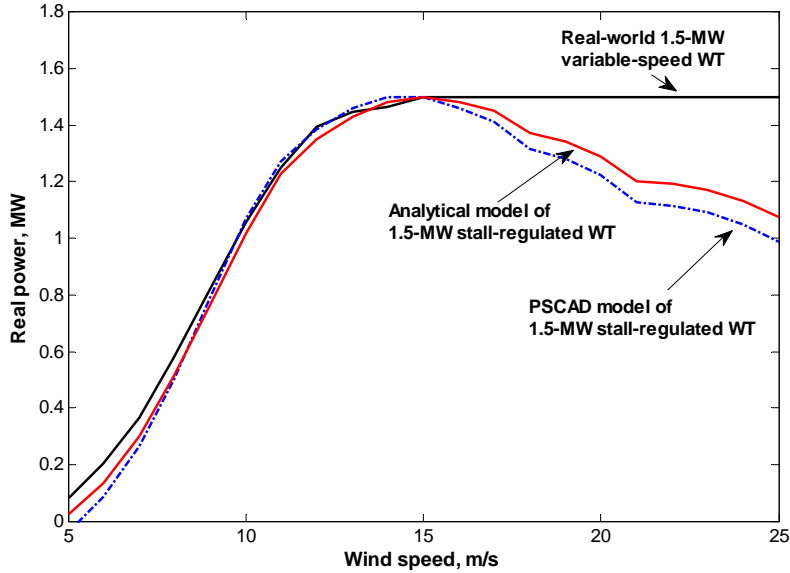


Fig. 2.10 Power curve by analytical calculation and PSCAD simulation

Figure 2.10 shows that the analytical result and the simulated result by PSCAD are comparable. The power output pattern of the analytical model is also very close to the output pattern of the real-world variable-speed wind turbine, up to the rated wind speed. The analytical wind turbine model starts producing power at 5 m/s, like the real-world wind turbine. The PSCAD model starts producing power at 6 m/s. Both analytical and PSCAD models produce 1.5 MW at the rated wind speed of 15 m/s. To produce the rated real power, the analytical wind turbine consumes 0.6052 MVAR of reactive power while the PSCAD wind turbine consumes 0.605 MVAR.

For wind speeds above 15 m/s, the analytical wind turbine behaves differently from the 1.5-MW variable-speed wind turbine. This is expected since the pitch angle of the wind turbine blades is fixed and the turbine produces less power when its rotor enters an aerodynamic-stall region. This is a correct behavior of a fixed-speed wind turbine.

The difference between the power curves of the analytical and PSCAD models are deemed due to difference in  $C_p$  calculation. The actual  $C_p$  is reproduced accurately for the analytical model using piece-wise linear interpolation. PSCAD [29] estimates  $C_p$  using certain interpolation technique which appears to be less accurate.

### 2.3.3.2 Torque, speed and power characteristics

The dynamic behavior of the analytical wind turbine model is validated by observing its torque, speed and power output variation characteristics for 20 seconds. All the considered quantities, shown in Fig. 2.11, 2.12 and 2.13, are calculated for the rated wind speed of 15 m/s. The respective results by PSCAD are shown along for comparison.

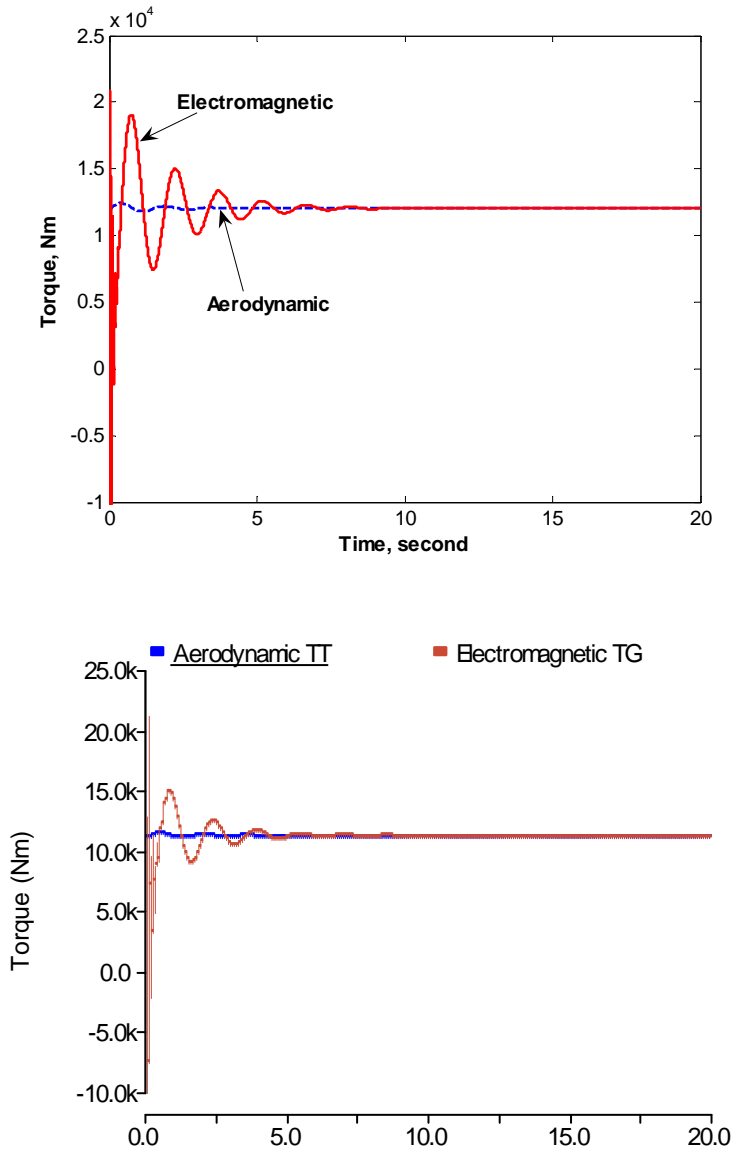


Fig. 2.11 Torque variation – analytical (upper) and PSCAD (lower)

From Fig. 2.11, the analytical result (upper figure) shows that the electromagnetic torque varies greatly for the first few seconds, then subsides and finally matches the aerodynamic torque,

whose oscillation is milder. This is a correct behavior as the two torques must match for the whole system to reach the steady state. The aerodynamic torque is relatively steady because the wind speed remains unchanged at 15 m/s for the entire calculation period (i.e. 20 seconds).

In this case the aerodynamic torque variation depends only on the ratio between the power coefficient  $C_p$  and the wind rotor speed (see equation 2.5). The power coefficient  $C_p$  increases when the wind rotor speed increases (left half of the  $C_p$ -curve, Fig. 2.4), so the relative change in the ratio is low. The PSCAD result (lower figure) has a similar trend but the degree of oscillation is lesser. Both models take around 10 seconds to reach the steady state.

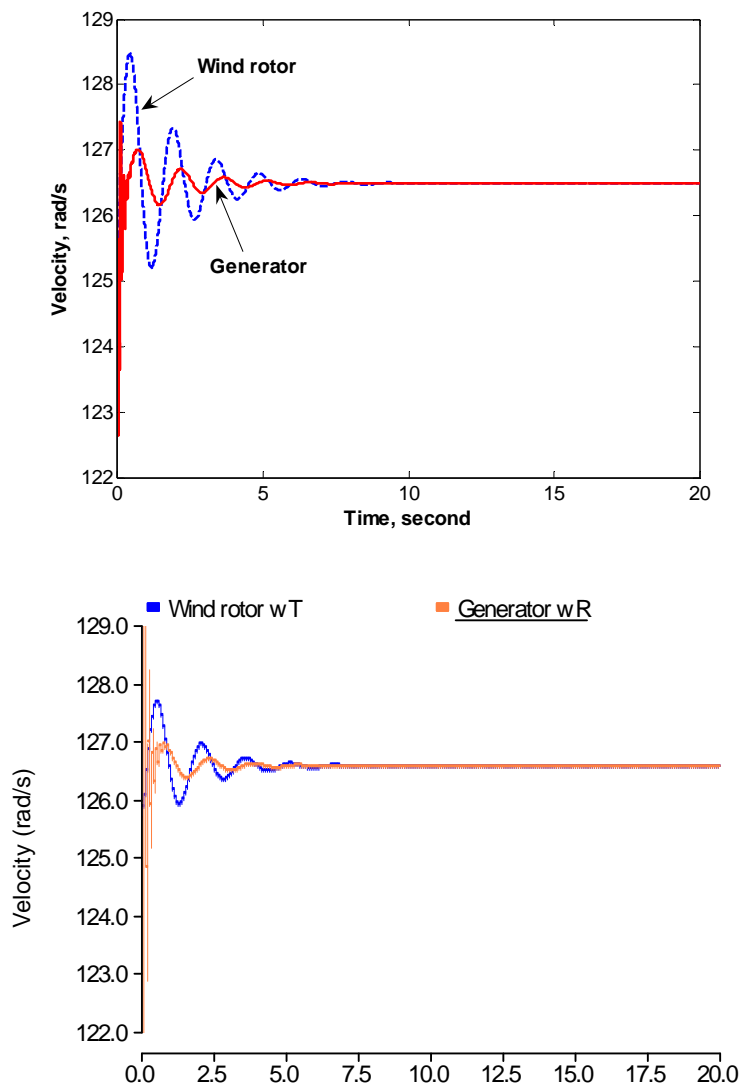


Fig. 2.12 Angular speed variation—analytical (upper) and PSCAD (lower)

Inspecting the angular speed variation for the analytical model (upper figure, Fig. 2.12), it is seen that the wind rotor speed oscillates at a greater degree than the generator rotor. This is because the wind rotor is far larger (and thus has larger moment of inertia) than the generator rotor. After around 10 seconds, the two speeds match. The same trend is shown for the PSCAD model (lower figure), again with a lesser degree of oscillation. The slip at the rated power output is -0.66% for the analytical model and -0.71% for the PSCAD model. The analytical model slip is a better match for the generator specified slip (-0.67%).

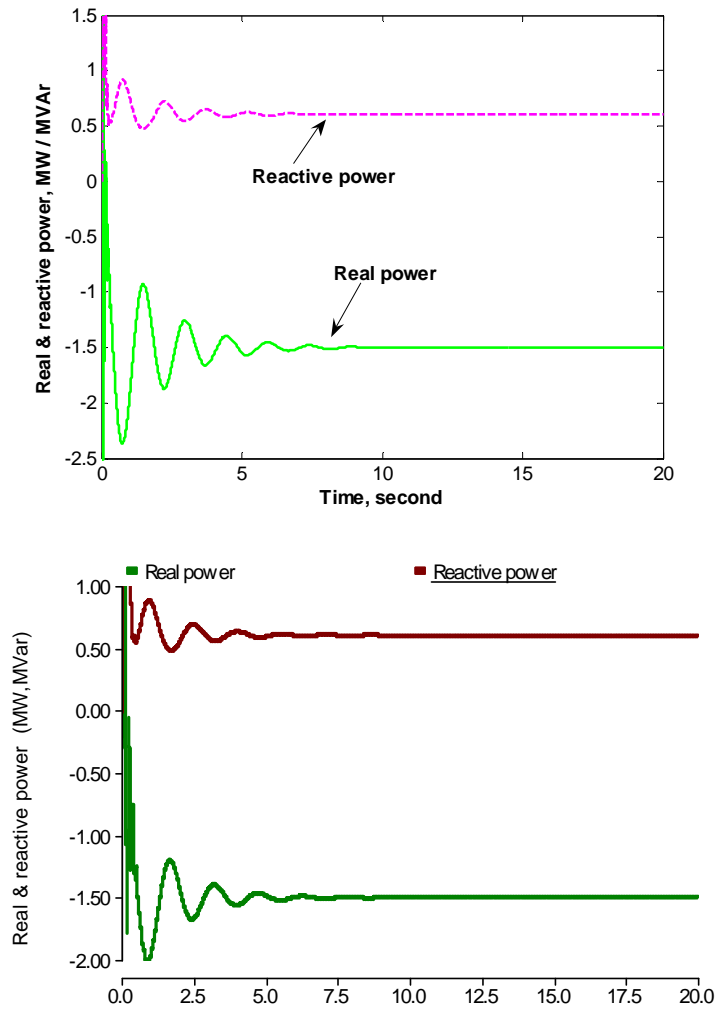


Fig. 2.13 Real and reactive power output – analytical (upper) and PSCAD (lower)

The power output profiles for the analytical and PSCAD models (upper and lower figures, Fig. 2.13) match each other well. Both models produce 1.5 MW of real power at the rated

wind speed and consume around 0.605 of reactive power. Both models output the rated power at the power factor of 0.9274. Again, the degree of oscillation for real power of the PSCAD model is lower than that of the analytical model. Since PSCAD does not provide sufficient details of its induction generator modeling and its integration method implementation, it is difficult to explain the differences.

### ***2.3.3.3 Transient stability performance of wind turbine model under a three-phase fault at the terminals***

**Scenario:** The wind turbine is connected to an infinite bus as shown in Fig. 2.9. This is a conventional connection scheme for transient stability studies [11]. The wind turbine is operated at the rated wind speed of 15 m/s. The wind speed is kept constant for the entire observed duration of 45 seconds. While the wind turbine is in the steady state at  $t = 12$  seconds, a balanced 3-phase fault with zero-impedance (i.e. bolted fault) is applied at the wind turbine bus  $WI$  (i.e. the induction generator terminals) and the wind turbines equations are solved. An iterative technique is used to find the critical clearing time  $t_c$ . The fault duration  $t_f$  is gradually increased from a few milliseconds to a certain value. For each  $t_f$ , the induction generator rotor speed is inspected to see if the machine speed returns to the steady state or is increasing towards some dangerous levels (runaway speed). The iterative technique is computationally intensive but can give very accurate results since it inspects all possible fault durations. For comparison, the same stall-regulated wind turbine model implemented in PSCAD is also run to find the respective  $t_c$ .

#### ***Results***

The obtained critical clearing time  $t_c$  are:

- Analytical model: 2.2484 seconds
- PSCAD model: 2.2495 seconds

The critical clearing time for the analytical model is less than that of the PSCAD model by 0.05%. The speed profiles of the two models for critical and runaway times are shown in Fig. 2.14 and 2.15.

It can be observed from Fig. 2.14 that both the wind rotor and the generator rotor start to accelerate at the instant the fault is applied (i.e. at  $t = 12$  seconds). At  $t = 14.2484$  seconds (i.e.  $12+t_c$  for analytical model), the fault is cleared, the speeds gradually reduce and finally return to the steady-state values about 30 seconds later (i.e. at  $t \sim 45$  seconds).

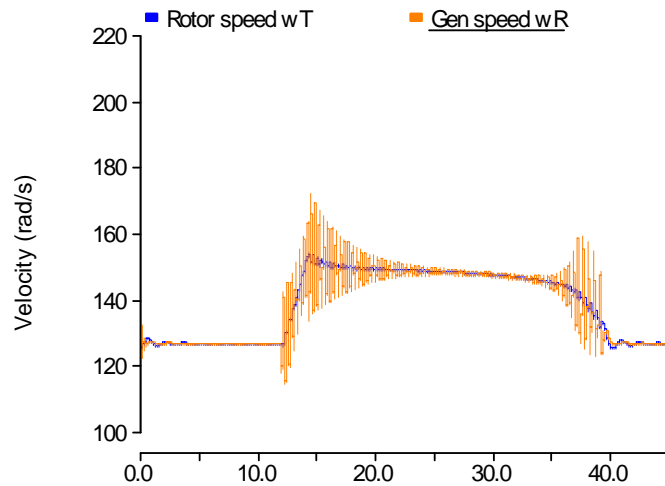
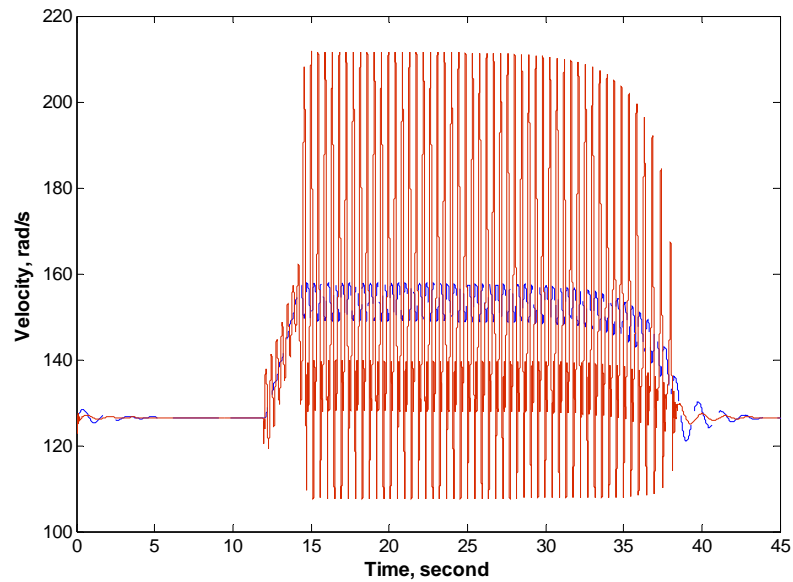


Fig. 2.14 Critical speed for analytical model (upper) and PSCAD (lower)

**Note:**  $t_c = 2.2484$  seconds for analytical model and  $t_c = 2.2495$  seconds for PSCAD model

The explanation is as follows. Since this is a bolted fault, the instantaneous voltages at the generator terminals immediately reduce to zero. As the consequence, the electromagnetic torque collapses and there is no opposing torque to balance the aerodynamic torque. The collapse of the electromagnetic torque also releases the potential energy stored in the wind turbine shaft (the shaft is twisted under the two opposing torques in steady state). These events cause the wind rotor and the generator rotor to accelerate. The wind rotor and the generator rotor accelerate with

different rates because their moments of inertia differ. Because of this and the shaft limited stiffness, both the wind rotor and the generator rotor swing [42, 51].

When the fault is cleared, the electromagnetic torque re-establishes and the machine decelerates. From power transfer viewpoint, the collapse of the terminal voltages prohibits the power transfer from the wind turbine to the grid. The trapped electric energy inside the machine releases itself primarily in the form of kinetic energy, so the machine accelerates. To decelerate the machine, the power transfer must be established in time before stability limit is reached. The discussion shows that the analytical wind turbine model behaves correctly under the fault condition.

Figure 2.14 (lower) shows that the speed oscillation of the PSCAD model is milder than that of the analytical model. This agrees with the results on the torque and speed characteristics under fault-free condition (Section 2.3.3.2). Though, the analytical and the PSCAD models have a similar critical clearing time. Both models take around 30 seconds to stabilize after the fault is cleared. Therefore, in terms of critical clearing time and stabilization duration, the two models are comparable. The analytical model appears to be more sensitive in capturing the transients. As said before, it is difficult to explain the differences because PSCAD does not provide sufficient details of its induction generator modeling and its integration method implementation.

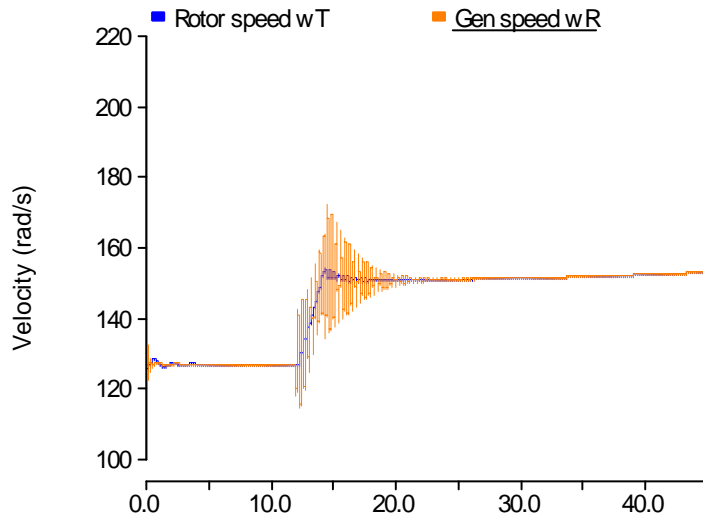
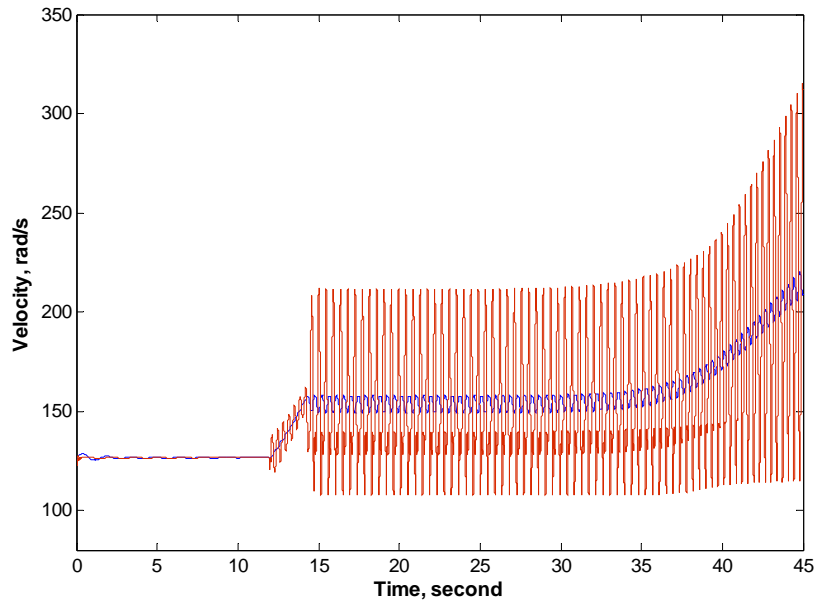


Fig. 2.15 Runaway speed for analytical model (upper) and PSCAD (lower)

**Note:**  $t_f = 2.2485$  seconds for analytical model and  $t_f = 2.25$  seconds for PSCAD model

Figure 2.15 shows that the wind turbine fails to stabilize itself as the fault duration exceeds the critical clearing time. In this case, the trapped power inside the machine appears to surpass the stability limit. After the terminal voltages recover and the power transfer re-establishes, the accumulated energy cannot be dissipated before the machine stability is lost.

## 2.4 DEVELOPMENT OF WIND FARM MODEL

A wind farm model can be developed based on the assumption that all wind turbines in the aggregate are identical and there is no dynamic interaction among them. In addition, all wind turbines are assumed to encounter the same wind speed profile so each wind turbine possesses an identical power output pattern. Two wind farm models are built as follows.

### *a) Detailed wind farm model*

With this approach, the wind farm model consists of individual wind turbines, which are connected individually to the wind farm collector bus. For the purpose of studying dynamic interaction between wind turbines, the wind source should be modelled uniquely for each wind turbine. However, the simulation time can be substantially long, especially when the wind farm consists of many small wind turbines. For this section study, a 15-MW wind farm is constructed from ten 1.5-MW wind turbines in which each turbine is represented individually. For comparison purpose, each wind turbine is exposed to the same wind-speed profile as in aggregated wind farm model in b) below.

### *b) Aggregate wind farm model*

In this approach, a wind farm is aggregated in the following manner. The wind farm is represented as a single aerodynamic and mechanical block with  $n$  number of identical induction machines. For a 15-MW wind farm, there will be one aerodynamic and mechanical block rated at 1.5-MW mechanical power with ten identical 1.5-MW induction machines. Using this approach, all wind turbines encounter the same wind source and all induction generators see the same aerodynamic torque. This approach does not allow dynamic interaction between wind turbines but it is deemed valid for most power system studies.

The above two models are implemented in PSCAD. The two wind farms models are connected based on the scheme shown in Fig. 2.9. The difference is that the grid has the short-circuit capacity of 300 MVA and the transformer is 20 MVA, 0.69kV $\Delta$ /Y34.5kV with a leakage reactance of 10%. The grid is considered sufficiently strong for hosting a 15-MW wind farm.

The power curves of the two 15-MW wind farm models are shown in Fig. 2.16.

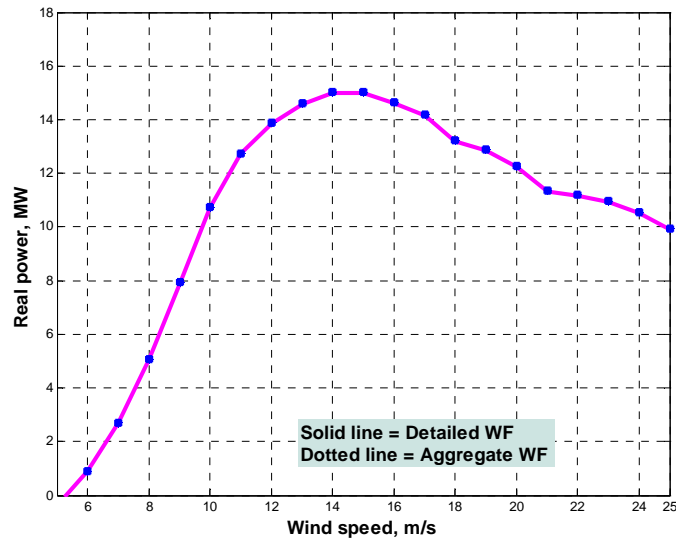


Fig. 2.16. Power curve of two 15-MW wind farm models

It is clearly observed that the power output profile of the aggregate wind farm model follows the power output profile of the detailed wind farm model very closely. There is insignificant difference in the power outputs of the two wind farm models. This means that, in terms of power output, the aggregate model can be used as a convenient equivalent replacement of the detailed model.

In a practical wind farm, wind turbines may experience different wind speed patterns at any time instant. In such a case, the wind farm can be divided into several groups of wind turbines of similar wind patterns and an aggregate wind farm model can be used to represent each group. Measured wind farm power output data can be used for studies that involve only wind farm power production (e.g. an optimal generation dispatch study).

## 2.5 CHAPTER CONCLUDING REMARKS

In this chapter, a detailed model for stall-regulated wind turbine is developed and validated. The model is verified using key characteristics, namely, power output, torque, speed, and transient stability performance under a 3-phase fault. The results show that the model behaves correctly. The model can be expanded or modified to represent other types of wind turbines, such as variable-speed pitch-controlled or DFIG. A wind farm model is also developed. The wind turbine model and the aggregate wind farm model will be used in subsequent studies for achieving the defined research objectives.

## Chapter 3

### **Analysis of voltage stability, optimal wind power penetration limits and benefit of energy storage systems**

#### **3.1 INTRODUCTION**

This chapter presents a pilot study to analyze and validate the proposed solution method of using energy storage systems (ESS) for solving the wind-farm related problems (see Section 1.1.2 for analysis). With reference to the research objectives and approach (Sections 1.2 and 1.3), the main goals of this study are as follows.

- (i) To establish criteria for analyzing voltage stability.
- (ii) To determine the critical wind power penetration levels based on voltage stability condition.
- (iii) To investigate possible benefits of ESS with respect to voltage stability and wind power penetration level.

Selection of voltage stability criteria is important for accurate evaluation of a power system stability condition. In this work, V-Q sensitivity, reactive reserve margin (or Q-reserve margin) and eigenvalue analysis are utilized since they are the most well-established voltage stability methods [11]. A small 6-bus power system is used to demonstrate the applicability of these criteria. Three case studies are carried out using Neplan [31], an off-the-shelf simulation package. An analytical calculation is done (with the aid of Matlab [30]) to demonstrate the selected voltage stability solution methods and validate the software results.

As shown in Case study 1, the 6-bus system voltage stability condition can be assessed accurately using the aforementioned methods. The results also show that the Q-reserve margin technique and the eigenvalue analysis can be used interchangeably. The method of eigenvalue analysis offers more advantages because it gives a system-wide view of stability condition. This technique will be used in subsequent analyses in Chapter 4 and 5.

Case study 2 shows that critical wind power penetration levels can be determined using voltage stability indicators. For example, the optimal wind power penetration level is the maximum amount of wind power that can be integrated into the system without reducing the

original stability level. The maximum wind power penetration level is the amount which the system can accept without pushing itself to the edge of voltage collapse.

Case study 3 implements a simplified solution of using an ESS to facilitate wind power integration and ensure the system voltage stability. The results show that the ESS-based solution is effective. The ESS helps maintain a steady power flow to the grid during considered 8-hour period. It also minimizes the wind farm impacts on the system voltage stability.

This pilot study offers significant benefits to subsequent research. First, it establishes a procedure for evaluating grid steady-state voltage stability condition (i.e. using either Q-margins or eigenvalues). Second, it demonstrates a technique for estimating critical wind power integration levels (using voltage stability indicators). Finally, it proves that the proposed ESS-based solution method for solving the wind-power-related problems is efficient. This forms a basis for implementing the method in a realistic and practical manner.

**Publication:** The work reported in this chapter has been published in the proceeding of *IEEE Power Engineering Society General Meeting 2007* with the title "Analysis of Voltage Stability and Optimal Wind Power Penetration Limits for a Non-radial Network with an Energy Storage System" [34].

## 3.2 ANALYTICAL VOLTAGE STABILITY SOLUTION AND SOFTWARE VALIDATION

### 3.2.1 Description of a 6-bus power system and wind farm

The 6-bus power system (Fig. 3.1) is a system derived from the large 27-bus regional grid of a large power utility (Section 1.3 and Appendix A3). It is strong network with two generators that supply power to the loads through three 138-kV lines. The total line length is 125 km and total load is 203.7 MW and 82.1 MVAR (219.6 MVA). The total generation capacity is 270 MVA. The difference between the total generation and total load (i.e. the spinning reserve) is 18.7%. Generator *Swing1* represents a stiff supply grid with the sending end voltage ( $V_s$ ) maintained at  $1.0\angle 0^\circ$  pu. The operational real power output of generator *Gen6* is 43 MW and the reactive power limits are +/-25 MVAR. The operational voltage at Bus 6 is set to be 1.0 pu. No transformer tap is set to raise the secondary-side voltages. The 6-bus power system hosts a large 140-MW wind farm which is connected to Bus 5.

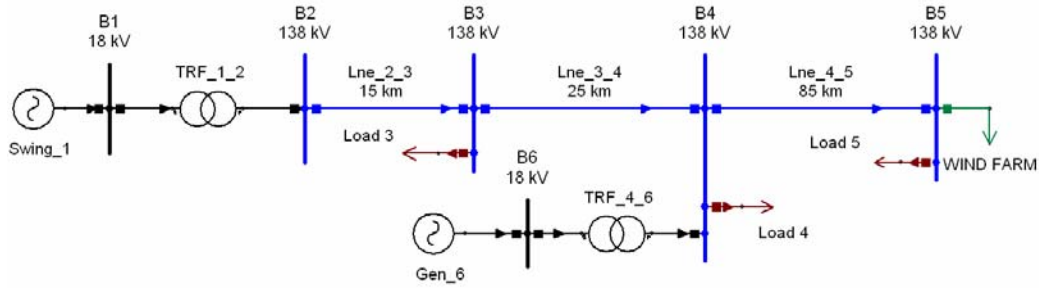


Fig. 3.1 Schematic diagram of the 6-bus power system with 140-MW wind farm

### 6-bus power system data

Generator <i>Swing1</i> :	220 MVA, 18 kV, $R=0.0008713 \Omega$ , $X_d=2$ pu
Generator <i>Gen6</i> :	50 MVA, 18 kV, $R=0.000052 \Omega$ , $X_d=2$ pu
Transformer <i>TRF12</i> :	300 MVA, 18 kV/138 kV, GY-GY, $R=0.154\%$ , $X=6.0304\%$
Transformer <i>TRF46</i> :	55 MVA, 18 kV/138 kV, GY-GY, $R=0.3\%$ , $X=10.05\%$
Line 23:	15 km, $R=0.0409132 \Omega/\text{km}$ , $X=0.375125 \Omega/\text{km}$ , $B=4.43$ microS/km
Line 34:	25 km, $R=0.0409132 \Omega/\text{km}$ , $X=0.375125 \Omega/\text{km}$ , $B=4.43$ microS/km
Line 45:	85 km, $R=0.135343 \Omega/\text{km}$ , $X=0.483124 \Omega/\text{km}$ , $B=3.425$ microS/km
Load 3:	$153.5 + j63.9$ MVA, PF= 0.923 lagging
Load 4:	$41.3 + j15.5$ MVA, PF = 0.936 lagging
Load 5:	$8.9 + j2.7$ MVA, PF = 0.957 lagging
Wind farm:	140 MW, PF=1.0

The system major load (Load 3) is connected to the main power source (i.e. *Swing1*) via a short and strong line (Line 23) which has small impedance. Load 4 is located near *Gen6* which feeds it. Load 5 is connected at the same bus as the wind farm and is fed through a relatively-weak and long line. This line has significantly higher impedance with the length more than twice that of Line 23 and Line 34 combined. The wind farm name plate rating is 140 MW. When the wind farm is offline, the system is in normal peak-load operation condition with the voltage profile within  $\pm 5\%$  limits (within the range of 95%–105% of the nominal values). This system condition is named Base case 1 and used as base for comparison.

As wind power output is of major interest in this study, the wind farm is modeled as a negative load with a real power output profile. The rationale for this modeling technique of wind farm is as follows. As explained in Section 1.1.2, small-disturbance (or steady-state) voltage stability is concerned with a system ability to control voltages following small disturbances, such as gradual changes in load. This type of voltage stability can be examined using steady-state techniques where the system dynamic equations are linearized at a given operating point [11]. As the result, solving the system differential equations is not required. Instead, only sets of algebraic equations need to be solved (see Equation 3.3 below). It is visible from (3.3) that, for power flow and steady-state voltage stability calculation, only step changes in power injection or absorption

is required. A wind farm injects real power into a power system and absorbs reactive power. Its output is intermittent depending on the availability of wind. Therefore, from power-flow viewpoint, it is like a power source that consumes reactive power but produces real power. In practice, wind farms are typically operated at unity power factor. Capacitor banks are usually installed to supply 100% of the farms reactive power demand in steady-state condition. Hence, for steady-state calculation, it suffices to model a wind farm as a power source that injects only real power into the grid and absorbs no reactive power. Neplan and many simulation software model such a power source as a negative load for power flow calculation. Note that the wind farm model developed in Chapter 2 includes all wind turbine dynamics and is more suitable for dynamic simulation, such as the analysis in Chapter 6. For a previous analysis that utilizes negative loads for modeling wind farms, see [52]. The real power output profile for the 140-MW wind farm is shown in Table 3.1.

Table 3.1 Wind farm real power output profile

<b>Variant</b>	1	2	3	4	5	6	7	8	9	10	11	12	13	14
<b>WF P, MW</b>	5	10	15	20	25	30	35	40	45	50	55	60	65	70
<b>Variant</b>	15	16	17	18	19	20	21	22	23	24	25	26	27	28
<b>WF P, MW</b>	75	80	85	90	95	100	105	110	115	120	125	130	135	140

### 3.2.2 Criteria for evaluating system voltage stability condition

A combination of three voltage stability techniques, namely, V-Q curve, V-Q sensitivity, and V-Q modal analysis are used for evaluating voltage stability condition. These are popular techniques for evaluating power system small-disturbance voltage stability [11]. See Section 1.1.2 for more details of voltage stability classification.

The 6-bus system voltage stability condition is evaluated using two main criteria: reactive reserve margin and smallest eigenvalues. The reactive reserve margin, or Q-reserve margin, is the VAR-distance measured from the point on the V-Q curve of interest where  $\partial V/\partial Q=0$  to the zero-Q line [11]. The Q-reserve margin chosen to represent the reactive power condition of the system is the margin calculated at the weakest bus. To determine the weakest bus, a V-Q sensitivity simulation is performed on the 6-bus power system under the condition of Base case 1. Bus 5 exhibits the largest V-Q sensitivity, indicating that it is most sensitive to any changes in reactive power (either injection or absorption) in the system. Therefore, it is chosen as the indicator of the system reactive power reserve condition. For this 6-bus system, there are four eigenvalues in total. They are calculated following V-Q modal technique and are used in parallel with the Q-reserve margin to judge the system stability condition.

To validate Neplan-based voltage stability results, first the V-Q self sensitivity for buses 2, 3, 4, 5 and the eigenvalues of the system are calculated using V-Q sensitivity and modal techniques. The code for this analytical calculation is written in Matlab. Then, the obtained analytical results are compared with those obtained by running voltage stability simulation using Neplan. The solution for the 6-bus system without the wind farm is Base case 1. The wind farm has 28 power output levels (Table 3.1) so there are 29 solutions sets to be solved for, including the base case.

### 3.2.3 Calculation of system V-Q self sensitivity and eigenvalues

The system V-Q self sensitivity and eigenvalues are calculated based on the theory in [53] and [11]. For brevity, only key equations are shown.

The 6-bus power system impedances are computed and converted to admittances with reference to the common base of 100 MVA. The lines are represented using  $\pi$ -model. Fig. 3.2 shows the equivalent circuit representation of the system with the common-base admittances in per unit.

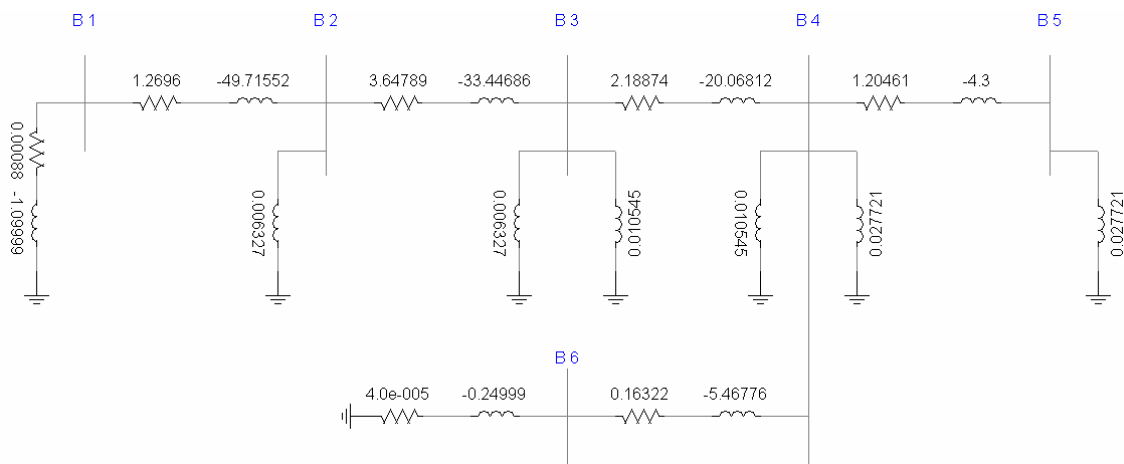


Fig. 3.2 Equivalent circuit representation of the 6-bus power system

Based on the circuit in Fig. 3.2, the network node admittance matrix  $Y_N$  (in per unit) of the system is given by

$$Y_N = \begin{bmatrix} 1.2696 - 49.7155i & -1.2696 + 49.7155i & 0 & 0 & 0 & 0 & 0 \\ -1.2696 + 49.7155i & 4.9175 - 83.1561i & -3.6479 + 33.4469i & 0 & 0 & 0 & 0 \\ 0 & -3.6479 + 33.4469i & 5.8366 - 53.4981i & -2.1887 + 20.0681i & 0 & 0 & 0 \\ 0 & 0 & -2.1887 + 20.0681i & 3.5566 - 29.7976i & -1.2046 + 4.3000i & -0.1632 + 5.4678i & 0 \\ 0 & 0 & 0 & -1.2046 + 4.3000i & 1.2046 - 4.2723i & 0 & 0 \\ 0 & 0 & 0 & -0.1632 + 5.4678i & 0 & 0 & 0.1632 - 5.4678i \end{bmatrix}$$

Generator admittances are not included in  $Y_N$  because it is assumed that the point of constant voltage is before the machine synchronous reactances. This is equivalent to assuming that the voltage magnitudes at bus  $B_1$  and  $B_6$  ( $V_1$  and  $V_6$ ) are 1.0 pu for all situations. Although this may not always hold true, the admittances of the generators are much smaller than those of the transformers (i.e.  $TRF12$  and  $TRF46$ ) so the exclusion of the admittances would not affect the accuracy of  $Y_N$  and the power flow results significantly [53].

With  $n$  being the number of the system buses, the power equations are given by the following formulae [53]

$$P_i = \sum_{j=1}^n V_i V_j Y_{ij} \cos(\theta_{ij} - \delta_i + \delta_j) \quad (3.1)$$

$$Q_i = -\sum_{j=1}^n V_i V_j Y_{ij} \sin(\theta_{ij} - \delta_i + \delta_j) \quad (3.2)$$

where

$P_i, Q_i$  = real and reactive power for bus  $i$ ;

$V_i, V_j$  = bus voltage magnitudes;

$\delta_i, \delta_j$  = bus voltage angles;

$Y_{ij}, \theta_{ij}$  = magnitude and angle of an element of the admittance matrix  $Y_N$ .

Based on (3.1) and (3.2), the expressions of  $P$  and  $Q$  for the buses 2, 3, 4 and 5 can now be written. For the PV-bus  $B_6$ , only the real power and the magnitude of  $V_6$  are available so there is an expression for  $P_6$  but no expression for  $Q_6$ . It is also noted that many elements of  $Y_N$  are zeros so the corresponding terms in  $P_i$  or  $Q_i$  can be eliminated. With reference to  $Y_N$ , the final power equations are:

$$\begin{aligned}
P_2 &= V_2 V_1 Y_{21} \cos(\theta_{21} - \delta_2 + \delta_1) + V_2^2 Y_{22} \cos \theta_{22} + V_2 V_3 Y_{23} \cos(\theta_{23} - \delta_2 + \delta_3) \\
P_3 &= V_3 V_2 Y_{32} \cos(\theta_{32} - \delta_3 + \delta_2) + V_3^2 Y_{33} \cos \theta_{33} + V_3 V_4 Y_{34} \cos(\theta_{34} - \delta_3 + \delta_4) \\
P_4 &= V_4 V_3 Y_{43} \cos(\theta_{43} - \delta_4 + \delta_3) + V_4^2 Y_{44} \cos \theta_{44} + V_4 V_5 Y_{45} \cos(\theta_{45} - \delta_4 + \delta_5) \\
&\quad + V_4 V_6 Y_{46} \cos(\theta_{46} - \delta_4 + \delta_6) \\
P_5 &= V_5 V_4 Y_{54} \cos(\theta_{54} - \delta_5 + \delta_4) + V_5^2 Y_{55} \cos \theta_{55} \\
P_6 &= V_6 V_4 Y_{64} \cos(\theta_{64} - \delta_6 + \delta_4) + V_6^2 Y_{66} \cos \theta_{66} \\
Q_2 &= -V_2 V_1 Y_{21} \sin(\theta_{21} - \delta_2 + \delta_1) - V_2^2 Y_{22} \sin \theta_{22} - V_2 V_3 Y_{23} \sin(\theta_{23} - \delta_2 + \delta_3) \\
Q_3 &= -V_3 V_2 Y_{32} \sin(\theta_{32} - \delta_3 + \delta_2) - V_3^2 Y_{33} \sin \theta_{33} - V_3 V_4 Y_{34} \sin(\theta_{34} - \delta_3 + \delta_4) \\
Q_4 &= -V_4 V_3 Y_{43} \sin(\theta_{43} - \delta_4 + \delta_3) - V_4^2 Y_{44} \sin \theta_{44} - V_4 V_5 Y_{45} \sin(\theta_{45} - \delta_4 + \delta_5) \\
&\quad - V_4 V_6 Y_{46} \sin(\theta_{46} - \delta_4 + \delta_6) \\
Q_5 &= -V_5 V_4 Y_{54} \sin(\theta_{54} - \delta_5 + \delta_4) - V_5^2 Y_{55} \sin \theta_{55}
\end{aligned}$$

Next, the expression for the Jacobian matrix is determined. The Jacobian matrix [11] (the first matrix on the right-hand side of 3.3) represents the sensitivity between power flow and bus voltage changes. The elements of the Jacobian matrix are found by taking the partial derivative of the above  $P_i$  and  $Q_i$  expressions with respect to  $V_i$  and  $\delta_i$ .

$$\begin{bmatrix} \Delta P \\ \Delta Q \end{bmatrix} = \begin{bmatrix} J_{P\delta} & J_{PV} \\ J_{Q\delta} & J_{QV} \end{bmatrix} \begin{bmatrix} \Delta \delta \\ \Delta V \end{bmatrix} \quad (3.3)$$

where

$\Delta P$  = incremental change in bus real power;

$\Delta Q$  = incremental change in bus reactive power;

$\Delta \delta$  = incremental change in bus voltage angle;

$\Delta V$  = incremental change in bus voltage magnitude.

The elements of  $J_{P\delta}$  are:

$$\begin{aligned}
j_{11} &= \frac{\partial P_2}{\partial \delta_2} = V_2 V_1 Y_{21} \sin(\theta_{21} - \delta_2 + \delta_1) + V_2 V_3 Y_{23} \sin(\theta_{23} - \delta_2 + \delta_3) \\
j_{12} &= \frac{\partial P_2}{\partial \delta_3} = -V_2 V_3 Y_{23} \sin(\theta_{23} - \delta_2 + \delta_3) \\
j_{13} &= \frac{\partial P_2}{\partial \delta_4} = 0; \quad j_{14} = \frac{\partial P_2}{\partial \delta_5} = 0; \quad j_{15} = \frac{\partial P_2}{\partial \delta_6} = 0; \\
j_{21} &= \frac{\partial P_3}{\partial \delta_2} = -V_3 V_2 Y_{32} \sin(\theta_{32} - \delta_3 + \delta_2) \\
j_{22} &= \frac{\partial P_3}{\partial \delta_3} = V_3 V_2 Y_{32} \sin(\theta_{32} - \delta_3 + \delta_2) + V_3 V_4 Y_{34} \sin(\theta_{34} - \delta_3 + \delta_4) \\
j_{23} &= \frac{\partial P_3}{\partial \delta_4} = -V_3 V_4 Y_{34} \sin(\theta_{34} - \delta_3 + \delta_4) \\
j_{24} &= \frac{\partial P_3}{\partial \delta_5} = 0; \quad j_{25} = \frac{\partial P_3}{\partial \delta_6} = 0; \\
j_{31} &= \frac{\partial P_4}{\partial \delta_2} = 0; \quad j_{32} = \frac{\partial P_4}{\partial \delta_3} = -V_4 V_3 Y_{43} \sin(\theta_{43} - \delta_4 + \delta_3) \\
j_{33} &= \frac{\partial P_4}{\partial \delta_4} = V_4 V_3 Y_{43} \sin(\theta_{43} - \delta_4 + \delta_3) + V_4 V_5 Y_{45} \sin(\theta_{45} - \delta_4 + \delta_5) \\
&\quad + V_4 V_6 Y_{46} \sin(\theta_{46} - \delta_4 + \delta_6) \\
j_{34} &= \frac{\partial P_4}{\partial \delta_5} = -V_4 V_5 Y_{45} \sin(\theta_{45} - \delta_4 + \delta_5) \\
j_{35} &= \frac{\partial P_4}{\partial \delta_6} = -V_4 V_6 Y_{46} \sin(\theta_{46} - \delta_4 + \delta_6) \\
j_{41} &= \frac{\partial P_5}{\partial \delta_2} = 0; \quad j_{42} = \frac{\partial P_5}{\partial \delta_3} = 0; \\
j_{43} &= \frac{\partial P_5}{\partial \delta_4} = -V_5 V_4 Y_{54} \sin(\theta_{54} - \delta_5 + \delta_4) \\
j_{44} &= \frac{\partial P_5}{\partial \delta_5} = V_5 V_4 Y_{54} \sin(\theta_{54} - \delta_5 + \delta_4); \quad j_{45} = \frac{\partial P_5}{\partial \delta_6} = 0; \\
j_{51} &= \frac{\partial P_6}{\partial \delta_2} = 0; \quad j_{52} = \frac{\partial P_6}{\partial \delta_3} = 0; \\
j_{53} &= \frac{\partial P_6}{\partial \delta_4} = -V_6 V_4 Y_{64} \sin(\theta_{64} - \delta_6 + \delta_4) \\
j_{54} &= \frac{\partial P_6}{\partial \delta_5} = 0; \\
j_{55} &= \frac{\partial P_6}{\partial \delta_6} = V_6 V_4 Y_{64} \sin(\theta_{64} - \delta_6 + \delta_4)
\end{aligned}$$

The elements of  $J_{PV}$ ,  $J_{Q\delta}$ , and  $J_{QV}$  are calculated in the similar manner. Since there is no expression for  $Q_6$  and  $V_6$  magnitude is assumed to be constant all the time, the corresponding

terms in  $J_{PV}$ ,  $J_{Q\delta}$ , and  $J_{QV}$  are absent. As the result, the sizes of  $J_{PV}$ ,  $J_{Q\delta}$ , and  $J_{QV}$  are 5 by 4, 4 by 5, and 4 by 4, respectively. For brevity, the expressions are not presented here.

For the base-case network, the bus voltage magnitudes and angles, found by solving the power flow equations using Newton-Raphson technique [53], are as following:

$$\begin{aligned} V_1 &= 1.0 \text{ pu}, & \delta_1 &= 0 \text{ deg} \\ V_2 &= 0.985 \text{ pu}, & \delta_2 &= -1.873 \text{ deg} \\ V_3 &= 0.961 \text{ pu}, & \delta_3 &= -4.640 \text{ deg} \\ V_4 &= 0.963 \text{ pu}, & \delta_4 &= -4.880 \text{ deg} \\ V_5 &= 0.956 \text{ pu}, & \delta_5 &= -6.068 \text{ deg} \\ V_6 &= 1.0 \text{ pu}, & \delta_6 &= -0.265 \text{ deg} \end{aligned}$$

The elements of the Jacobian matrix corresponding to the power flow solution of Base case 1 are:

$$J_{P\delta} = \begin{bmatrix} 80.6825 & -31.7791 & 0 & 0 & 0 \\ -31.4459 & 50.0100 & -18.5641 & 0 & 0 \\ 0 & -18.5471 & 27.7604 & -3.9801 & -5.2331 \\ 0 & 0 & -3.9341 & 3.9341 & 0 \\ 0 & 0 & -5.2584 & 0 & 5.2584 \end{bmatrix}$$

$$J_{PV} = \begin{bmatrix} 4.8438 & -1.9990 & 0 & 0 \\ -5.0510 & 4.0091 & -2.0219 & 0 \\ 0 & -2.1876 & 2.9941 & -1.0734 \\ 0 & 0 & -1.2370 & 1.0589 \\ 0 & 0 & 0.2772 & 0 \end{bmatrix}$$

$$J_{Q\delta} = \begin{bmatrix} 4.7712 & 1.9204 & 0 & 0 & 0 \\ 4.9753 & -6.9214 & 1.9461 & 0 & 0 \\ 0 & 2.1015 & -3.7079 & 1.0265 & 0.5800 \\ 0 & 0 & 1.1907 & -1.1907 & 0 \end{bmatrix}$$

$$J_{QV} = \begin{bmatrix} 81.9100 & -33.0807 & 0 & 0 \\ -31.9243 & 50.7279 & -19.2871 & 0 \\ 0 & -19.3068 & 28.5195 & -4.1620 \\ 0 & 0 & -4.0874 & 4.0574 \end{bmatrix}$$

The elements of the Jacobian matrix can also be verified using the partial-derivative expressions for  $J_{P\delta}$  (shown above),  $J_{PV}$ ,  $J_{Q\delta}$ , and  $J_{QV}$  (not shown). Substituting the final values of  $V_1$  through  $V_6$  and  $\delta_1$  through  $\delta_6$  (i.e. the base-case power flow solution) into the expressions gives

the same  $J_{P\delta}$ ,  $J_{PV}$ ,  $J_{Q\delta}$ , and  $J_{QV}$  as shown above. This helps further verify the accuracy of the power flow solution. Since the substitution is simple, it is left as an exercise for interested readers.

Recall that the sub-matrices of the Jacobian matrix are given in (3.3) as

$$J = \begin{bmatrix} J_{P\delta} & J_{PV} \\ J_{Q\delta} & J_{QV} \end{bmatrix}$$

The reduced Jacobian matrix  $J_R$  is calculated using (3.4) [11]

$$J_R = [J_{QV} - J_{Q\delta} J_{P\delta}^{-1} J_{PV}] \quad (3.4)$$

$$J_R = \begin{bmatrix} 82.2032 & -33.2011 & 0.0000 & 0.0000 \\ -32.7234 & 51.2454 & -19.4992 & -0.0001 \\ 0.0000 & -19.5547 & 29.0404 & -4.4385 \\ 0.0000 & 0.0000 & -4.4617 & 4.3779 \end{bmatrix}$$

The bus self and mutual V-Q sensitivities are the inverse of  $J_R$ . The V-Q self-sensitivity values of Bus 2, 3, 4, or 5 are the respective diagonal elements of the inverse matrix  $J_R^{-1}$  [11].

$$\Delta V \Delta Q^{-1} = J_R^{-1}$$

$$(J_R)^{-1} = \begin{bmatrix} 0.0193 & 0.0180 & 0.0143 & 0.0145 \\ 0.0177 & 0.0445 & 0.0354 & 0.0359 \\ 0.0141 & 0.0355 & 0.0690 & 0.0700 \\ 0.0144 & 0.0362 & 0.0703 & 0.2997 \end{bmatrix}$$

The V-Q self-sensitivities for Bus 5, Bus 4, Bus 3, and Bus 2, in the stated order, are 0.2997, 0.0690, 0.0445, and 0.0193.

Using modal analysis technique [11], voltage stability characteristics are determined via the eigenvalues and eigenvectors of the reduced Jacobian matrix  $J_R$ . The system eigenvalues are the elements of the diagonal eigenvalue matrix  $\Lambda$  of  $J_R$  in (3.5).

$$J_R = \xi \Lambda \eta \quad (3.5)$$

where  $\xi$  = right eigenvector matrix of  $J_R$

$\eta$  = left eigenvector matrix of  $J_R$

$\Lambda$  = diagonal eigenvalue matrix of  $J_R$

The 6-bus system eigenvalues under the condition of Base case 1 are:

$$\lambda_1 = 3.0512, \quad \lambda_2 = 13.6468, \quad \lambda_3 = 45.5025, \quad \lambda_4 = 104.6664$$

The V-Q sensitivities and eigenvalues for the remaining variants (shown in Table 3.1) are calculated similarly.

### 3.2.4 Comparison of analytical and Neplan-based results

The analytical voltage stability solution for the base-case 6-bus power system is presented in Section 3.1.3 above. The 6-bus power system is then simulated using Neplan for the respective voltage stability solutions (i.e. Base case 1, and 28 variants with the 140-MW wind farm). Table 3.2 and 3.3 show the selected results for Base case 1, Variant 6 (WF P=30MW) and Variant 20 (WF P=100MW) obtained analytically using Matlab and the corresponding results given by Neplan. While increasing wind power injection, the system loads are always at peak and the operational real power output of generator *Gen6* is kept constant at 43 MW. The system power supply-demand balance is regulated by the swing generator *Swing1*.

Table 3.2 Selected analytical and software-based V-Q self-sensitivities

Bus name	Base case 1			Variant 6: WF P=30MW			Variant 20: WF P=100MW		
	Neplan	Analytical	Diff, %	Neplan	Analytical	Diff, %	Neplan	Analytical	Diff, %
Bus 5	0.2997	0.2997	0.000	0.2944	0.2944	0.000	0.3118	0.3118	0.000
Bus 4	0.0690	0.0690	0.000	0.0689	0.0689	0.000	0.0726	0.0726	0.000
Bus 3	0.0445	0.0445	0.000	0.0444	0.0444	0.000	0.0454	0.0454	0.000
Bus 2	0.0193	0.0193	0.000	0.0193	0.0193	0.000	0.0194	0.0194	0.000

Table 3.3 Selected analytical and software-based eigenvalues

Base case 1			Variant 6: WF P=30MW			Variant 20: WF P=100MW		
Neplan	Analytical	Diff, %	Neplan	Analytical	Diff, %	Neplan	Analytical	Diff, %
3.0513	3.0512	-0.003	3.1001	3.0999	-0.006	2.9092	2.9091	-0.003
13.6490	13.6468	-0.016	13.7142	13.7119	-0.017	13.5613	13.5591	-0.016
45.5067	45.5025	-0.009	45.6042	45.6000	-0.009	45.2777	45.2734	-0.009
104.6754	104.6664	-0.009	104.7861	104.7771	-0.009	104.4714	104.4623	-0.009

**Note:** Plus sign (+) = increase and minus sign (-) = decrease

It is visible that the Neplan-based results are basically the same as the analytical results. The difference between the two sets of results ranges from zero to a fraction of a percent. The two solutions, therefore, are fully compatible. We can now be confident to utilize Neplan for subsequent analyses. The following three case-studies are performed using Neplan.

### 3.3 CASE STUDY 1: ANALYSIS OF WIND FARM IMPACTS ON 6-BUS POWER SYSTEM

This case study aims at identifying and quantifying the wind farm impacts on system voltage stability. The results would help clarify and justify the need for mitigation measures, such as using an energy storage system (ESS).

**Setting:** The 140-MW wind farm (WF) is connected at Bus 5 (Fig. 3.1). Its power output is gradually increased from 5 MW to 140 MW in 5-MW increments. This results in 28 power output levels, or variants (Table 3.1). Note that, apart from specific wind farm power output level, each variant has other properties such as power loss and voltage stability characteristics. The network condition without the wind farm (Base case 1) is used as base for comparison purposes.

#### *Power loss profile*

The system total real power losses (or P losses) for Base case 1 and the variants with the wind farm operational are shown in Fig. 3.3. The wind farm first helps reduce the total P losses at its lower power production but increases the losses at higher output levels.

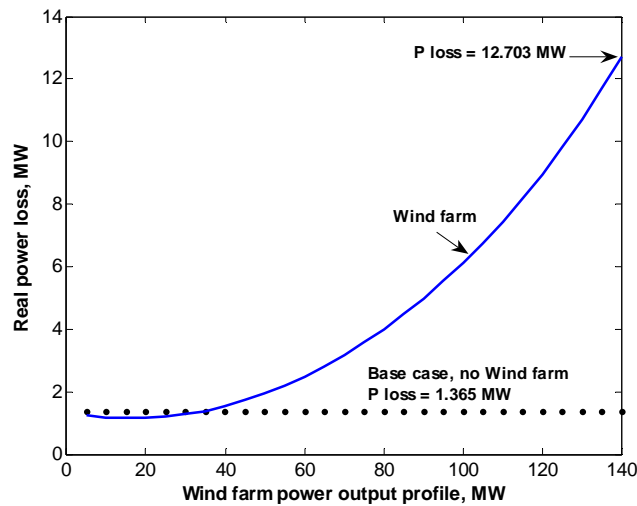


Fig. 3.3 System real power losses under various wind power generation levels.

Compared to Base case 1, the loss reduction is achieved for the wind power production range from 5 to 30 MW. The highest loss reduction is 15.8%, obtained when the wind farm outputs 15 MW. Visibly, the main reason for the loss reduction is that the wind farm supplies power to the local load (8.9 MW for Load 5), leading to the smaller power flow from *Swing1* (see Fig. 3.1 for the 6-bus system component layout). With the wind farm operational, most or all feeding power to Load 5 does not have to go through Line 45, which is a long line with high impedance (i.e. higher loss).

However, when the wind farm power production becomes high, the losses rise dramatically, up to 830.6% (12.703 MW). The obvious reason is that the wind power now goes in the reverse direction to the system major load (Load 3) through the high-loss Line 45. The power flow over Line 34 also becomes stronger, causing additional losses on the same line.

### ***Evaluation of system voltage stability condition***

We now evaluate the system voltage stability condition by comparing the system reactive reserve margins for four selected variants (i.e. four wind power output levels) with that of Base case 1 (69.36 MVAR). High Q-reserve is desired for voltage stability.

Figure 3.4 shows that the system has more Q-reserve (71.64 MVAR) when the wind farm power production is relatively low, such as in Variant 6 (WF P=30 MW). However, the wind farm quickly exhausts the system reactive reserve as its increasing power amount is injected into the system. The Q-reserve margins for Variant 20, 24, and 28 are 56.19 MVAR, 47.24 MVAR, and 36.54 MVAR respectively. The Q-reserve margin for Variant 28 is shown by a double-sided arrow in Fig. 3.4. Other Q-reserve margins are measured similarly. The Q-reserve for Variant 28 is reduced by 47.4% compared to that of the base case, showing that the system voltage stability condition significantly deteriorates as the farm output becomes high. The V-Q curves are also narrower, indicating that the system is more vulnerable to voltage instability.

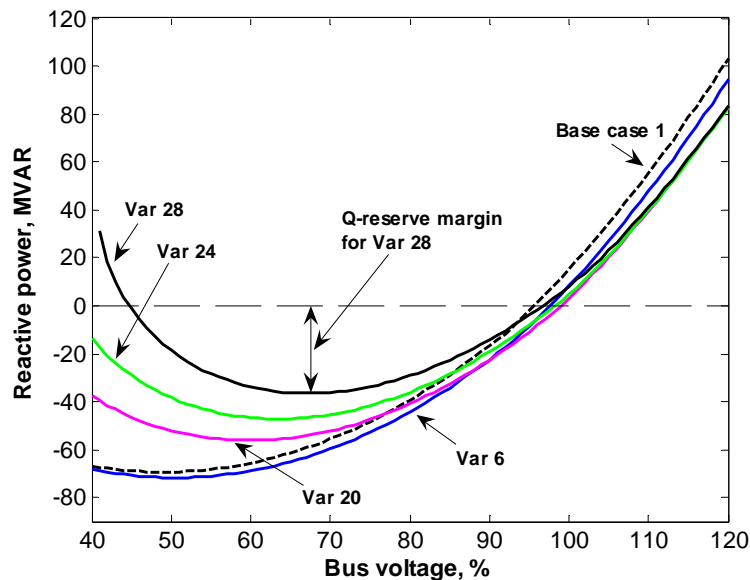


Fig. 3.4 Selected V-Q curves calculated at Bus 5

**Note:** Variant 6: WF P = 30 MW; Variant 20: WF P=70 MW  
Variant 24: WF P=100 MW; Variant 28: WF P=140 MW

Table 3.4 System eigenvalues for four selected variants

<b>Base case 1</b>	<b>Variant 6</b>	<b>Variant 20</b>	<b>Variant 24</b>	<b>Variant 28</b>
<b>WF=0 MW</b>	<b>WF=30 MW</b>	<b>WF=70 MW</b>	<b>WF=100 MW</b>	<b>WF=140 MW</b>
3.0513	3.1001	2.9092	2.1708	1.9541
13.6490	13.7142	13.5613	11.0932	10.8662
45.5067	45.6042	45.2777	42.8893	42.4347
104.6754	104.7861	104.4714	104.0193	103.5058

Table 3.4 shows the system eigenvalues for the above four selected variants. For the 6-bus system, there are four eigenvalues for each system condition (i.e. Base case 1, Variant 6, and so on). The system eigenvalues for the selected variants confirm the findings using the V-Q curves. The eigenvalues are improved (i.e. larger than those of Base case 1) for Variant 6 where the V-Q curve indicates better Q-reserve margin, meaning that the system is more voltage-stable. All the eigenvalues for Variant 20 through Variant 28 are worse than the corresponding values of Base case 1, indicating that the voltage stability condition is worsen in these cases. This result agrees with what shown by the respective V-Q curves.

***Remarks for Case study 1***

The wind farm has positive impacts on the network when its power production is relatively comparable with the local load. It helps reduce real power losses and improve the voltage stability condition. However, as the wind farm output exceeds the local power consumption significantly, the strong reverse power flow increases the losses and lowers the system stability. This judgment is based on the system real power losses and two voltage-stability criteria, namely, system reactive reserve margins and eigenvalues.

This finding is an interesting one. To date, wind farm high demand for reactive power is often considered as the main factor that affects the stability condition of power networks. This case study reveals that, even with full reactive compensation, a strong (or excessive) reverse power flow from the wind farm could also worsen the system stability (by exhausting the network reactive power reserve and increasing power losses).

The system steady-state voltage stability condition shown by Q-reserve margins is comparable with the indication by eigenvalues. Though, it is noted that using eigenvalue indicator is more advantageous. The eigenvalues provide a system-wide view of voltage stability while the Q-reserve margins are tied to a particular bus (Bus 5 in this study). For analyzing large systems, using Q-reserve margin would be very cumbersome due to the need to calculate a large number of V-Q curves for measuring the Q-margins.

### 3.4 CASE STUDY 2: DETERMINATION OF MAXIMUM-POSSIBLE WIND POWER PENETRATION LEVELS

Case study 2 determines how much wind power should or could be integrated while maintaining an acceptable voltage stability condition for the system. The results are used together with the results of Case study 1 in operating the ESS in Case study 3.

**Setting:** The wind farm is connected at Bus 5 as shown in Fig. 3.1. Its power production is gradually increased from 5 MW in 5-MW increments until the system power flow calculation fails to converge. Power flow divergence is an indication that the system is approaching the edge of voltage collapse. At or near this limit, V-Q curve calculation cannot be performed [11]. It is clear that further injection of wind power in this situation is impossible. To explore this limit, the wind farm output is allowed to exceed its original rating (i.e. 140 MW). The amount of integrated wind power (the penetration level) is determined with respect to different voltage stability conditions, which are represented by the system Q-reserve margins and four smallest eigenvalues. Base case 1 is used for comparison purposes. Note that, since the system is at peak load and peak generation in the base case, this is a lowest voltage stability condition without the wind farm. It represents a conservative situation for voltage stability evaluation.

#### Results

The main results obtained for this case study are shown in Fig. 3.5 and Table 3.5. Figure 3.5 plots the amount of wind power that can be integrated into the 6-bus system versus the respective reactive reserve margin. Table 3.5 contains the system eigenvalues for the investigated conditions, which correspond to the wind power injection levels shown Fig. 3.5.

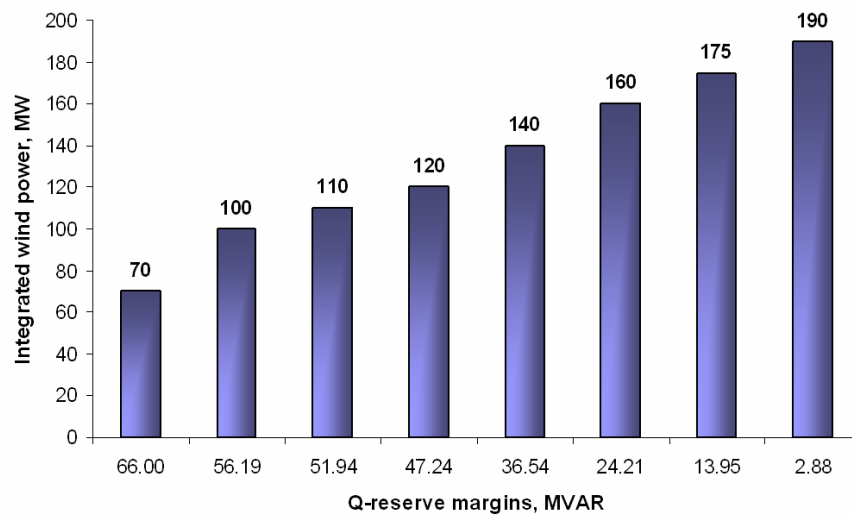


Fig. 3.5 Amount of integrated wind power versus Q-reserve margin

The wind power injection levels shown in Fig. 3.5 and Table 3.5 correspond to the numbered variants, as following: Variant 14 (70 MW), Variant 20 (100 MW), Variant 22 (110 MW), Variant 24 (120 MW), Variant 28 (140 MW), Variant 32 (160 MW), Variant 35 (175 MW), Variant (190 MW).

Table 3.5 System eigenvalues for different wind power injection levels

System eigenvalues, MVAR/%								
Base case 1	Variant 14	Variant 20	Variant 22	Variant 24	Variant 28	Variant 32	Variant 35	Variant 38
1	2	3	4	5	6	7	8	9
3.0513	3.0427	2.9092	2.2553	2.1708	1.9541	1.6439	1.2952	0.6330
13.6490	13.6790	13.5613	11.1799	11.0932	10.8662	10.5378	10.1725	9.5072
45.5067	45.5123	45.2777	43.0661	42.8893	42.4347	41.7903	41.0862	39.8321
104.6750	104.7030	104.4714	104.2200	104.0190	103.5060	102.7840	102.0040	100.6360
Change in system eigenvalues compared to Base case 1, %								
10	11	12	13	14	15	16	17	18
0.00	-0.28	-4.66	-26.09	-28.86	-35.96	-46.12	-57.55	-79.25
0.00	0.22	-0.64	-18.09	-18.73	-20.39	-22.79	-25.47	-30.35
0.00	0.01	-0.50	-5.36	-5.75	-6.75	-8.17	-9.71	-12.47
0.00	0.03	-0.19	-0.44	-0.63	-1.12	-1.81	-2.55	-3.86

**Note:** For Column 11-18, plus sign (+) = increase and minus (-) = decrease.

The analysis of the obtained results reveals three major wind power penetration levels with respect to three critical voltage stability limits for the 6-bus system, as following.

**Penetration level 1:** 70 MW of wind power, or 34.36 % of the system demand, based on the total real power demand of 203.7 MW. For this penetration level, the voltage stability condition (Variant 14) is essentially the same as that of the original system (Base case 1). The Q-reserve margin is 66 MVAR (Fig. 3.5), which is less than that of Base case 1 (69.36 MVAR) by 4.85%. The system eigenvalues are close to those of Base case 1 (Column 1, 2 and 11, Table 3.5).

**Penetration level 2:** 110 MW, or 54% of the system demand. The respective voltage stability limit (Variant 22) is reduced by around 25% compared to that of the original system (Base case 1). The value of 25% is based on the fact that the system Q-reserve margin for Variant 22 (51.94 MVAR, Fig. 3.5) is reduced by 25.12% and the system smallest eigenvalue is decreased by 26.09% (Column 13, Table 3.5). However, the system normal operation is still possible with the voltage profile within +/-5% limits. There is no line or generator overload.

**Penetration level 3:** 190 MW, or 93.27% of the system demand. The system reactive reserve is almost exhausted (2.88 MVAR, Fig. 3.5) and the eigenvalues are reduced by up to 79.25% compared to those of Base case 1 (Column 18, Table 3.5). A penetration level higher than this causes the system to become voltage-unstable and can lead to voltage collapse. Simulation

shows that, when the wind farm power is increased to 194 MW, the system power flow fails to converge. Calculation of V-Q curve is impossible because V-Q sensitivity is too large. This indicates that the maximum wind power penetration level for the 6-bus system is around 190 MW. Other lower penetration levels may also be defined in observance of the respective voltage stability limits, but the three identified penetration levels correspond to three most important voltage stability conditions of the 6-bus system.

### ***Remarks for Case study 2***

The selected three voltage stability techniques (i.e. V-Q curve, V-Q sensitivity and V-Q modal analysis) can be used effectively to determine different penetration levels of wind power for a power network.

For the 6-bus system, three most important penetration levels are identified. Penetration level 1 is 70 MW of wind power, or 34.36 % of the system demand. At this penetration level, the static voltage stability condition of the original system is maintained. At Penetration level 2 (110 MW, or 54%), the system stability condition is reduced by around 25%, but its normal operation is still possible. Penetration level 3 (190 MW, or 93.27%) corresponds to a lowest stability condition of the system. Beyond this limit, the system enters voltage-unstable region that could lead to voltage collapse. The knowledge of these limits (penetration levels) is useful since they indicate the boundaries for the system safe operation.

Case study 1 and 2 show that, in many situations, wind power integration negatively impacts the system voltage stability condition. A solution, therefore, is needed to mitigate the adverse impacts. In Case study 3, application of an energy storage system (ESS) is investigated to learn if the ESS can improve wind power penetration and the system voltage stability.

### **3.5 CASE STUDY 3: APPLICATION OF AN ENERGY STORAGE SYSTEM FOR IMPROVING WIND POWER INTEGRATION AND VOLTAGE STABILITY**

In this case study, the operation and the effectiveness of an ESS are investigated.

**Setting:** The wind farm is connected to Bus 5 as shown in Fig. 3.1. Its power production for 8 hours is shown in Fig. 3.6 and Column 2 of Table 3.6. An energy storage system (ESS), modeled as a negative load, is connected at the same bus as the wind farm. The storage system is controlled to store and release wind energy according to the schemes developed in Table 3.6 where Column 3 is the charge and Column 4 is the discharge scheme. Base case 1 is used for comparison purposes.

**Assumptions:** (a) It is assumed that the 6-bus system demand (i.e. total load) and the matching generation stay at their peaks (i.e. the condition in Base case 1) for the considered 8 hours. This is a conservative scenario for voltage stability evaluation since the system stability is at a lowest level under the peak-load condition. (b) For each hour of consideration, the wind farm power output is unchanged. In practice, a wind farm power output changes every minute or even every second. In this case study, hourly-averaged wind power production is considered. (c) Wind farm power output for any hour is known with 100-percent accuracy. This is possible because wind farm output history is used in this study. (d) The ESS capacity is sufficiently large to store all wind energy as desired. For each hour of consideration, the ESS charging rate is fast enough to store all surplus energy during that 1-hour period.

### ***Selection of charge-discharge reference point for ESS***

The reference point is essential for the ESS operation since it indicates when the ESS is to start to store wind power or to release it. In case a control system for the ESS is modeled explicitly (likely in dynamic simulation), this point would be a reference point for the control system.

It is not straightforward to set this reference point. If it is too low and the wind farm power output is high, a large amount of wind power would have to be diverted into the ESS. This means that the ESS size would have to be very large, resulting in higher ESS capital cost. In addition, less wind power is channeled into the power system in this situation. If the reference is too high, the system stability may be affected because of the excessive wind power flow. In [54, 55] the wind power plant power output of 0.9 pu is the control objective. In [56] the real power reference is chosen to be the wind farm average real power. This study uses a grid-based approach. It selects the reference point based on the overall voltage stability condition of the power network. The core idea is that the reference is chosen so as to meet two criteria simultaneously: (i) to maintain the network voltage stability and (ii) to channel a maximum-possible amount of wind power into the system.

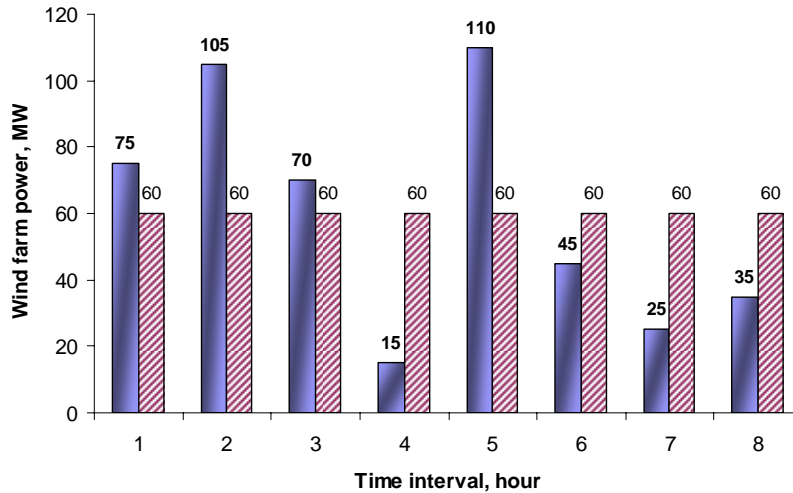


Fig. 3.6 Uncontrolled wind farm output and target power profile for 8 hours

**Note:** Figure 3.6 shows the uncontrolled 140-MW wind farm power production for 8 hours (i.e. without the ESS) and the desired power profile (i.e. with the ESS). The set of blue-filled bars is the wind farm power profile and the set of stripe-bars is the target power profile.

The results of Case study 1 and 2 show that channeling around 70 MW of wind power (i.e. 34.36 % of the system demand, or Penetration level 1) into the 6-bus system could maintain the original stability condition (Base case 1). Therefore, to be more conservative, the reference point of 60 MW is chosen for the ESS. For example, if the wind farm outputs 75 MW, 60 MW is allowed to go freely into the grid and 15 MW is diverted to the ESS for storing. In the opposite situation, if the wind farm outputs less than 60 MW, say 50 MW, the ESS releases 10 MW (provided the power is available in the storage) to the system. The final goal is to ensure a wind-power flow of around 60 MW to the system at all times. Certainly, if the wind farm power production is low, an output of less than 60 MW is acceptable since the amount does not affect the voltage stability condition of the original system.

#### ***Calculation of power charge-discharge profiles for ESS***

Given the wind farm 8-hour power profile and the reference point of 60 MW, it is possible to calculate the amount of wind power that should be stored in the ESS and the amount that the ESS should release during each hour. The result is shown in Table 3.6 where Column 3 shows the amount of wind power to be stored in the ESS for every hour while Column 4 indicates the hourly power that the ESS should discharge. Column 5 shows the cumulative energy in the ESS, which is available for discharge during each hour. The combined hourly power output from the wind farm and the storage system is calculated and shown in Column 6. This is the hourly wind power amount channeled into the grid from the wind farm point of connection.

Table 3.6 Calculation of power charge-discharge profile for ESS

Time Interval, hour	Wind farm power, MW	Power to ESS, MW	ESS output, MW	Cumulative energy in ESS, MWh	Combined output of WF & ESS, MW
1	2	3	4	5	6
1	75	15	0	15	60
2	105	45	0	60	60
3	70	10	0	70	60
4	15	0	45	25	60
5	110	50	0	75	60
6	45	0	15	60	60
7	25	0	35	25	60
8	35	0	25	0	60

The constant target power profile of 60 MW used in this case study is a special case. It is envisioned that, in practice, the desired combined output between a wind farm and an ESS would not be constant all the time. This is because the grid load demand varies during any day. In this situation the ESS benefit would also be different. Though, even with this special case, the below results clearly show that the ESS-based method is effective. However, more realistic conditions need to be considered, such as different wind farm power output profiles, ESS charging rate, and/or size for any ESS-based practical application etc. This is done in the subsequent studies in chapters 4 through 6.

## Results

The main simulation results are plotted in Fig. 3.7 and Fig. 3.8.

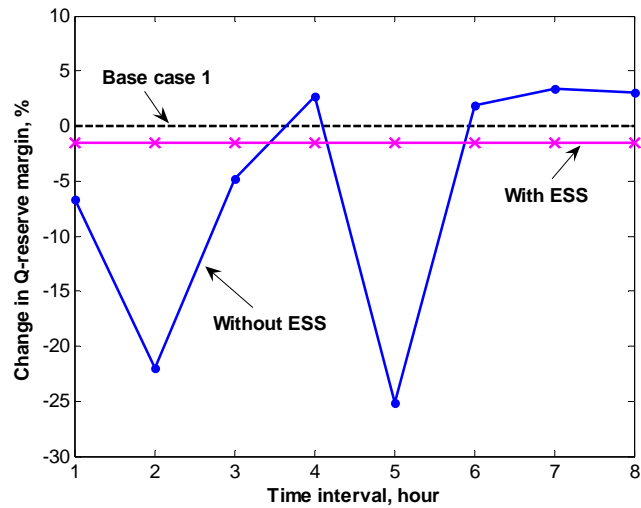


Fig. 3.7 Change in Q-reserve margin with and without ESS

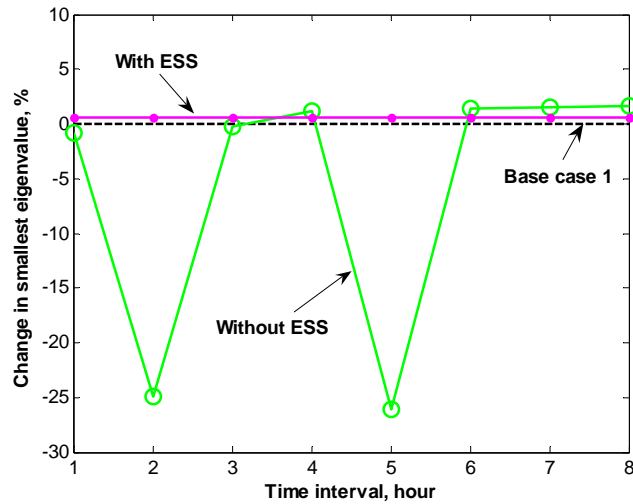


Fig. 3.8 Change in system smallest eigenvalue with and without ESS

Without the ESS, the results show that the system voltage stability condition varies dramatically as the wind farm power production goes up and down. At times the system Q-reserve margin is improved by around 3% while at other times the margin drops by up to 25.13% (Fig. 3.7, Time interval 5). The system eigenvalues, shown in Fig. 3.8, agree with this finding. The smallest eigenvalue is reduced by up to 26.09% (Fig. 3.8, Time interval 5) as the wind farm

injects up to 110 MW into the system. Operation of the 6-bus system in this situation is clearly undesirable because the stability condition deteriorates considerably under the farm high outputs (e.g. 105 MW at Time interval 2, 110 MW at Time interval 5).

With the ESS operational, a steady wind power flow of 60 MW is maintained for the entire 8-hour period. The system reactive reserve margin stays close to that of Base case 1 with a slight decrease of 1.54% (Fig. 3.7). On the other hand, the system eigenvalues are improved, as shown in Fig. 3.8. This means that the ESS helps increase the voltage stability limit for the 6-bus system. All the wind power produced by the wind farm is integrated into the system.

For the 8-hour period, the ESS releases a total amount of 120 MWh of wind power (sum of Column 4, Table 3.6). Without the ESS, either this amount of wind power has to be thrown away, or be integrated into the system at the cost of lowering stability. The maximum amount of energy that the ESS has to carry is 75 MWh (during the 5th hour, Column 5, Table 3.6). It follows that the ESS would need to be sized at around 75 MWh to meet the storage requirement for the 8 hours of consideration. Given the wind farm capacity of 140 MW, the ESS size is about half of the wind farm rating.

### ***Remarks for Case study 3***

Overall, the results obtained in this case study show that using an energy storage system to increase wind power penetration is effective. The ESS helps integrate all the power produced by the wind farm during the 8-hour period of consideration. In addition, it improves the system voltage stability slightly. Another advantage of the ESS is that it increases the system spinning reserve, thanks to the energy available in the storage for certain periods. For instance, at the 5th hour, the stored energy available in the ESS is 75 MWh (Column 5, Table 3.6). As a result, during this hour, the original system spinning reserve (50.4 MVA, or 18.7%) increases to 125.4 MVA, or 46.4%. Larger spinning reserve implies better voltage stability since the system has more power to support voltage and frequency during the time interval.

By using steady-state analyses, other useful information is also obtained. It includes the total energy released by the ESS during the 8-hour period and the maximum energy that the ESS is to carry during an hour-time. The information may be used for estimating an appropriate ESS size and its economic benefit.

### **3.6 CHAPTER CONCLUDING REMARKS**

In this chapter, a pilot study is conducted to prove that it is possible to use energy storage systems to mitigate wind farm negative impacts on power system voltage stability while facilitating wind power integration into the power grid.

A three-step solution using an energy storage system is developed and demonstrated by three case studies. The ESS effectiveness is evaluated on a small but realistic 6-bus non-radial power system that hosts a large wind farm. The results show that the ESS-based solution is efficient. All wind power produced during an 8-hour period has been integrated into the system while its voltage stability condition is maintained.

The above finding gives the base and confidence to proceed with the development of a more sophisticated application using ESS for reducing wind farm power output variation and improving grid voltage stability. The application development is the content of the following chapter.

## Chapter 4

### Development and analysis of an ESS-based application for regulating wind farm power output variation

#### 4.1 INTRODUCTION

The proposed solution based on energy storage systems is demonstrated to solve the wind-farm-related problems by three simplified case studies in Chapter 3. In this chapter, the solution is developed in a detailed and realistic manner using real-world wind farm and power system data. The main goals are defined as follows.

- (i) To define a framework for the ESS-based application, i.e., the steps one should follow to design an ESS for regulating a wind farm output fluctuation.
- (ii) To develop a technique to calculate the desired target power output profile, i.e., the combined output that a wind farm and the associated ESS should produce for the grid benefit.
- (iii) To develop an operation scheme for ESS, i.e., ESS charge-discharge scheme.
- (iv) To quantify ESS benefits in terms of voltage stability, wind power integration, and ability to reduce the mismatch between wind farm output and the grid load demand.

To achieve the goals stated in (i)–(iii), optimization theory and engineering design concepts are applied. With respect to the goal defined in (iv), the ESS benefit in terms of wind power integration is measured using additional integrated wind power amount. The voltage-stability benefit is validated using eigenvalue analysis. The ESS ability to reduce the mismatch between the farm output and the grid demand is assessed using coefficient of correlation. The study is carried out using the real-world 27-bus transmission grid (Section 1.3 and Appendix A3) and actual wind farm data. Matpower [32] and Matlab [30] are used as computational tools. Matpower is a publicly available Matlab-based program that performs power flow and optimal power flow calculations. The computing codes are written in Matlab.

A case study with a 183-MW wind farm connected to 27-bus transmission grid shows that the defined framework for the ESS-based application is useful. Following this framework, one can design an ESS for use with the wind farm successfully. The proposed technique for calculating the desired output uses optimal power flow to determine the best output profile,

achievable by the aggregate system for the benefit of the grid. The term “benefit” is defined as “minimizing the total cost of grid generated power”. Regulating the wind farm output according to the desired profile causes the farm to behave like a dispatch-able source while taking into account the cost of system generation. This technique, to the best knowledge of the author, is a completely new approach. For considered ESS rating (1–183 MW and 0.5–8 hours) the increase in wind energy integration is between 0.1%–32.9%. In addition, the ESS can increase the grid steady-state voltage stability by a net amount between 2.7%–22.3%, compared to the case where the wind farm output variability is completely unregulated. For the mentioned range of ESS rating, the mismatch between the wind farm output and the grid load-demand can be reduced by 0.1%–77.7%.

**Publication:** The work reported in this chapter has been published in the proceeding of *IEEE Power & Energy Society General Meeting 2009* with the title "Development and analysis of an ESS-based application for regulating wind farm power output variation" [35].

## 4.2 PROBLEM ANALYSIS AND SOLUTION

### 4.2.1 Problem analysis

It is known that, as wind comes and goes, the wind farm power output varies greatly. The power output usually does not match the grid load demand. It can be low when the load demand is high or high when the load demand is low. The power output variability and demand-mismatch have two drawbacks. The first is that wind power produced at times of low demand may have little or no economic value. The second is that the grid voltage stability can decrease due to the surplus or shortage of power from time to time (i.e. the power supply-demand balance is not preserved). To solve the problems, it is proposed to use an energy storage system for regulating the wind farm output, so as to reduce its variability, as well as to make it a better match for the grid demand. The scenario of using an ESS with a wind farm, defined as an “aggregate system”, to regulate the farm power output is illustrated in Fig. 4.1.

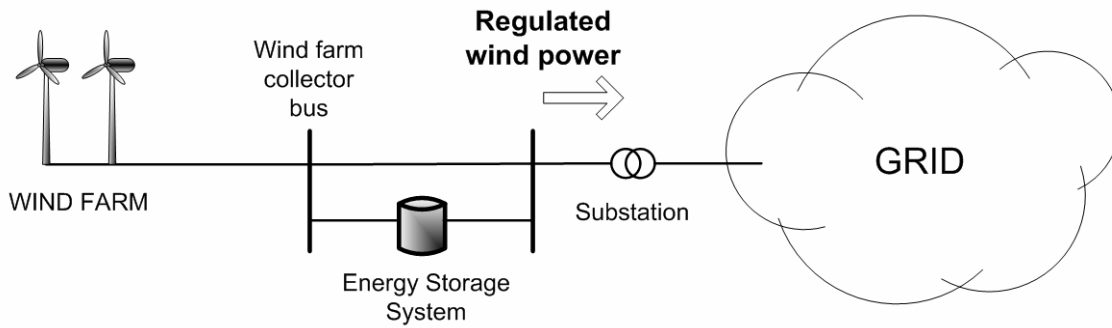


Fig. 4.1 Scenario of using ESS for regulating wind farm output variability

Under the scenario, the ESS is connected in parallel with the wind farm. Normally, the wind farm power is channeled directly into the grid. In case there is a surplus in wind power, the surplus power is diverted to the ESS for storage. When the wind farm output decreases (i.e. there is a deficit of wind power), the energy stored in the ESS is discharged to make up for the deficit. The combined output of the wind farm and the ESS is the regulated wind power to the grid.

The surplus or the deficit in wind power is determined based on a reference power profile. This power profile is the dispatch profile desired by the grid where the wind farm is connected. Therefore, the reference power profile is also named the “desired output”. For details of how to calculate the reference power profile, see Section 4.2.2.

At any time  $t$ , the wind power surplus is the positive difference between the wind farm output level and the respective desired output level. Conversely, the negative difference is the power deficit. All wind farm power output is channeled directly into the grid whenever there is no surplus power. In this way, the ESS is used to regulate only part of the wind farm output. Partial-output regulation potentially helps reduce the ESS capacity required for the application. Given the currently-high cost of ESS, this approach is advantageous.

**Important concepts of ESS:** The rating of an ESS includes two components, the rating of the power conversion unit (i.e. the power rating in MW) and the rating of the energy storage unit (i.e. the energy rating in MWh). ESS of different technologies may have very different characteristics. Although this study does not require specification of ESS technology, large-scale storage is needed because today wind farms are large (i.e. with the rating of tens to hundreds of MW). Therefore, large-scale storage ESS, such as pumped hydroelectric energy storage (PHES) and compressed-air storage systems (CAES), are of primary interest. For these ESSs, the efficiency of the energy storage unit is included as part of the system overall efficiency.

Therefore, the ESS energy rating  $E$  is calculated simply as  $E = P \times t$ , where  $P$  is the rating of the power conversion unit and  $t$  is the discharge duration [57, 58].

#### 4.2.2 Solution – Steps for implementing ESS-based application

The implementation of an ESS-based application requires consideration of both technical and economic issues.

On the technical side, it is very important to determine an appropriate wind power output profile, which is most beneficial to the grid where the wind farm is connected. This is the output that the aggregated system (i.e. the wind farm and the ESS) should produce for the grid benefit. Hence, the output is called the desired output profile. Next, a charge-discharge scheme for the ESS is to be developed. The scheme directs the ESS to store unwanted wind power and appropriately re-dispatch it later. It is used in conjunction with the desired output profile, which serves as the reference for charge-discharge operation. Furthermore, the effects of the ESS need to be quantified and analyzed to find out if the application is technically-sound.

On the economic side, the cost and benefit of the ESS must be considered before the ESS project can be implemented. The technical analysis of ESS effects provides required information for the economic analysis.

Following the above discussion, the major steps for implementing an ESS-based application are defined as follows.

- **Step 1 – Reference power profile:** Based on the grid condition, such as load, line, generator power cost, to determine the desired output profile, or the reference power profile, for the wind farm of interest. This is the ideal power output that the wind farm and the associated ESS should produce for the grid benefit.
- **Step 2 – Charge-discharge scheme:** To develop a charge-discharge scheme for the ESS which directs the ESS operation to facilitate wind power integration.
- **Step 3 – ESS efficacy:** To quantify and analyze the effects of ESS in terms of wind power integration, voltage stability, and load-demand mismatch reduction. These criteria are deemed essential in evaluating the ESS efficacy.
- **Step 4 – ESS sizing:** To determine the optimal power and energy ratings for the ESS so as to maximize the ESS net benefit. The net benefit results from subtracting the ESS total cost from the total benefit. This is named “ESS-sizing” problem and is solved using an optimization-based technique. The ESS benefits, such as increased wind power integration and voltage stability improvement, and ESS costs are

included in an objective function. The function is then optimized to find the ESS optimal rating.

The following study focuses on the first three steps (i.e. Step 1 through 3), which are technical analyses. A separate study is conducted on the issue of ESS-sizing (i.e. Step 4) and presented in Chapter 5.

### **4.3 FORMULATION OF A CASE STUDY**

This case study demonstrates the implementation of an ESS-based application for regulating the power output of a large wind farm connected to a transmission grid. The case study follows the first three steps defined in Section 4.2.2.

#### **4.3.1 Description of 27-bus power system and wind farm**

The power system used for this study is a reduced 27-bus version of the regional network of a large power utility. To form the 27-bus system, all transmission lines of 138-kV and 345-kV voltage are preserved. All under-69-kV systems are removed and modeled as lumped loads. The 27-bus system consists of four 345-kV transmission lines and 19 138-kV lines. There are six lumped loads (load points) and seven generators on the system, including a wind farm and a swing generator. The total generation capacity is 1499.5 MVA and the total load is 1148.6 MVA. The spinning reserve is 23.4% and the total load power factor is 0.97 lagging. The online diagram with peak-load power flow for the 27-bus grid is shown in Appendix A3.

The wind farm is a combination of several large groups of wind turbines with the total name-plate rating of 183 MW. The ESS is connected in parallel with the wind farm as shown in Fig. 4.1. All the load and wind farm data are for the particular year of 2005. The load profiles are for 365 days in 30-min resolution, derived based on the assumption that the system demand remain unchanged during every 30-minute period.

#### **4.3.2 Technique for determining desired output profile**

The desired output profile for the wind farm (Step 1, Section 4.2.2) is determined as follows. An equivalent conventional generator is assumed to be located in place of the 183-MW wind farm. Then, an optimal power flow (OPF) calculation is done to determine the generator dispatch profile, which is considered as the desired output profile of the wind farm. This is the output that the aggregate system (the wind farm and the associated ESS) should produce for the grid benefit. The term “benefit” is defined as “minimizing the total cost of grid generated power”.

The optimal power flow calculates the best dispatch profile for the assumed generator in coordination with all generators on the power system so as to minimize the total cost of power generation. Meanwhile, the basic requirements for normal system operation such as the supply-demand balance, line power-carrying capability and generator limits, are satisfied. Therefore, the dispatch profile of the equivalent generator is the optimal and desired power output for the wind farm and the ESS to achieve.

The assumption for this approach is that the generation cost of the equivalent generator corresponds to the cost of the wind power generation. The assumed generator is considered equivalent and representative of the wind farm when their average power outputs are identical. This is achieved by adjusting the rating of the assumed generator.

The OPF-based technique for determining the combined output of wind farm and ESS offers a great advantage. Regulating the wind farm output according to the desired profile makes the wind farm behave like a dispatch-able power source while taking into account the cost of system generation. The closer the combined output is to the desired output, the more beneficial it is to the grid because the total cost of power generation is minimized.

As said before, a publicly available optimal power flow (OPF) Matlab-based software named Matpower [32] is used for all OPF calculations. Following the research principle, Matpower results are validated using analytical calculation before use. The validation is presented in Appendix A4.

### ***Brief description of optimal power flow solution method***

The optimal power flow problem is formulated as follows [32]. The OPF vector of variables  $x$ , which includes the voltage angles  $\theta$  and voltage magnitudes  $V$  at each bus, and real and reactive power generator injections  $P_g$  and  $Q_g$ , is defined as

$$x = [\theta \ V \ P_g \ Q_g]^T$$

The optimal power flow problem is

$$\min_x \sum_i (f_{1i}(P_{gi}) + f_{2i}(Q_{gi})) + \frac{1}{2} wHw^T + C_w^T w \quad (4.1)$$

Subject to

$$\begin{aligned}
1) \quad & g_p(x) = P(\theta, V) - P_g = 0 \\
2) \quad & g_q(x) = Q(\theta, V) - Q_g = 0 \\
3) \quad & g_{s_f}(x) = |S_f(\theta, V)| - S_{\max} \leq 0 \\
4) \quad & g_{s_t}(x) = |S_t(\theta, V)| - S_{\max} \leq 0 \\
5) \quad & l \leq Ax \leq u \\
6) \quad & x_{\min} \leq x \leq x_{\max}
\end{aligned} \tag{4.2}$$

In (4.1)  $f_{1i}$  is the cost of active and  $f_{2i}$  is the cost of reactive power for generator  $i$  at a given dispatch point. The OPF problem in (4.1) determines the optimal dispatch power at a given dispatch point for each generator on the power system of interest so as to minimize the total cost of the system generated power while satisfying a set of constraints specified in (4.2) [32].

In (4.2),  $g_p(x)$  and  $g_q(x)$  are active and reactive power balance equations, respectively.  $P(\theta, V)$  and  $Q(\theta, V)$  are the total real and reactive load power demands which depend on the system bus voltages and voltage angles.  $P_g$  and  $Q_g$  are the total generated real and reactive power outputs.  $g_{s_f}(x)$  and  $g_{s_t}(x)$  specify the apparent power flow limits of lines *from* and *to* end. All  $S$  are magnitudes of apparent power.  $S_f(\theta, V)$  and  $S_t(\theta, V)$  are vectors of calculated apparent power (magnitude) for lines *from* and *to* end, respectively.  $S_{\max}$  is the vector of apparent power limits for lines. The fifth set of constraints is general linear constraints such as constraints that define the generator P-Q capability curves. The sixth set of constraints contains the lower and upper limits imposed on the variables. For further details on OPF formulation, see Matpower User's Manual [32].

For calculating the desired output profile, the lower and upper limits of real and reactive power are imposed on the grid generators by specifying their P-Q capability curves. For each generator, the P-Q capability curve is modeled as a box constraint, which is defined by the respective  $P_{\min}$ ,  $P_{\max}$ ,  $Q_{\min}$ , and  $Q_{\max}$ . Simulation of the 27-bus system under a peak load condition using Newton-Raphson power flow method shows that the reactive power outputs of all generators are well inside the Q-limits. Therefore, simple box constraints are satisfactory. Concerning the power generation cost, only the active power cost  $f_{1i}$  is considered. The limits for the bus voltages are 95%–105% of the nominal values

The active power cost curves are approximated by quadratic polynomials based on data obtained from [53, 59, 60]. For developing the cost curves of the system generators, only the fuel cost is considered. The cost of generation includes the fuel cost, the labor cost, supplies and

maintenance, but the fuel cost is the dominant component [53, 61]. Therefore, the fuel-cost curves (i.e. plot of the cost of fuel input in \$/h versus output power in MW) are good estimators of the generators' power costs. In addition, quadratic functions are adequate for representing the relationship between generated real power and cost for generators [53]. The generators' limits and active power cost functions are provided in Table 4.1. The cost function of generator  $i$  is of the form  $C_i = \gamma_i P_i^2 + \beta_i P_i + \alpha_i$  where  $P$  is the generator output in MW. The generator limits are of the form  $P_{i(\min)} \leq P_i \leq P_{i(\max)}$  and  $Q_{i(\min)} \leq Q_i \leq Q_{i(\max)}$ .

Table 4.1 Generator limits and cost data [53, 59, 60]

Generator name	Pmax MW	Pmin MW	Qmax MVAR	Qmin MVAR	Coefficients of cost functions			Estimated heat rate MBtu/MWh
					$\gamma$	$\beta$	$\alpha$	
Gen1008	595	10	238	-30	0.0809	5.6	111	7.74
Gen5343	150	10	43.95	-43.95	0.0999	6.95	137	9.55
Gen1000	450	10	450	-450	0.0849	5.9	117	8.12
Gen7038	42	10	12	-12	0.53	37.1	520	9.50
Gen5017	88.2	10	1E-6	-1E-06	0.22	5.4	250	9.20
Gen5019	86.8	10	1E-6	-1E-06	0.42	31.5	400	9.05
Gen4016	100	10	1E-6	-1E-06	0.25	5.5	152	9.30

The last three generators (*Gen5017*, *Gen5019* and *Gen4016*) are operated at the unity power factor. Their Q-limits are set to small values for the OPF program. Generator *Gen4016* is the assumed generator and placed at Bus 4016 where the 183-MW wind farm of consideration is located. The desired output profile for the wind farm (i.e. the output profile of *Gen4016*) is found by running Matpower OPF with the 27-bus power system data. The optimal dispatch profiles of the system 5 other generators (except for the Swing generator) are also found. They will be used later for establishing the optimal condition for quantification of the system voltage stability.

### 4.3.3 Development of ESS charge-discharge scheme

The ESS charge-discharge scheme (Step 2, Section 4.2.2 ) is designed so as to make the wind farm power output match the desired output as much as possible while facilitating wind power integration. The main rule is that the ESS accumulates wind energy and re-dispatches it whenever there is an opportunity. In other words, it increases wind power integration by maximizing the discharged energy. To determine the discharged energy accurately, the ESS charge-discharge efficiency, or the two-way efficiency, is considered. For bulk energy storage technologies defined in a Sandia National Laboratories study [58], the two-way efficiency ranges from 0.65 to 0.78. For this study, the two-way efficiency of 0.73 is chosen. This is a

representative efficiency because it is approximately the averaged efficiency of the bulk storage technologies listed in [58]. It is close to the efficiency of the two most promising storage technologies for wind power management, namely pumped hydroelectric storage (0.75) and compressed-air energy storage (0.73) [58]. Assuming that the charge efficiency is equal to the discharge efficiency, one way efficiency is 0.865. The inputs of the ESS operation scheme are the measured unregulated power output for the year 2005 of the 183-MW wind farm, and the desired output profile determined in Section 4.2.2. The diagram for ESS charge-discharge scheme is shown in Fig. 4.2.

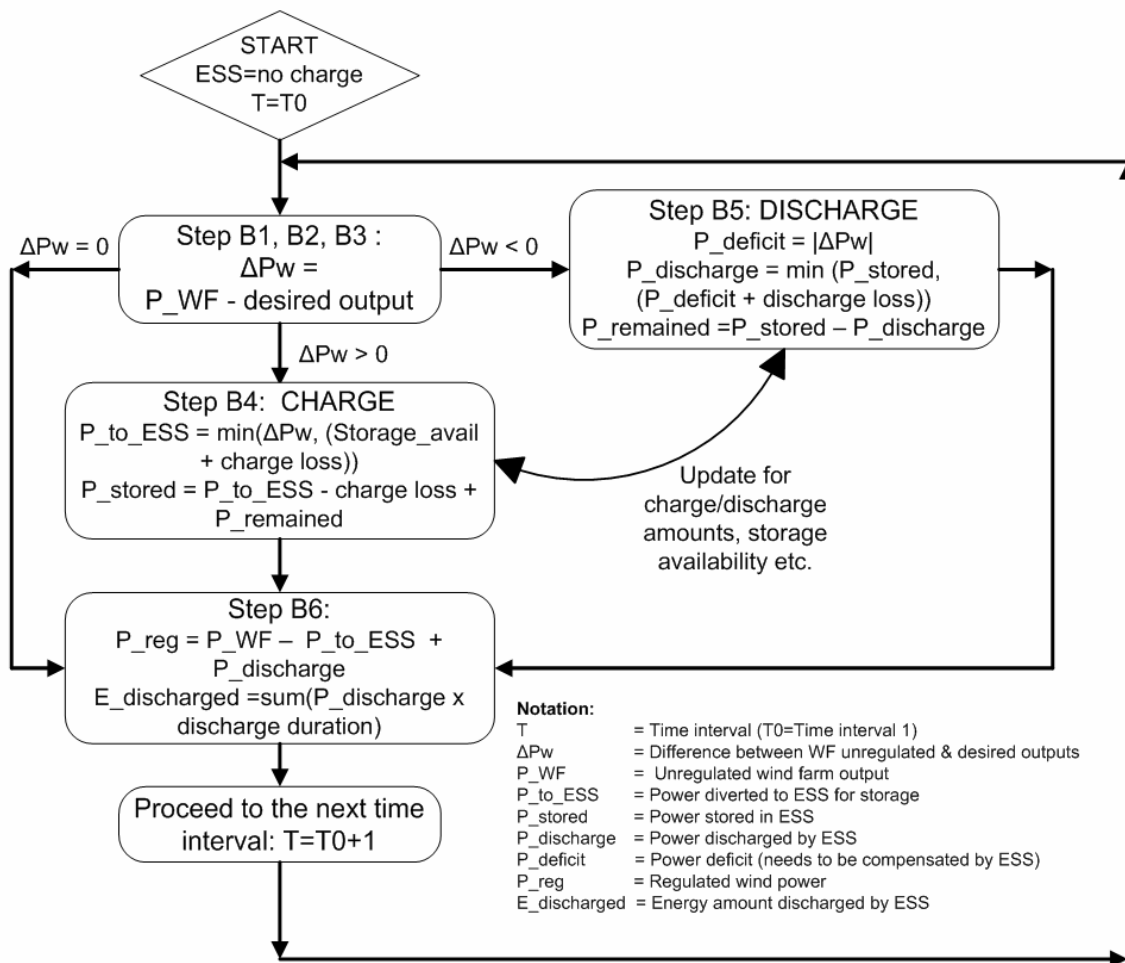


Fig. 4.2 Diagram for ESS charge-discharge scheme

The main features of ESS charge-discharge scheme are as follows.

- **Reference output profile:** The desired output profile (determined in Section 4.3.2) is the reference for the ESS to charge or discharge. As discussed in Section 4.2.1, wind power surplus is the positive difference between the wind farm output and the desired output. Conversely, the negative difference is the power deficit.
- **Charge:** For any time interval, if there is a wind power surplus, the surplus power is diverted into the ESS as much as possible. The ESS is assumed to have the ability to store the amount of power during the time period less the charge efficiency, up to its power or energy limit. If the ESS is full, the surplus power is allowed to integrate into the grid. However, this energy amount is considered to have no economic value because the power is not desired by the grid at the time.
- **Discharge:** For any time interval, the ESS discharges if there is a power deficit, aiming at compensating for the full deficit amount. In case the available energy in the ESS is insufficient for this purpose, all the stored energy is dispatched to make up the deficit as much as possible. The remaining deficit is compensated by the system other generators. The ESS discharged efficiency is considered.
- The ESS maximizes the discharged wind energy by accumulating and re-dispatching the wind energy whenever there is an opportunity. The multiple charge-discharge cycles of the ESS can be scheduled accurately because the data (historical wind farm output, charge-discharge reference) are known with 100-percent certainty. The output to the grid is the combined output of the wind farm and the ESS. The cumulative discharged energy for the year is the total energy dispatched by the ESS over 17,520 time intervals (365 x 24 x 2).

#### 4.3.4 Techniques for quantifying ESS efficacy

As said in the solution for designing the ESS-based application (Step 3, Section 4.2.2), the ESS efficacy is evaluated using three criteria, as follows.

- (i) Effect on wind power integration;
- (ii) Effect on grid voltage stability;
- (iii) Effect on reducing the mismatch between the grid demand and the wind farm output (i.e. the grid demand mismatch).

The techniques for measuring the effects are presented below.

#### ***4.3.4.1 Technique for quantifying ESS effect on wind power integration***

To measure the ESS efficacy in increasing wind power integration, the total amount of wind energy discharged by the ESS during the year of consideration is calculated for different ESS ratings. The discharged energy is the additional amount of wind energy that is integrated into the grid thanks to the use of the ESS.

All possible ESS ratings are considered for computing the annual discharged energy, as follows. The considered ESS power rating is changed from 1 MW to 183 MW (i.e. up to the wind farm nameplate rating) in 1-MW increment. This results in 183 power rating variants. Meanwhile, the discharge duration (i.e. energy rating) is varied from 0.5 hour to 8 hours in a 0.5-hour increment. This results in 16 energy rating variants. The power and energy variants are then combined to create different ESS rating-combinations. A combination is the rating for an ESS. For example, 60 MW and 5 hours are the power and energy rating of the 60MW/5h ESS. As the result, there are 2,928 combinations (183 x 16) or 2,928 ESS ratings. For clear presentation, each combination is called an ESS-variant. Note that each ESS-variant consists of two ratings, namely, a power rating in MW and an energy rating in hours.

For each ESS-variant, the discharged energy amount is calculated for the year of interest by replicating the ESS operation for the year (i.e. 2005). Note that this calculation technique does not require knowledge of the analytical relation between the ESS rating and discharged energy. There are 2,928 ESS-variants for which 2,928 discharged energy amounts are calculated. Consideration of such a large number of ESS-variants facilitates observation of how the discharged energy varies with respect to ESS rating.

#### ***4.3.4.2 Technique for quantifying ESS effect on grid voltage stability***

The system steady-state voltage stability condition is assessed using the V-Q modal analysis, or the eigenvalue analysis. For the grid voltages to be stable, all the eigenvalues (eigenvalues are real) must be greater than zero. The larger the eigenvalues, the more stable the system. For details of the eigenvalue analysis, refer to [11]. Since the power system of interest is not very large (27 buses), the system smallest eigenvalue is used as a single indicator of its voltage stability condition. By monitoring this eigenvalue, the variation of the lower limit of the system voltage stability can be obtained.

Note that the reactive reserve (i.e. Q-reserve) margin technique is not used here because it requires a huge amount of calculation of V-Q curves. As shown in Chapter 3, eigenvalue analysis provides a system-wide view of stability condition and is equivalent to Q-reserve margin

technique. Therefore, it is used as the sole technique for quantifying steady-state voltage stability in this study.

For quantifying the changes in the system stability, three scenarios are established, as follows.

- *Optimal scenario*: The system original condition with no wind farm, no ESS and all generators dispatch profiles are optimal (i.e. determined by the optimal power flow).
- *Base scenario*: The system condition under the optimal scenario but with the wind farm operational where its output is completely unregulated.
- *ESS-related scenario*: The system condition under the base scenario with the ESS operational for regulating the wind farm output variation.

The ESS effect on the grid voltage stability is quantified as follows. The system load profiles for the year are in 30-min resolution. This is equivalent to dividing the year of interest into 17,520 time intervals ( $365 \times 24 \times 2$ ). The dispatch profiles for the system generators, determined by optimal power flow (Section 4.3.2), are also in 30-min resolution. For consistency, the 183-MW wind farm power output profile is also averaged every 30 minutes to make it a 30-min resolution profile.

For each time interval of the 17,520 intervals, the system smallest eigenvalue is calculated. The stability condition for a time interval is called a stability event. Next, all the eigenvalues of the base scenario (i.e. with wind farm operational) are ranked descending and the bottom 8,539 eigenvalues are selected. This portfolio (i.e. 8,539 eigenvalues) will be used as base case for comparison when validating the grid stability conditions with ESS. The reason for selecting this portfolio is as follows. The smallest eigenvalue of the 27-bus system under peak load condition is 1.4028. Simulation shows that the system is in normal operation condition with all bus voltages within +/-5% limits (i.e. between 95–100% of the nominal values). In addition, there is no generator or transmission line overload. The eigenvalue of 1.4028 is obtained under peak load condition and hence considered a lower stability limit. The magnitude of the selected 8,539 eigenvalues ranges from 1.211 to 1.4. Comparing the three eigenvalues, the grid stability lower limit is reduced by 0.2%–13.7% due to the 183-MW wind farm operation. This means that the selected portfolio essentially includes all worsen eigenvalues. Observation of this portfolio would reveal the true voltage stability condition of the 27-bus grid.

With an ESS in operation to regulate the wind farm output, the grid stability condition is expected to improve (i.e. the smallest eigenvalue becomes larger) most of the time. However, for certain stability events (out of 8,539), the stability level may be reduced compared to the base

scenario, where the wind farm output is completely unregulated. This is because the aggregated system (the wind farm and the ESS) is operated to achieve the desired output profile. As described in Section 4.3.2 and 4.3.3, the desired output profile is calculated using optimal power flow, which aims at reducing the total cost of generated power. Therefore, at times the ESS operation may lower the grid stability level to some extent for maximizing the overall economic benefit, provided the grid safe operation limits are not violated. The operation limits are supply-demand balance, line power-carrying capability and generator limits (see Section 4.3.2). It follows that the grid overall stability improvement is actually *net improvement*, resulting from subtracting the number of reduced eigenvalues from total improved eigenvalues.

From the above discussion, the net improvement in the grid stability because of ESS is calculated as follows.

- (i) For each of the considered ESS-variants (2,928 in total), compare the ESS-related 8,539 eigenvalues with the respective base-scenario eigenvalues.
- (ii) Count the number of improved eigenvalues thanks to the ESS operation. This sum is called GAIN.
- (iii) Count the number of reduced eigenvalues because of the ESS operation. This sum is called LOSS.
- (iv) The net improvement in the grid stability condition (in percentage) is computed as  $100 \cdot (\text{GAIN} - \text{LOSS}) / 8,539$ .

#### ***4.3.4.3 Technique for quantifying ESS effect on demand mismatch reduction***

The grid demand mismatch reduction is measured using coefficient of correlation (*CR*) where the correlation between the ESS-regulated output and the grid demand (i.e. the desired output) is calculated and plotted for different ESS ratings. Recall that the ESS-regulated output is the combined output between the wind farm and the ESS.

***Interpretation of coefficient of correlation:*** A parameter used to characterize the variation-relation between two parameters  $x$  and  $y$ . The range of values of the coefficient of correlation is  $[-1,1]$ . The negative sign means the two considered parameters  $x$  and  $y$  vary in the opposite direction (i.e. mismatch) and the positive sign means that they vary in the same direction. The absolute value of *CR* is the degree of correlation. If  $CR = 0$  the parameters  $x$  and  $y$  have no correlation [62]. In this study context,  $x$  is either the wind farm unregulated power output or the ESS-regulated output while  $y$  is the grid demand (i.e. the desired output). Therefore, the

closer the  $CR$  is to the value of  $-1$ , the worse the mismatch between the two outputs. Likewise, as  $CR$  goes from  $-1$  to  $0^-$ , the mismatch lessens.

#### **4.4 CASE STUDY RESULTS AND ANALYSES**

The obtained ESS effects on (i) wind power integration, (ii) grid voltage stability, and (iii) load-demand mismatch reduction, are presented in the following sections. The results are specific to the 27-bus transmission grid and the 183-MW wind farm. However, the approach used in this study would apply to other power systems.

##### **4.4.1 ESS effect on wind power integration**

Recall that there are 2,928 rating-combinations between the ESS power rating (1–183 MW) and discharge duration (0.5–8 hours) which are called ESS-variants. The ESS ability to store surplus wind energy and re-dispatch the stored energy depends on its rating. Figure 4.3 illustrates how the total amount of discharged energy over the year of interest varies as the power rating of the ESS changes. The discharge duration is fixed to facilitate clear presentation. In Fig. 4.3, “Dd=8h” means “the ESS discharge duration (i.e. energy rating) is 8 hours”.

From Fig. 4.3 it is visible that, for any discharge duration (i.e. 1 hour, 2 hours, etc), the amount of wind energy saved and discharged by the ESS (discharged energy) increases as the ESS power rating increases. For any power rating (e.g. 170 MW) the ESS with longer discharge duration (i.e. higher energy rating) can store and integrate more wind energy into the power system. In other words, the larger the ESS, the higher its ability to regulate the wind farm output. This result is logical and expected.

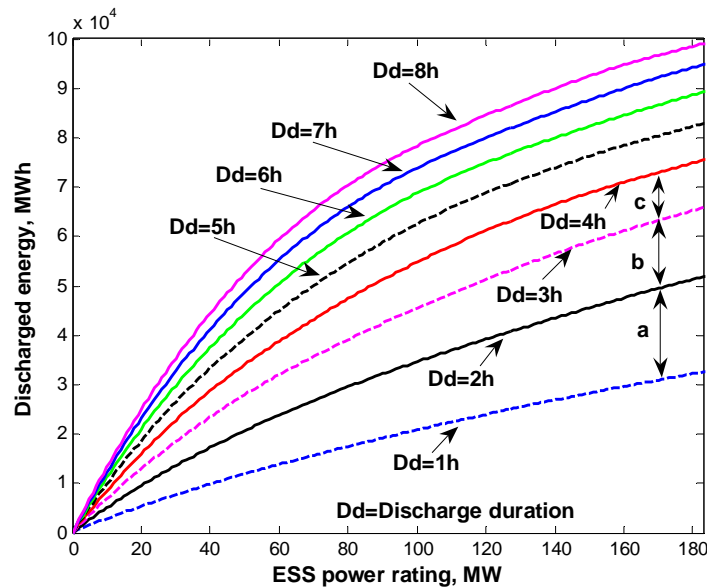


Fig. 4.3 Discharged wind energy versus ESS rating

The relationship between the ESS rating and discharged energy is non-linear. For a given ESS power rating, as the discharge duration increases, the discharged energy increases by large amounts at first, then by smaller amounts. One can infer based on this observation that doubling an ESS rating does not necessarily increase the discharged energy twice. Therefore, to maximize the ESS overall benefit, its rating must be optimized.

Taking the same power rating of 170 MW as an example, the increases in discharged energy for energy ratings of 2, 3, and 4 hours, compared to that of the respective immediate-lower energy rating, are “a”, “b”, and “c” where  $a \gg b \gg c$ .

Quantitatively, for the power rating 170 MW, the annual discharged energy for the ESS with 1-hour energy rating is 30941.8 MWh. The discharged energy for the 2-hour energy rating is 49501.8 MWh i.e. 60-percent increase compared to that for 1-hour energy rating. Likewise, the increases in discharged energy for 3-hour energy rating versus 2-hour, 4-hour versus 3-hour, 5-hour versus 4-hour are 27.8%, 15.4%, 10.1%, respectively. The increases in discharged energy for 6-hour versus 5-hour, 7-hour versus 6-hour, and 8-hour versus 7-hour are just in the range of 4.9%–7.8%.

Overall, for the chosen 170-MW ESS power rating, the discharged energy increases fast when the discharge duration increases from 1 to 5 hours. By contrast, the discharged energy increases at a slower rate when the discharge duration is raised to 6, 7 and 8 hours. The similar trend can be obtained by visual inspection of Fig. 4.3 for other ESS power and energy ratings.

This result leads to an interesting observation that the best discharge duration should be between 1 and 5 hours. The estimation could be useful when determining the optimal rating for the ESS.

Without the ESS, the integrated wind energy for the year (i.e. 2005) is 300,577 MWh. The integrated energy is the amount channeled into the grid freely without the aid of the ESS and with economic value (i.e. with payment). The surplus wind power which cannot be stored by the ESS is channeled into the grid without payment. Therefore, it does not count towards the integrated energy. The smallest ESS (1MW/0.5h) can save additional 182.5 MWh and the biggest ESS (183MW/8h) can save 99,027.8 MWh for that year. Comparing the additional energy amounts for the two ESSs with the integrated energy (300,577 MWh), the increase in wind energy integration is between 0.1%–32.9%.

#### **4.4.2 ESS effect on grid voltage stability**

Recall that the reactive reserve margin (i.e. Q-reserve) technique is not used to evaluate the ESS effect on grid voltage stability because it requires a huge amount of calculation of V-Q curves. Eigenvalue analysis is used as the sole technique because it provides a system-wide view of the grid stability condition and is equivalent to Q-reserve margin technique.

The ESS ability to supply reactive power is not considered in this study, because of the following reason. The small-disturbance voltage stability of interest primarily involves grid steady-state conditions. It is assumed that the 183-MW wind farm is operated at unity power factor and its reactive demand is fully met by capacitor banks in steady-state. As the result, the ESS is not used for supplying the farm with reactive power, but for regulating the farm real power output only. Its impact on the grid voltage stability, therefore, results from its ability to reduce the farm real power output variation. The ESS ability to stabilize a wind farm by dynamic reactive supply is investigated in Chapter 6.

Recall that the grid overall stability improvement by the ESS operation is actually *net improvement*, resulting from subtracting the number of reduced eigenvalues from total improved eigenvalues. For details of the net improvement calculation, see Section 4.3.4.2.

Figure 4.4 shows the percentage net improvement in the system voltage stability. For clear presentation, the ESS discharge duration is fixed while its power rating is varied. By regulating the wind farm power output variability, the ESS raises the system stability limit by at least 2.7% compared to the base case. The 2.7-percent net improvement is for the discharge duration of 0.5 hours and is not shown in Fig. 4.4. Overall, the stability improvement by the ESS ranges from 2.7% to 22.3%.

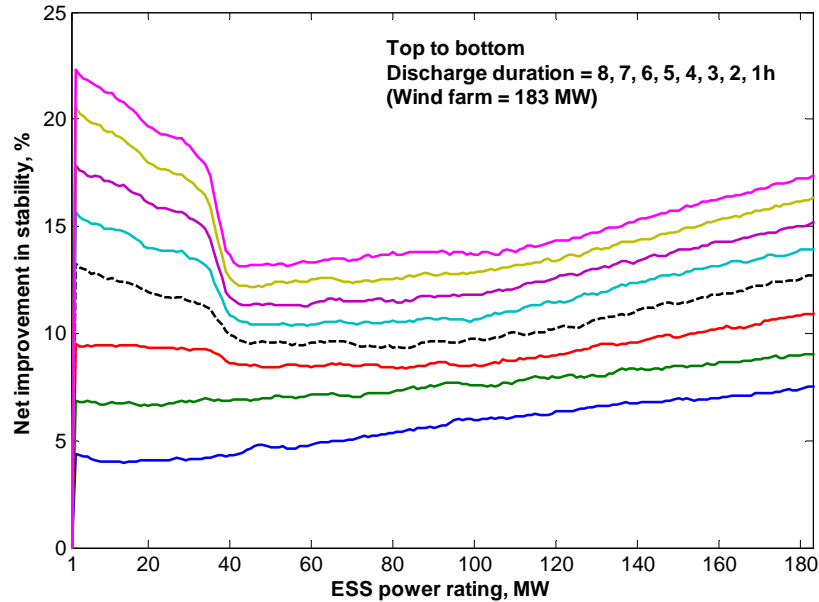


Fig. 4.4 Voltage stability net improvement vs. ESS rating

The relationship between the system net stability increase and the ESS rating is nonlinear. Visual inspection of Fig. 4.4 shows that higher net stability improvement is achieved for the ESS power rating range of 1–35 MW and the energy rating range of 4–8 hours. In Section 4.4.1 it is estimated that the ESS energy rating should be between 1–5 hours. Combining the results, the ESS best rating is estimated to be in the range of 1–35 MW and 4–5 hours. This finding may be useful when solving the ESS sizing problem in Chapter 5.

However, because of the nonlinearity of the relationship between ESS rating and either discharged energy or voltage stability improvement, the best rating can be found only by optimization. The optimal rating is likely a trade-off between the ESS benefits and its cost.

#### 4.4.3 ESS effect on load-demand mismatch reduction

It is obvious that ESS with different ratings have different impacts on demand mismatch reduction because their abilities to store and re-dispatch wind power (i.e. to regulate the wind farm output) differ. To visualize how an ESS can mitigate the demand-mismatch, a 60MW/5h ESS is chosen and its effect on regulating the wind farm output is plotted for two days. The power rating of 60 MW is 32.8% of the farm name-plate rating (183 MW). Likewise, the value of 32.8% is a representative capacity factor for wind farms in general. The energy rating of 5 hours

is selected based on the previous analyses in Section 4.4.1 and 4.4.2, which show that 5-hour discharge duration may be an optimal ESS energy rating.

The ESS impact on the demand mismatch reduction is also quantified using coefficient of correlation for the considered range of ESS rating (1–183 MW and 0.5–8 hours). This analysis would give a more comprehensive view of the ESS ability to reduce the mismatch between the wind farm and the grid demand (i.e. the desired output).

#### 4.4.3.1 Load-demand mismatch reduction by observation

Figures 4.5 and 4.6 illustrate how the wind farm output variation is regulated by the 60MW/5h ESS for a winter day and a summer day. The dotted blue line is the wind farm unregulated output (the farm natural output). The black-x line is the desired output, which is the target for the aggregate system (the wind farm and the ESS) to achieve for the grid benefit. The red bold line is the aggregate system output, or the farm regulated output by the ESS.

Recall that the surplus wind power output level is the output that exceeds the respective desired output level. Conversely, the output that is below the respective desired output is the deficit. For example, in Fig. 4.5 and 4.6, areas 1 and 3, which are bounded by the dotted blue and the black-x lines and lie above the desired-output line, represent the wind power surplus. Areas 2, lying below the desired-output line, represent the power deficit.

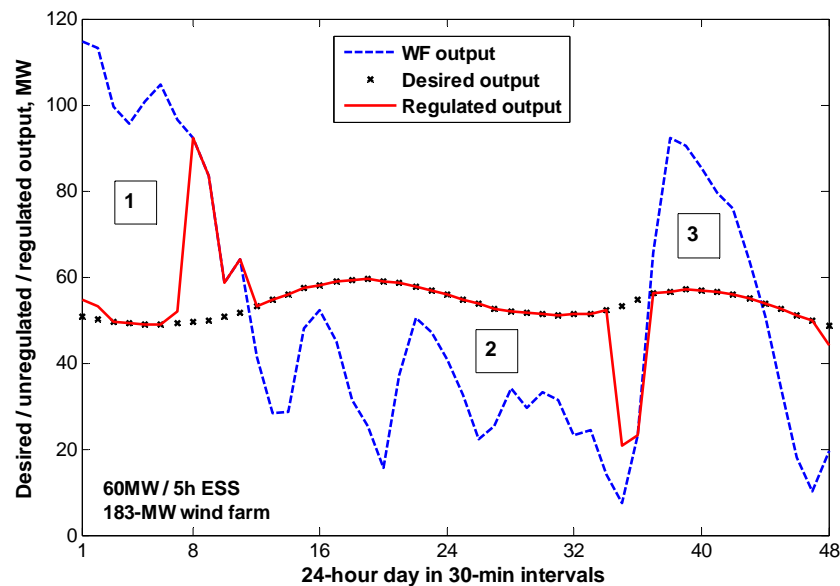


Fig. 4.5 Regulated wind farm output for a winter day (Feb 05, 2005)

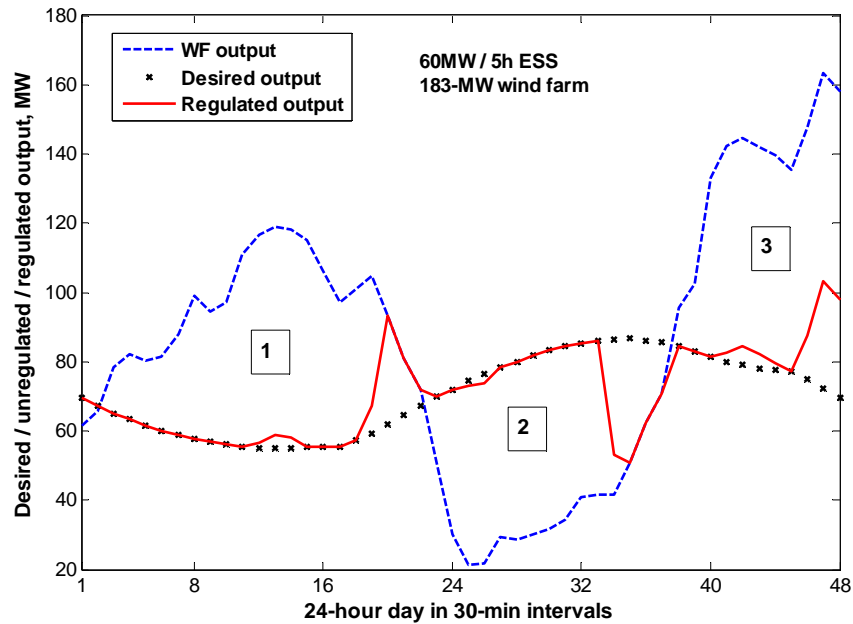


Fig. 4.6 Regulated wind farm output for a summer day (Jul 24, 2005)

From Fig. 4.5, during the early hours of the winter day, the 60MW/5h ESS stores certain amount of wind power surplus (Area 1). It is visible that the ESS cannot store all the surplus wind power of Area 1, so some wind power surplus is allowed to integrate into the system. This is why the regulated output (red bold line) goes up instead of following the desired output (black-x line) exactly. Later, the ESS discharges the stored power when the wind farm power output drops below the desired output (Area 2 represents the deficit power and duration). The regulated output follows the desired output tightly for most of the deficit duration, meaning that the ESS is able to compensate for most of the deficit power. The ESS charges again when the wind farm output exceeds the desired output (Area 3). After that, it releases the stored energy again as the farm output drops. A similar situation can be observed from Fig. 4.6.

Overall, the 60MW/5h ESS regulates the 183-MW wind farm output effectively during the two observed days. The two figures show that the regulated output matches the respective desired output most of the time. For the winter day, the ESS performs two charge-discharge cycles during the 24-hour period. For the summer day, it charges two times and discharges once.

#### 4.4.3.2 Load-demand mismatch reduction by coefficient of correlation

Figure 4.7 shows how the demand-mismatch is reduced by the ESS with different ratings using coefficient of correlation. Table 4.2 shows the values of correlation coefficient for selected ESS ratings and the percentage reduction in demand-mismatch.

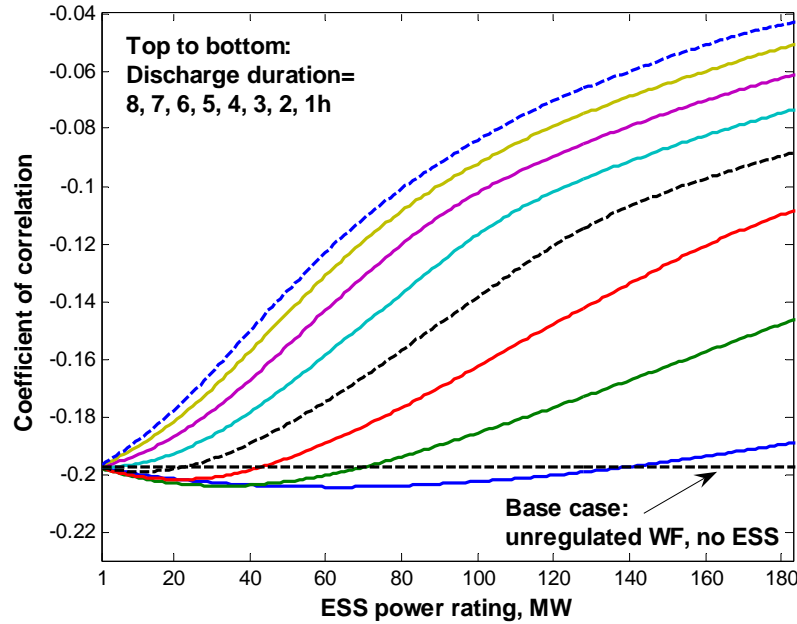


Fig. 4.7 Correlation between regulated 183-MW wind farm output and grid demand

Table 4.2 Correlation coefficient and reduction in demand-mismatch

ESS power rating, MW	ESS discharge durations, hours							
	1 h	2 h	3 h	4 h	5 h	6 h	7 h	8 h
20 MW	-0.2016	-0.2032	-0.2018	-0.1982	-0.1928	-0.1871	-0.1818	-0.1779
60 MW	-0.2045	-0.2005	-0.1891	-0.1748	-0.1586	-0.1430	-0.1311	-0.1230
100 MW	-0.2026	-0.1857	-0.1627	-0.1386	-0.1169	-0.1023	-0.0923	-0.0840
140 MW	-0.1974	-0.1674	-0.1339	-0.1071	-0.0915	-0.0792	-0.0689	-0.0603
180 MW	-0.1898	-0.1479	-0.1099	-0.0896	-0.0746	-0.0625	-0.0521	-0.0440
	Demand-mismatch reduction, %							
20 MW	-2.1	-2.8	-2.2	-0.3	2.4	5.3	8.0	9.9
60 MW	-3.5	-1.5	4.3	11.5	19.7	27.6	33.6	37.8
100 MW	-2.5	6.0	17.7	29.8	40.8	48.2	53.3	57.5
140 MW	0.1	15.3	32.2	45.8	53.7	59.9	65.1	69.5
180 MW	3.9	25.2	44.3	54.7	62.2	68.4	73.6	77.7

**Note:** For demand-mismatch reduction, positive sign (+) means that demand-mismatch reduction is achieved; negative sign (-) means that the mismatch worsens.

In Table 4.2, the percentage reduction is calculated based on the coefficient of correlation of the base case (i.e.  $-0.1976$ ). For example, the percentage reduction for the 100MW/2h ESS is computed as  $100 \times (-0.1976 - (-0.1857)) / (-0.1976) = 6\%$ .

Figure 4.7 and Table 4.2 show that, as the ESS rating increases, the correlation coefficient becomes less negative in general. This means that the mismatch between the ESS-regulated output and the desired output is reduced. In other words, the ESS is able to regulate wind farm output and make it a better match for the system demand. The degree of mismatch reduction increases as the ESS becomes larger. A 20MW/5h ESS can reduce the mismatch by 2.4% while a 60MW/5h ESS can reduce the mismatch by 19.7%. Very large ESS, such as 140MW/6h or 180MW/7h can lower the mismatch by 59.9% and 73.6%, respectively. Overall, the reduction in demand-mismatch by the ESS ranges from 0.1% to 77.7%. This result is specific to the 183-MW wind farm output profile but may be an estimation for other wind farm outputs.

#### 4.5 CHAPTER CONCLUDING REMARKS

This study develops the solution steps required for implementing an application using energy storage systems (ESS) for regulating wind farm power output variation. The ESS-based application implementation and its effects are evaluated via a case study. Three key ESS effects are accessed, namely, (i) wind power integration, (ii) grid voltage stability, and (iii) load-demand mismatch reduction. The obtained results have led to the following conclusions:

- (i) ***Technique for calculating desired output profile:*** The proposed technique uses optimal power flow to determine the best output profile achievable by the aggregate system for the benefit of the grid. The term “benefit” is defined as “minimizing the total cost of grid generated power”. Regulating the wind farm output according to the desired profile causes the farm to behave like a dispatchable power source while taking into account the cost of system generation.
- (ii) ***Wind power integration and grid voltage stability:*** Installing the ESS to regulate the wind farm output variability proves to be beneficial. By storing surplus wind energy and re-dispatching it appropriately, the ESS increases wind energy integration by 0.1%–32.9%. In addition, ESS can raise the system voltage stability by 2.7% to 22.3%, compared to the case where the wind farm output variability is completely unregulated. The results are specific to the 183-MW wind farm and ESS rating of 1–183 MW and 0.5–8 hours. The impacts of

optimal ESS on increasing wind power integration and steady-state voltage stability are further investigated in Chapter 5 with 17 wind farms.

- (iii) ***Demand-mismatch reduction:*** The ESS is very effective in reducing the mismatch between the wind farm output and the grid demand. An average-size ESS may be able to reshape the wind farm output to match the system demand many days during the considered year. For the ESS rating of 1–183 MW and 0.5–8 hours, the demand-mismatch reduction ranges from 0.1% to 77.7%. The result is specific to the 183-MW wind farm output profile but may be an estimation for other wind farm outputs.

Overall, the developed solution steps are applied successfully for designing an ESS-based application. The remaining important task in the application design is to find the optimal rating for ESS (i.e. solving the ESS unit-sizing problem). This is essential because an ESS project, like any project, can be implemented only if it is cost-justified. The technique for optimizing ESS rating is presented in Chapter 5.

## Chapter 5

### Determination of ESS optimal rating and impacts on wind power integration and voltage stability

#### 5.1 INTRODUCTION

Determining optimal rating for ESS, or sizing of ESS, is the last step defined in the framework for designing an ESS-based application (Section 4.1.2, Chapter 4). The ESS-based application is also called wind power firming application because the ESS helps make wind farm output “firmer”, i.e. more deterministic and less variable. Unit-sizing of ESS is deemed the most important task in the application design. An ESS project, like any project, can be implemented only if it is cost-justified. Therefore, the formulation of the ESS optimal-sizing problem must take into account all possible ESS costs and benefits. The solution for the problem is the ESS optimal rating, which actually consists of two sub-ratings – the power rating in MW and the energy rating in hours.

This study is related to the previous study in Chapter 4 as follows. The previous study outlines the framework for the ESS-based application. It provides a broad picture of the ESS efficacy. For example, the ESS impacts on wind power integration and voltage stability are obtained for a wide range of ESS rating (1–183 MW and 0.5–8 hours). In this study, economic requirements of ESS are considered in addition to its technical efficacy (e.g. ability to regulate wind farm output variability and enhance stability). A wide range of ESS rating is to be narrowed down to an unique rating by balancing ESS benefits and cost. From optimization viewpoint, the unique ESS rating is a global optimum or a local optimum for the ESS-sizing problem. For implementing the ESS-based application, knowledge of the ESS unique rating is required. Following the above discussion, the goals of this study are:

- (i) To formulate and solve the ESS-sizing problem for the ESS optimal rating;
- (ii) To analyze the economic aspects of ESS in terms of cost, revenue and profit;
- (iii) To quantify the ESS impacts in terms of wind power integration and grid steady-state voltage stability with respect to its optimal rating.

With respect to the defined goals, a novel optimization-based method (also called direct-calculation method), is proposed for solving the ESS-sizing problem. The method employs formulation of a cost-based objective function, discretization of this function, and exhaustive search of the function values to find the ESS optimal rating. The ESS benefits, such as increased wind power integration and voltage stability improvement, and ESS cost are included in the objective function.

The effectiveness of the solution method is validated by a case study with a large data set of 14 wind farms with diverse characteristics, a wide range of ESS rating (0.5–165 MW and 0.5–8 hours) and 27-bus grid realistic load conditions. For the 27-bus grid description, see Section 4.3.1 and Appendix A3. The ESS technology under consideration is compressed-air energy storage (CAES). The ESS impacts on wind power integration and grid steady-state voltage stability are quantified using the techniques in Section 4.3.4.1 and 4.3.4.2, respectively. The ESS switching operation is also obtained. All computing codes are written in Matlab.

The results show that the proposed method works well with the large data set. An optimal ESS rating can be found for a wind farm with a high degree of accuracy. The results show a significant trend that may be used to estimate CAES rating for similar wind farms without rigorous calculation. For wind farms with rating of 91.5–210 MW and a capacity factor of 33% or better, the optimal ESS power rating is 9%–14% (10.5–19 MW) of the farm nameplate capacity. The optimal ESS energy rating (i.e. the optimal discharge duration) is between 4 and 4.5 hours. The result is based on the ESS operating under the developed charge-discharge scheme and being able to discharge 100% of accumulated energy. Recall that the previous study in Chapter 4 estimates the best ESS rating to be in the range of 1–35 MW and 4–5 hours, which is relatively close to the exact result by optimization.

The use of ESS improves wind power integration. Overall, the enhancement in wind energy integration is 1.7%–8%. Of the 14 evaluated ESSs, 13 ESSs achieve a net increase in stability between 8.3% and 18.3%. On average, the ESSs perform 2.5–3.1 switching operations per day, which is beneficial in preserving the equipment life.

**Publication:** Part of the work presented in this chapter has been published in the proceeding of *IEEE Power & Energy Society General Meeting 2008* with the title "Sizing Energy Storage Systems for Wind Power Firming: An Analytical Approach and a Cost-Benefit Analysis" [36].

## **5.2 ANALYTICAL SOLUTION: PROBLEM ANALYSIS, FORMULATION, AND SOLUTION**

### **5.2.1 Problem analysis and formulation**

The author's review of the literature finds that little work has been done in the area of energy storage sizing for large grid applications up to 2007, which is the year this study had been carried out. A few studies found are [63] and [64], which were published in 2003 and 2005, respectively. In the 2003-study [63], the authors presents an algorithm for calculating the optimal dispatch of an energy storage system. The algorithm takes into account the short-term energy exchange and the expected imbalance penalties of a 10-MW wind farm. The 2005-report of the Sandia Lab [64] describes a methodology for estimating power and discharge duration ratings of storage systems for deferring upgrades of congested transmission and distribution nodes. The review's finding suggests a need for further research in this area.

As discussed in the introductory section, this study considers economic requirements of ESS in addition to its technical efficacy (e.g. ability to regulate wind farm output variability and improve stability). A unique ESS rating, which is required for implementing the ESS-based application, is to be found by balancing the ESS benefits and cost. The reason for considering economic factors is simple – any ESS project is feasible only if it is cost-justified. Therefore, profit is naturally the control factor over the ESS-sizing process.

The profit of an ESS project is the amount obtained by subtracting the ESS cost (i.e. ESS financial requirement) from the project total revenue (i.e. the ESS monetary benefits). To calculate the profit, ESS cost and benefits must be determined. The following are the possible benefits of the ESS-based application:

- Integrating (selling) more wind energy into the power grid;
- Generation capacity firming;
- Improved grid voltage stability;
- Improved grid reliability;
- Environmental-related benefit, such as reduced green-house gas emission.

It is logical that the identified benefits are used as criteria for determining the optimal rating of the ESS. Hence, the ESS sizing problem can be formulated as an optimization problem where the goal is to find an optimal rating of the ESS so as to maximize the net benefit (i.e. profit).

Taking into account the above five benefit factors, the cost-based objective function can be defined as

$$B = M_E + M_{CF} + M_{VS} + M_{RL} + M_{EV} - M_{ESS} \quad (5.1)$$

where

- $B =$  Net profit (i.e. benefit) obtained per year, [\$/year].
- $M_E =$  Revenue (money) earned from saving and integrating an amount of wind power into the grid that otherwise not integrated, [\$/year]. The additional energy is called ESS discharged energy. Further explanation for this benefit term is provided in Section 5.3.1.
- $M_{CF} =$  Revenue from wind farm capacity firming. This benefit results from avoiding the need to add other generation equipment [65], [\$/year].
- $M_{VS} =$  Revenue from improved voltage stability, [\$/year];
- $M_{RL} =$  Revenue from improved reliability, [\$/year].
- $M_{EV} =$  Revenue from environmental considerations, [\$/year].
- $M_{ESS} =$  Annual financial requirement of ESS. Based on [65], this is the monies needed to service debt or equity capital used to purchase and install, or lease the ESS, including operation and maintenance costs and tax effects. Simply speaking, this is the annualized cost of the ESS. Utilities must meet this revenue before making any profit [\$/year]. Details of calculating this term are provided in Section 5.3.3.

It follows that the ESS-sizing problem is

$$\text{Max}_{\langle \text{ESS rating} \rangle} B = M_E + M_{CF} + M_{VS} + M_{RL} + M_{EV} - M_{ESS} \quad (5.2)$$

All the terms on the right-hand side of (5.2) are assumed to be functions of ESS rating. A specific problem may be subjected to certain constraints or boundary conditions, depending on detailed formulation and/or solution method.

***Alternate problem formulation:*** The ESS-sizing problem can be formulated as a “maximizing investment return rate” problem. Return rate is the ratio between the net profit and the total cost (i.e. the investment). Maximizing return rate is an indirect way of maximizing profit. Since maximizing profit is more straightforward, it is chosen for this study. The formulation using return rate, however, may be interesting and is left for future study.

***Partial problem and staged solution:*** The ESS-sizing problem in (5.2) may be formulated with less than five identified benefit terms, in case a benefit term is hard to quantify. In this case the problem is named a “partial problem” and the solution is called a “staged

solution”. Yet a staged solution can provide useful information such as initial estimate of the project profit. This helps utilities in the decision-making process such as deciding whether to proceed with the project comprehensive feasibility study. Other variables, such as the benefit terms other than the five terms in (5.2), may also be included in the same manner. Irrespective of the number of included terms, the problem may be solved using the same solution method, described in the following Section 5.2.2. This is the flexibility of the proposed method.

### **5.2.2 Problem solution**

The problem in (5.2) may be solved in two ways, namely, (a) Solution by conventional optimization methods and (b) Solution by direct calculation method. The solution by conventional optimization methods means “solving the problem by traditional differential-based optimization methods”. It requires, in general, knowledge of the analytical form of the objective function. For this to happen, the analytical form of all the terms on the right-hand side of (5.2) must be determined. Determining the analytical objective function is sometimes complicated. Therefore, a new method is proposed. It is called the “direct-calculation method” or “optimization-based method” for identification. The name “optimization-based” results from the fact that the method employs optimization concepts, such as formulation of an objective function, finding an optimum etc. The difference is that it solves the ESS-sizing problem in (5.2) by discretization of the objective function and exhaustive search of the function values instead of using differential calculus.

The proposed direct-calculation method works as follows. Based on the problem characteristics, a sufficiently-large set of variable-values is selected. Next, the values of the objective function are calculated based on the selected variable-values. The obtained values of the objective function form a pool of solution candidates. Finally, a search is performed to find the maximum (or maxima) of the objective function within the pool of candidates. The maximum (or maxima) and the variable-values associated with them forms the desired solution. In short, this method combines discretization of the objective function and exhaustive search of the function values to find the desired solution.

For the ESS-sizing problem, the variable-values are various ESS power and energy ratings. The calculated values of the objective function are the net profit amounts specific to the considered ESS ratings. The desired maximum is the largest profit for the ESS and the associated variable-values are the ESS optimal power and energy ratings.

The proposed method is particularly useful in solving the ESS unit-sizing problem in (5.2) because the analytical form of several terms on the right hand side of (5.2) is hard to

determine. For this problem, it is envisioned that the set of variable-values can be bounded. Suppose we want to find the optimal rating for an ESS for use with a 150-MW wind farm. Then, the power rating of the ESS (i.e. a maximum variable-value) can be limited to 150 MW. As discussed in Section 4.2.1, the ESS regulates only part of the wind farm power output. Therefore, it is likely that the ESS optimal power rating is less than the farm nameplate rating. As estimated in Chapter 4, the ESS best energy rating could be between 1–5 hours. In an extreme scenario, the ESS energy rating may be up to a few days or weeks. Even if that is the case, the set of ESS ratings can still be bounded. Hence, it follows that the number of solution candidates (i.e. ESS profit) is limited. This ensures the feasibility of the proposed solution method. Section 5.3 presents a case study to demonstrate the method efficacy.

#### ***Steps for solution by direct calculation method***

- 1) ***Step 1:*** Based on the problem characteristics, such as wind farm, ESS technology, and possible benefits, formulate a cost-based objective function according to the model defined in (5.2).
- 2) ***Step 2:*** Select a range of ESS power rating and energy rating (i.e. discharge duration). All possible combinations between the ESS power and energy rating (called ESS-variants) within the selected range form a set of variable-values (or a set of ESS-variants) for consideration.
- 3) ***Step 3:*** Calculate the net profit  $B$  for the set of ESS-variants selected in Step 2 based on the objective function formulated in Step 1. The obtained profit amounts form a pool of solution candidates.
- 4) ***Step 4:*** Perform an exhaustive search for the highest profit within the pool of solution candidates obtained in Step 3. The ESS rating (i.e. power rating and discharge duration) associated with this profit is the desired optimal rating.

### **5.3 FORMULATION OF A CASE STUDY**

In this case study, the direct-calculation method is applied to determine the optimal ESS ratings for 14 wind farms. It is followed by an analysis of the economic aspects of the ESS projects (revenue, cost and profit), and quantification of the ESSs impacts on wind energy integration and steady-state voltage stability. The available data are the farms measured power outputs for a year, the 27-bus power system (Section 4.2.1 and Appendix A3), and the time-series annual demand of a large power utility. The energy storage technology under consideration is compressed-air energy storage (CAES). CAES is selected because it is found to be very cost

effective for bulk energy storage and relatively commercially-matured [66]. The data for wind farms, system demand, and CAES costs are selected during the period 2004–2006.

### ***Reformulation of objective function***

Among the five benefit terms in (5.2), it is recognized that the revenue from discharged energy  $M_E$  may be calculated directly based on ESS rating, although it may not be expressed as a function of ESS rating analytically. The revenue from wind farm capacity firming  $M_{CF}$  may be expressed as a function of ESS rating.

However, the remaining three benefit terms are difficult to determine. There is no established technique to express, say,  $M_{VS}$ , the revenue from improved voltage stability, as a function of ESS rating, or in terms of money. Two common criteria for measuring grid voltage stability are reactive reserve margin and eigenvalues [11]. Unlike discharged wind energy, voltage stability is not an item for direct sale. Rather, it is indirectly related to energy sale through ensuring a required condition for grid normal operation, which enables electricity delivery and sale. Therefore, it is very involved to express voltage stability as a function of ESS rating or in monetary terms. One faces a similar situation with the revenue from improved reliability  $M_{RL}$ , and the revenue from environmental considerations  $M_{EV}$ . To overcome the difficulty, the ESS-sizing problem in (5.2) is re-formulated as follows:

$$\text{Max}_{\langle \text{ESS rating} \rangle} \quad B = M_E + M_{OTHER} - M_{ESS} \quad (5.3)$$

The benefit term  $M_{OTHER}$  includes four remaining benefit terms in (5.2). This formulation allows one to by-pass any of the four benefit terms that cannot yet be determined and proceed to find a staged solution. Following the solution steps in Section 5.2.2, for each wind farm, first the net profit  $B$  is calculated for different ESS rating combinations (i.e. ESS variants), then a search is performed for the highest profit and the associated ESS rating i.e. the desired solution.

### **5.3.1 Calculating revenue from discharged energy**

The main idea behind generating this revenue is to store and integrate into the grid the wind energy that would otherwise be lost. The revenue is calculated as follows.

Wind farm output profiles may be classified into two main types, namely, non-firm (or unregulated output) and desired output. The unregulated output profile is the natural output of the wind farm, which is the energy converted by the farm turbines for a period of time, such as one year. The desired output is the most beneficial output for the grid, where “beneficial” means “minimizing the total cost of grid generated power” (see Section 4.3.2 for further explanation).

As shown in Chapter 4, a wind farm unregulated output profile poorly matches the desired output profile in general. This results in discarding certain amount of wind power on many occasions. Typically, at a given time  $t$ , the wind farm output that exceeds the desired output level has to be reduced. This means that a significant amount of wind energy is left unconverted, not integrated into the grid (i.e. the energy is lost). Even when some of the surplus wind power is allowed to be integrated into the grid, its value is likely to be low because it is sold at time of low demand. Therefore, one of the major objectives when installing the ESS is to save the surplus wind power and later integrate it into the grid appropriately.

Following the above discussion, in this study, all the output data of the 14 wind farms are considered unregulated outputs. Furthermore, it is assumed that, at any time  $t$ , any amount of wind power that exceeds the desired output level (the surplus wind power) either has to be stored by the ESS, or is allowed to integrate into the grid without payment. Integration of the excess wind energy forces the grid other generators to reduce their outputs for ensuring the supply-demand balance. This may raise the total cost of the grid generated power to some extent. It is ideal to make the combined output (of a wind farm and its associated ESS) an exact match for the desired output. Though, certain reduction in the total cost of generated power is achieved just by bringing the combined output closer to the desired output. Therefore, it is still worthwhile regulating the wind farm output fluctuation. The revenue from discharged energy  $M_E$  is generated by selling the energy discharged by the ESS. As explained before, this is the additional amount of integrated wind energy that would not be integrated without the ESS.

The annual revenue obtained from saving and integrating more wind energy into power grid (i.e. the energy discharged by the ESS over a year) is calculated as

$$M_E (\$/year) = \text{Energy price } (\$/MWh) \times \text{Discharged energy } E_{DC} (MWh) \quad (5.4)$$

Since the energy price is known, the remaining task is to calculate the energy discharged by the ESS for the year of interest. Without knowing the analytical relation between ESS rating and discharged energy, this amount of energy is found by replicating ESS operation for one year. The replication of ESS operation is possible for any ESS rating variant of interest by using each wind farm power output profile, the respective desired output, and the ESS charge-discharge scheme (defined in Section 4.3.3).

The desired output profile is determined using optimal power flow (OPF) which is presented in Section 4.3.2. A brief description of the technique is provided here for reader convenience. An equivalent conventional generator is assumed to be placed in the considered

wind farm location. Then, OPF is used to find the output of the generator. The assumed generator output is the desired output. The rating of the assumed generator is adjusted so that its average output and the wind farm unregulated average output are identical. For very large wind farms, if its unregulated average output is larger than the average optimal output (determined by OPF for the wind farm), the OPF output is chosen to be the desired output. For example, the maximum average optimal output determined by OPF for Wind farm A is 61 MW. Wind farm A unregulated average output is 65 MW. Then, the rating of the assumed generator will not be adjusted further and the desired average output for Wind farm A is dictated by the OPF, i.e. 61 MW. For the 27-bus system and connection point bus *B4016* (see Appendix A3), this condition needs to be enforced upon two largest wind farms WF13 and WF14 (Table 5.1).

As said before, the annual discharged energy amount for each of the 14 wind farms of interest is determined by replicating the operation of the respective ESS for one year. This technique is previously presented in Section 4.3.4.1. The considered CAES power rating is 0.5–165 MW in 0.5-MW increment (i.e. 330 power rating variants) and the discharge duration is 0.5–8 hours in 0.5-hour increment (i.e. 16 energy rating variants). Therefore, the total ESS-variants is  $330 \times 16 = 5,280$ . As the result, 5,280 discharged energy amounts are calculated for the 5,280 ESS-variants.

### 5.3.2 Calculating revenue from other benefits

As said earlier,  $M_{OTHER}$  includes four benefit terms, namely, revenue from wind farm capacity firming  $M_{CF}$ , revenue from improved voltage stability  $M_{VS}$ , revenue from improved reliability  $M_{RL}$ , and revenue from environmental considerations  $M_{EV}$ .

The annual revenue from wind farm capacity firming  $M_{CF}$  results from avoiding the need to install new generation equipment and the increased value of wind farm integrated power. Based on [65], a standard assumption of wind generation correlation with peak demand is 30%, meaning that an ESS with the same nameplate rating as a wind farm can be used to firm up 70% of the farm output. Therefore, the ESS capacity firming benefit is claimed to be equal 70% of the annual carrying cost of a new combined-cycled power plant (CCPP) (i.e. avoided plant, \$65/kW-year), or \$45.5/kW-year ( $0.7 \times \$65/\text{kW-year}$ ). However, according to [67], the figure of \$45.5/kW-year may be an over-optimistic estimation. Overall, at the time of this calculation, the procedure or value accepted by the power industry for determining  $M_{OTHER}$  is lacking.

Therefore, it is assumed that, for the considered ESS power rating of 0.5–165 MW and discharge duration of 0.5–8 hours, combination of the four remaining benefits,  $M_{OTHER}$ , is a function of ESS rating and is worth \$45.5/kW-year.

$$M_{OTHER} (\$/year) = 45,500 (\$/MW - year) \times ESS \text{ power rating } (MW) \quad (5.5)$$

It should be emphasized that this assumption is made to enable a stage solution to the ESS-sizing problem in (5.2). As a consequence, the obtained results are valid under this assumption holding true. Though, a staged solution is deemed adequate for the study goals, namely, development of a method for determining optimal ESS rating and analysis of the ESS impacts with respect to the optimal rating.

### 5.3.3 Calculating ESS annual financial requirement

The ESS technology of interest in this case study is compressed-air storage system (CAES). The CAES annual financial requirement is determined based on the cost information for CAES bulk storage in [66]. Assuming the system life-cycle of 20 years, the ESS annual financial requirement is calculated as [66]

$$M_{ESS} (\$/year) = FCR \times TC (\$) + OM (\$/MW - year) \quad (5.6)$$

$$TC (\$) = C_{PCU} (\$) + C_{ESU} (\$) + BOP (\$)$$

where

$M_{ESS}$  = Annual financial requirement of ESS, [\$/year];

$FCR$  = Fixed charge rate, used to convert a plant total capital cost to annuity equivalent i.e. annual carrying charges for capital equipment [65].

For this case study,  $FCR = 0.12$

$TC$  = Total capital cost of ESS, [\$];

$OM$  = Fixed operation and maintenance cost, [\$/MW-year];

$C_{PCU}$  = Cost of ESS power conversion unit equipment, [\$];

$C_{ESU}$  = Cost of ESS energy storage unit, [\$];

$BOP$  = Balance of plant cost i.e. the cost involving systems whose power conversion unit is used both in charge and discharge modes, [\$].

$$C_{PCU} (\$) = \text{Power-related cost } (\$/MW) \times ESS \text{ power rating } (MW)$$

$$C_{ESU} (\$) = \text{Energy-related cost } (\$/MWh) \times \text{Energy rating } (MWh)$$

$$BOP (\$) = BOP \text{ cost } (\$/MWh) \times ESS \text{ energy rating } (MWh)$$

Recall that the rating of an ESS includes two components, the rating of the power conversion unit (i.e. the power rating in MW) and the rating of the energy storage unit (i.e. the energy rating in MWh). For CAES, the efficiency of the energy storage unit is included as part of the system overall efficiency. Therefore, the ESS energy rating  $E$  is calculated simply as  $E = P \times t$ , where  $P$  is the rating of the power conversion unit and  $t$  is the discharge duration [57, 58].

### 5.3.4 Wind farm, system demand, and CAES data

The raw data of power output profiles of the 14 wind farms are in 1-minute resolution and so is the 27-bus grid load demand profiles. All the profiles are averaged every 30 minutes to produce 30-min-resolution profiles. The desired output profiles for 14 wind farms, calculated using optimal power flow, are also in 30-minute resolution. A separate analysis done by the author shows that the use of 30-min resolution for wind farm output profiles is adequate for accurate calculation of discharged energy. Calculation of annual energy output for the 14 farms based on the original 1-min resolution and the derived 30-min resolution profiles leads to similar results with insignificant difference. The basic wind farm data are summarized in Table 5.1, where the farms are arranged in ascending order in terms of nameplate capacity. The CAES-related information, which is obtained from [65, 66], is presented in Table 5.2. The tables use several important terms, whose explanation is provided in the section beneath them.

Table 5.1 Data summary for 14 wind farms

Wind farm name	Wind farm rating, MW	Capacity factor CF	Wind farm name	Wind farm rating, MW	Capacity factor CF
1	2	3	4	5	6
WF1	28.5	0.2670	WF8	142.0	0.4078
WF2	80.0	0.2418	WF9	150.0	0.3788
WF3	82.5	0.2654	WF10	159.7	0.2372
WF4	91.5	0.4130	WF11	160.0	0.3352
WF5	100.0	0.1930	WF12	160.5	0.2810
WF6	114.0	0.4090	WF13	210.0	0.3673
WF7	120.6	0.3499	WF14	278.2	0.2782

Table 5.2 CAES cost data and other information [65, 66]

Item	Value	Item	Value
Discharged energy price, \$/MWh	50	Charge or discharge efficiency	0.865
Power-related cost, \$/MW	425,000	ESS life, years	20
Energy-related cost, \$/MWh	3,000	Other benefits $M_{OTHER}$ , \$/MW-year	45,500
Balance of plant (BOP) cost, \$/MWh	50,000	Considered ESS power rating, MW	0.5–165
Fixed O&M cost, \$/MW-year	2,500	Considered discharge duration, hour	0.5–8
Fixed charge rate (FCR)	0.12		

**CAES charge or discharge efficiency:** The CAES round-trip efficiency [66] (i.e. both charge and discharge) is 0.73, or the two-way loss is 0.27. Assumed that one-way loss, either charge or discharge, is 50% of the two-way loss, one-way efficiency is 0.865.

**Discharged energy price:** Assuming that the surplus wind energy (i.e. the input energy for the ESS) has zero-value while the output energy can be sold for \$50 per MWh on average, the net revenue per MWh of ESS-saved energy is \$50.

**Capacity factor:** Capacity factor is a performance parameter used to monitor and assess the productivity of an individual wind turbine and a complete wind power plant. It is the ratio of actual net energy production to the product of the plant power rating times the calendar time interval of interest. For example, annual capacity factor of a wind farm is calculated as follows:  $Annual\ energy\ production / (Farm\ power\ rating * 8760\ hours)$  [38, 68].

## 5.4 CASE STUDY RESULTS AND ANALYSES

The problem in (5.3) is solved for 14 wind farms using the direct calculation technique as described in Section 5.2.2. The considered CAES power rating is 0.5–165 MW in 0.5-MW increment (i.e. 330 power rating variants) and the discharge duration is 0.5–8 hours in 0.5-hour increment (i.e. 16 energy rating variants). Hence, the total ESS-variants is  $330 \times 16 = 5,280$ . The solution method aims to find the optimal rating of the 5,280 rating variants for each wind farm.

### 5.4.1 ESS optimal rating versus wind farm rating

The optimal ESS rating is presented in Table 5.3, Column 4 and 5. Column 6 contains the ratio between the ESS optimal power rating and the respective wind farm nameplate rating. For example, the ESS optimal power rating for WF1 is 2.5 MW and the wind farm nameplate rating is 28.5 MW. Then, the ratio is calculated as  $100 \times (2.5/28.5) = 8.8\%$ . For convenient observation, the ESS optimal ratings for wind farms 1–7 and wind farms 8–14 are reproduced in Fig. 5.1 and 5.2, respectively.

Table 5.3 ESS optimal ratings for 14 wind farms

Wind farm name	Wind farm rating, MW	Capacity factor, CF	ESS optimal power rating, MW	ESS optimal discharge duration, hour	ESS power rating vs. WF rating, %
1	2	3	4	5	6
WF1	28.5	0.2670	2.5	3	8.8
WF2	80.0	0.2418	5.5	4	6.9
WF3	82.5	0.2654	5.0	3	6.1
WF4	91.5	0.4130	10.5	4	11.5
WF5	100.0	0.1930	3.5	3	3.5
WF6	114.0	0.4090	15.5	4.5	13.6
WF7	120.6	0.3499	13.0	4.5	10.8
WF8	142.0	0.4078	16.0	4.5	11.3
WF9	150.0	0.3788	17.5	4.5	11.7
WF10	159.7	0.2372	5.5	3	3.4
WF11	160.0	0.3352	16.5	4	10.3
WF12	160.5	0.2810	7.0	3	4.4
WF13	210.0	0.3673	19.0	4.5	9.0
WF14	278.2	0.2782	30.5	4.5	11.0

Table 5.3, Fig. 5.1 and 5.2 shows that the optimal ESS power rating (i.e. MW-rating) varies from wind farm to wind farm in general. Larger wind farms (e.g. WF6, WF8, WF9, WF11, WF13, WF14) tend to require bigger storage systems than smaller wind farms (e.g. WF1, WF5). The optimal discharge duration ranges from 3 to 4.5 hours. The ratio between ESS power rating and wind farm rating is 3.4%–13.6% (Column 6, Table 5.3).

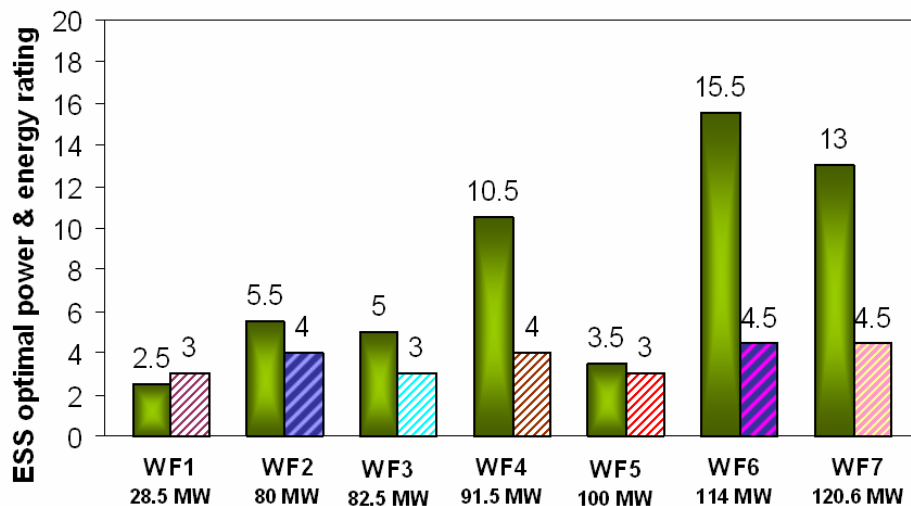


Fig. 5.1 ESS optimal power and energy rating for wind farms 1–7

**Note:** For each group of two columns, the first is optimal power rating in MW and the second is optimal energy rating in hours.

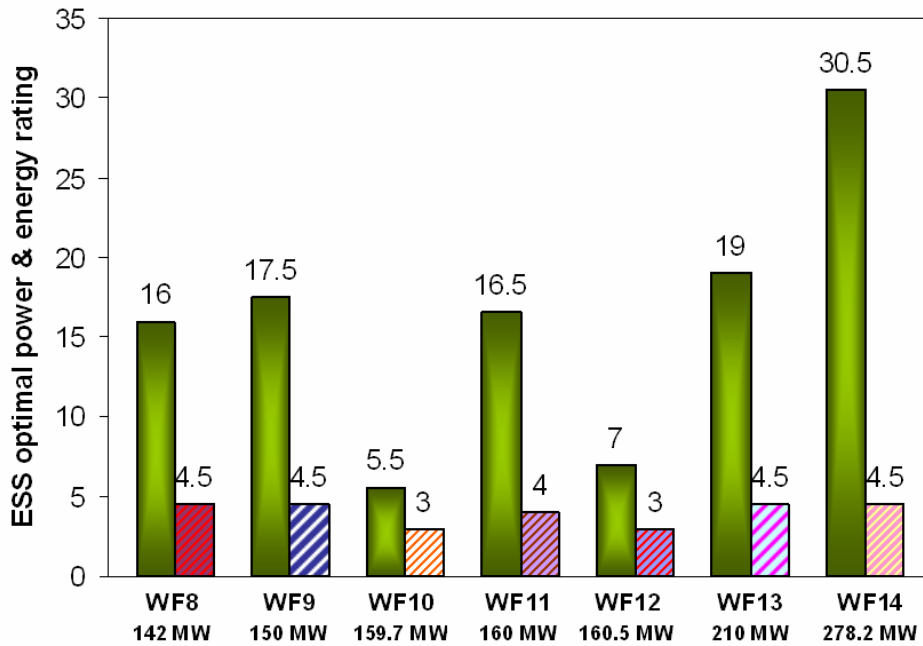


Fig. 5.2 ESS optimal power and energy rating for wind farms 8–14

**Note:** For each group of two columns, the first is optimal power rating in MW and the second is optimal energy rating in hours.

Another observed trend is that, for wind farms with capacity of 91.5–210 MW and capacity factor (Column 3) of around 33% or better, the ESS optimal power rating is 10.5–19 MW, or around 9%–14% of the wind farm rating (Column 6). For the wind farms, shaded in Table 5.3, the optimal discharge duration (i.e. energy rating) is between 4 and 4.5 hours. The trend is interesting since it may be used as some “rule of thumb” for fast estimating of CAES optimal rating. In the previous study, the ESS best rating is estimated to be in the range of 1–35 MW and 4–5 hours (Section 4.4.1 and 4.4.2). The estimation is relatively close to the accurate calculation by the optimization-based method.

### ***Discussion***

It is noted that, in practice, an ESS (CAES in this case study) may not be built in exact ratings as the optimal in Column 4–5. However, any rating is possible if utilities lease the ESS capacity. For example [69], purchasing hydro storage and shaping service is now possible. Furthermore, applying the ESS-application design concept, several wind farms may be served by one big energy storage system. In this case, the output of a number of wind farms may be aggregated and an optimal ESS rating can be found for them.

### 5.4.2 Revenue, cost and profit versus ESS optimal rating

Profitability of an ESS project is of great interest for any utility or developer who plans to use ESS for wind farms. Figures 5.3 and 5.4 plot the total revenue, total cost and the net profit for the 14 ESS projects that correspond to 14 wind farms. The ESS rating is optimal for all cases. The specific values are given in Table 5.4.

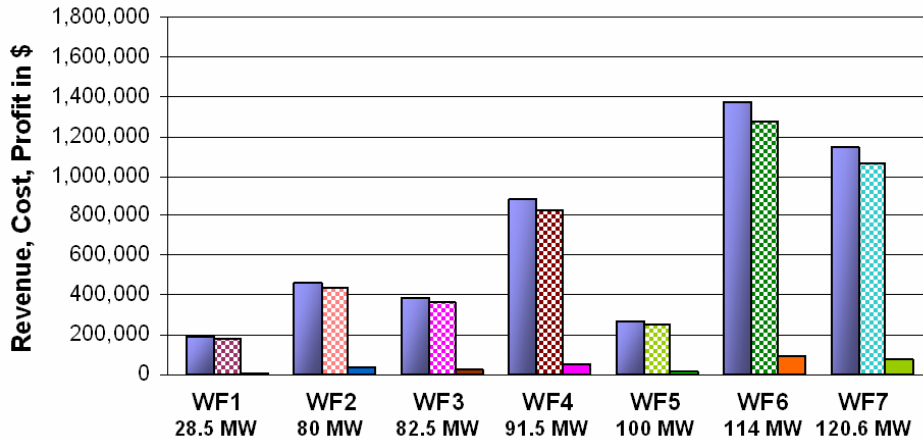


Fig. 5.3 Revenue, cost and profit for wind farms 1–7

**Note:** For each group of 3 columns, the first from left is revenue, the second is cost, and the third is net profit

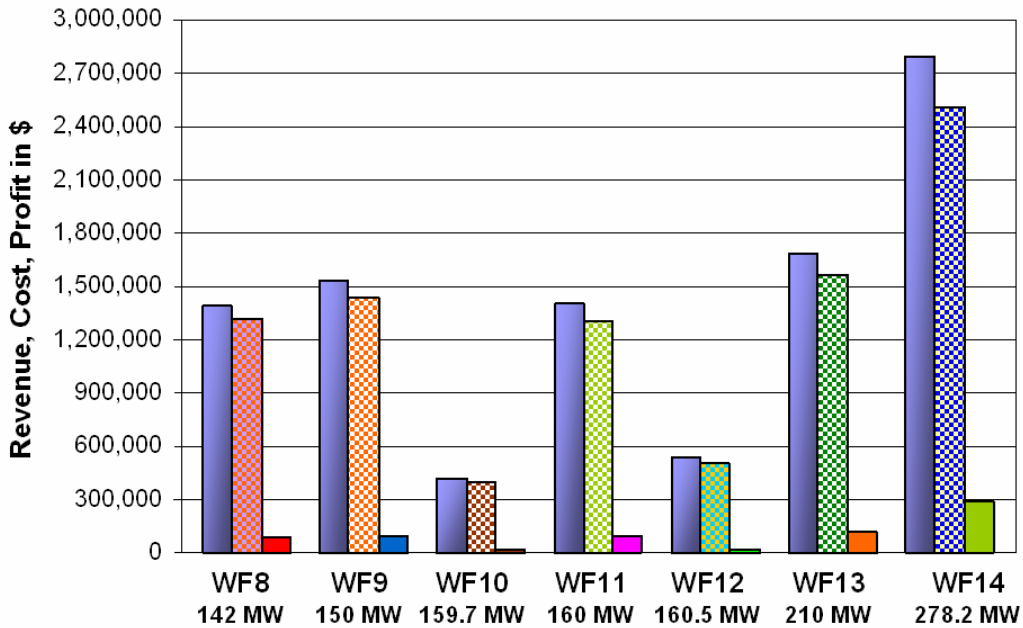


Fig. 5.4 Revenue, cost and profit for wind farms 8–14

**Note:** For each group of 3 columns, the first from left is revenue, the second is cost, and the third is net profit

Table 5.4 Cost and return rate for 14 ESS projects

Wind farm name	WF rating, MW	Capacity factor, CF	Total revenue, \$	ESS cost, \$	Net profit, \$	Return rate, %	Discharged energy, MWh	Energy cost, \$/MWh
1	2	3	4	5	6	7	8	9
WF1	28.5	0.2670	194,073	181,450	12,623	7.0	1,606	113.0
WF2	80.0	0.2418	466,709	434,170	32,539	7.5	4,329	100.3
WF3	82.5	0.2654	388,446	362,900	25,546	7.0	3,219	112.7
WF4	91.5	0.4130	885,328	828,870	56,458	6.8	8,152	101.7
WF5	100.0	0.1930	268,943	254,030	14,913	5.9	2,194	115.8
WF6	114.0	0.4090	1,371,570	1,272,860	98,710	7.8	13,326	95.5
WF7	120.6	0.3499	1,145,314	1,067,560	77,754	7.3	11,076	96.4
WF8	142.0	0.4078	1,397,247	1,313,920	83,327	6.3	13,385	98.2
WF9	150.0	0.3788	1,536,525	1,437,100	99,425	6.9	14,805	97.1
WF10	159.7	0.2372	415,806	399,190	16,616	4.2	3,311	120.6
WF11	160.0	0.3352	1,400,300	1,302,510	97,790	7.5	12,991	100.3
WF12	160.5	0.2810	534,501	508,060	26,441	5.2	4,320	117.6
WF13	210.0	0.3673	1,679,726	1,560,280	119,446	7.7	16,305	95.7
WF14	278.2	0.2782	2,792,528	2,504,660	287,868	11.5	28,096	89.1

In Table 5.4, the rate of return in Column 7 is obtained by dividing the net profit by the corresponding ESS cost i.e. the annualized investment. For example, for wind farm WF1, the return rate is calculated as  $100 \times (181,450/194,073) = 7.0\%$ . The storage energy cost (Column 9) is calculated by considering only the discharged energy and the ESS cost. For wind farm WF1, the storage energy cost is calculated as  $181,450/1,606 = 113 \text{ $/MWh}$ .

Figures 5.3, 5.4 and Table 5.4 show that all ESS projects are profitable with a return rate between 4.2% and 11.5% (Column 7, Table 5.4). Eight projects yield the return rate of 7% or better. The farms with this performance are shaded in Table 5.4.

Though, it should be emphasized that the result is based on the assumption that combination of four ESS benefits (capacity firming, increased voltage stability, increased reliability, and environmental considerations) is worth \$45.5/kW-year. If this holds true, the ESS projects can be attractive to developers with the annual return rate of 4.2%–11.5%. In a worst-case scenario, where the four benefits cannot be claimed, the storage energy cost ranges from 89.1–120.6 \$/MWh (Column 9).

### 5.4.3 Revenue component

It is worth looking at the project revenue component since it provides information on how each benefit-component impacts the total obtained monies.

In figures 5.5 and 5.6, the revenue from discharged energy is the lower portion of each column while the revenue from other benefits is the upper part. The percentage proportion of discharged energy to other revenue for each wind farm is shown on top of each column. The first value is for discharged energy and the second value is for other revenue.

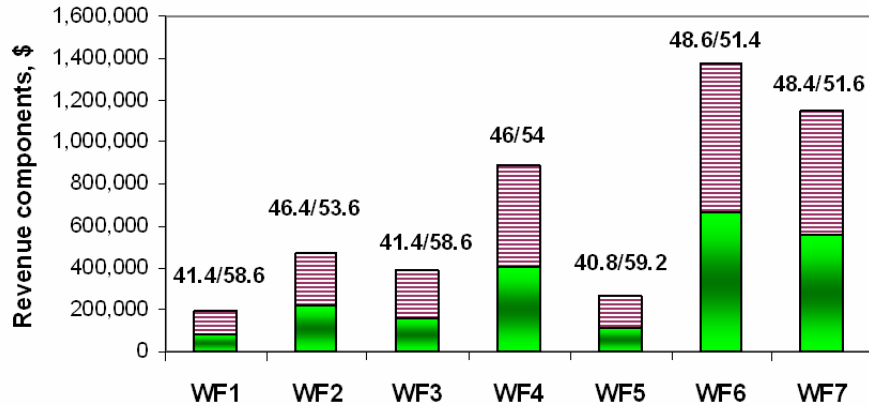


Fig. 5.5 Revenue component for wind farms 1–7

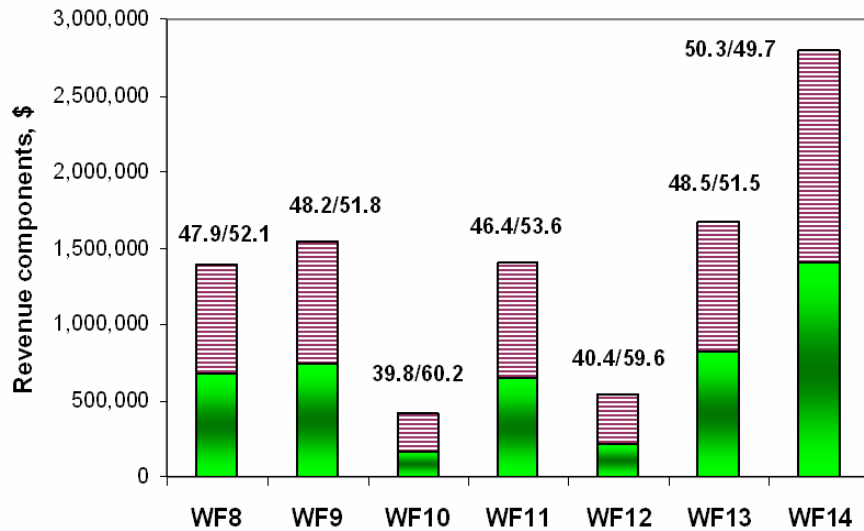


Fig. 5.6 Revenue component for wind farms 8–14

The revenue from discharged energy accounts for 39.8%–48.6% of the total revenue. Other benefit factors have a slightly-higher impact on the total revenue for most ESS projects (41.2–52.4%). The only exception is wind farm WF14 for which the ratio between discharged energy and other revenue is 50.3%/49.7%. This proportion shows that discharged energy plays a dominant role in total revenue. It suggests that significant revenue can be generated just by using ESS to store and re-dispatch wind energy appropriately.

### 5.4.4 Relation between ESS discharge duration and profit

Figures 5.7 and 5.8 show the relationship between the ESS discharge duration and the profit for 14 wind farms. In the figures, a curve shows how profit varies as the discharge duration changes. For each curve, the ESS power rating corresponding to the highest profit is the optimal rating. The ESS optimal power ratings are provided in Table 5.3.

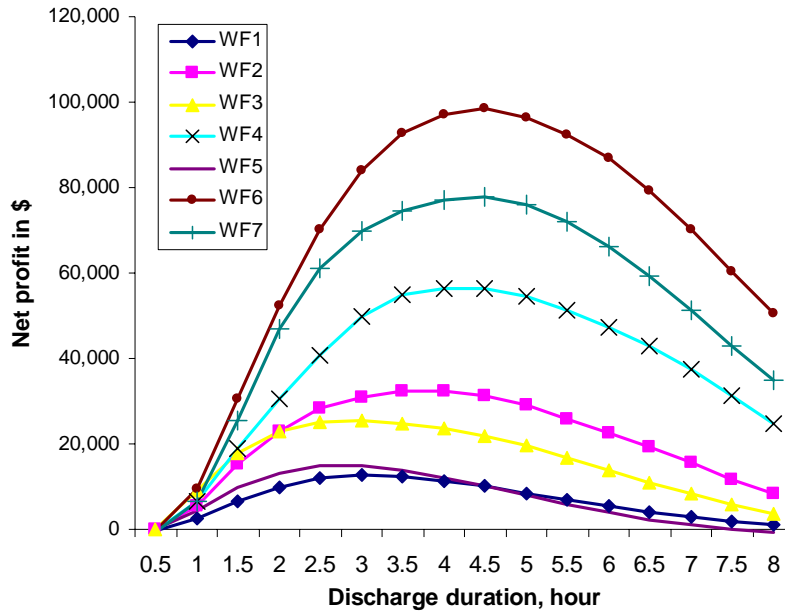


Fig. 5.7 ESS discharge duration versus profit for wind farms 1–7

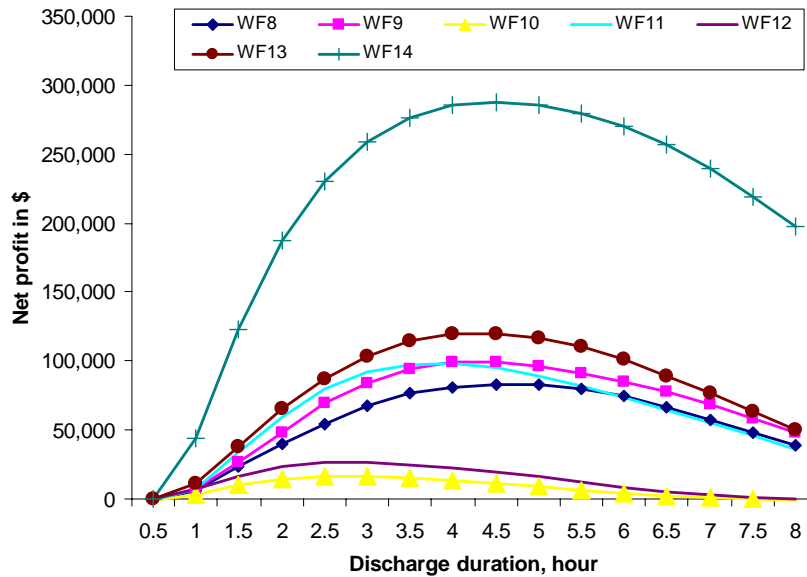


Fig. 5.8 ESS discharge duration versus profit for wind farms 8–14

Both figures show that there is a unique discharge duration for which the profit is maximized. As said above, the highest profit on each curve correspond to an ESS optimal power rating. This suggests that the discharge duration is as important as the power rating of a storage system for its rating to be completely “optimal”. For the 14 wind farms, the optimal discharge duration range is 3–4.5 hours (Table 5.3). The finding also suggests that the obtained solution for the ESS-sizing problem, i.e. the ESS optimal rating, is unique.

### 5.4.5 ESS switching behavior

Figure 5.9 shows one-day operation for the optimal ESS associated with wind farm WF9 (150 MW). The ESS optimal rating is 17.5MW/4.5h. A summary of switching operation of the 14 optimal ESSs is provided in Table 5.5, Fig. 5.10 and Fig. 5.11. A switching operation is defined as the event where an ESS makes one of the following operation-mode changes: (a) charge to discharge, (b) discharge to charge, (c) charge to charge, or (d) discharge to discharge.

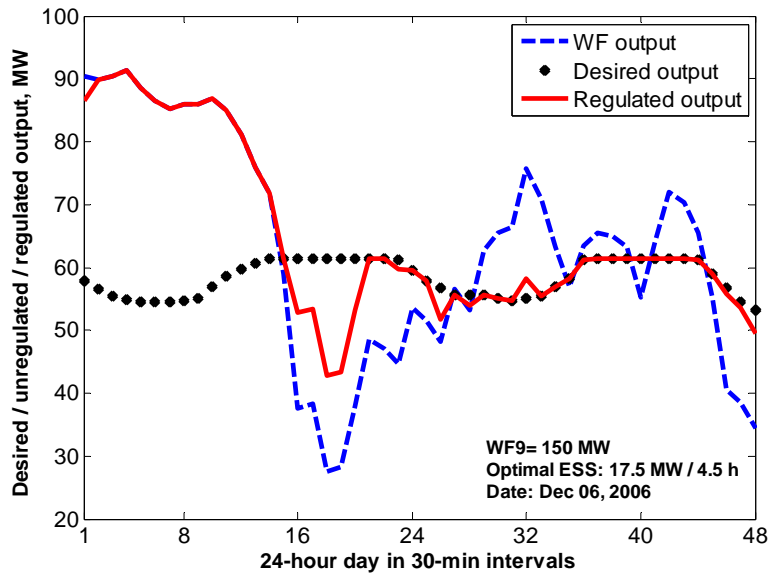


Fig. 5.9 ESS switching operation for one day

By visual inspection of Fig. 5.9, between 8am and 10am of the winter day, the farm output (blue curve) dropped below 30 MW. The ESS was able to compensate for part of this deficit amount, raising the regulated output (red curve) above 40 MW. Between 10am and 10pm that day (i.e. 12 hours), the ESS could regulate the farm output to be a good match for the grid demand (i.e. the desired output). For the 24-hour period, the ESS performed 5 switching operations.

Table 5.5 ESS switching operation for 365 days

Wind farm name	Wind farm rating, MW	Capacity factor, CF	ESS optimal rating		Number of days with # of switching operations			Total number of switching operations	Average switching operation per day
			MW	hour	Zero to 2	3 or 4	5 or more		
1	2	3	4	5	6	7	8	9	10
WF1	28.5	0.2670	2.5	3	193	88	84	1051	2.9
WF2	80.0	0.2418	5.5	4	193	89	83	1084	3.0
WF3	82.5	0.2654	5	3	188	86	91	1120	3.1
WF4	91.5	0.4130	10.5	4	195	113	57	989	2.7
WF5	100.0	0.1930	3.5	3	193	74	98	1105	3.0
WF6	114.0	0.4090	15.5	4.5	202	103	60	996	2.7
WF7	120.6	0.3499	13	4.5	211	89	65	950	2.6
WF8	142.0	0.4078	16	4.5	211	88	66	932	2.6
WF9	150.0	0.3788	17.5	4.5	209	103	53	952	2.6
WF10	159.7	0.2372	5.5	3	207	87	71	993	2.7
WF11	160.0	0.3352	16.5	4	217	85	63	919	2.5
WF12	160.5	0.2810	7	3	199	77	89	1057	2.9
WF13	210.0	0.3673	19	4.5	198	103	64	987	2.7
WF14	278.2	0.2782	30.5	4.5	174	119	72	1096	3.0

In Table 5.7, the number of days where an ESS performs zero, one or two switching operations is shown in Column 6. Similarly, the numbers of days with 3–4 switching operations and 5 or more operations are provided in Column 7 and 8, respectively. For each wind farm, the sum of columns 6 through 8 is 365 days. For example, for wind farm WF1, the sum is 193+88+84=365. Column 9 shows the total number of switching operations for 365 days. Column 10 contains the daily average of switching events, obtained by dividing the total number of switching operations by 365 days. Taking wind farm WF2 as an example, the daily switching average is calculated as 1084/365 = 3 times. The number of days with (a) zero to 2, (b) 3 or 4, and (c) 5 or more switching operations is converted to percentage on 365-day base and shown graphically in Fig. 5.13 and 5.14. For instance, the number of days where the optimal ESS associated with wind farm WF1 performs zero to 2 switching operations is 193. Then, the percentage is calculated as  $100 \times (193/365) = 52.9\%$ .

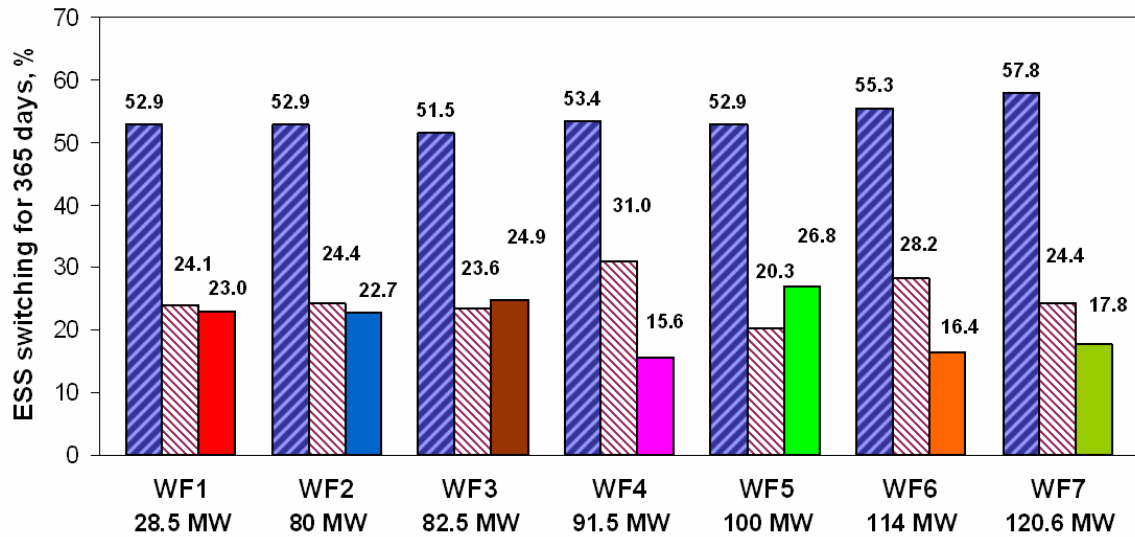


Fig. 5.10 ESS switching behavior for wind farms 1–7

**Note:** For each group of three columns, the first is the number of days with zero to 2 switching operations, the second is the number of days with 3 or 4 operations, the third is the number of days with 5 or more operations; all are in percentage on 365-day base.

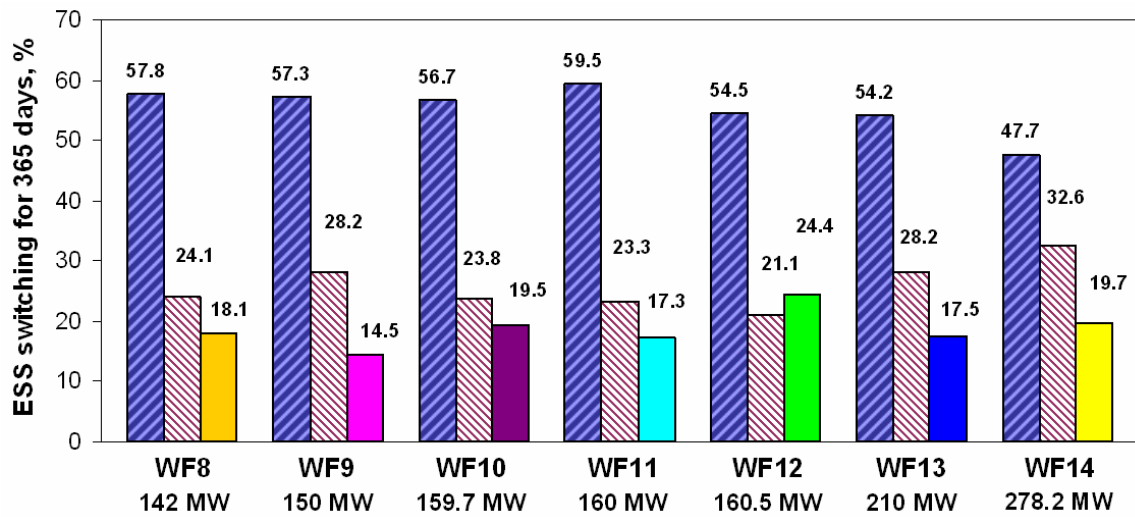


Fig. 5.11 ESS switching behavior for wind farms 8–14

**Note:** For each group of three columns, the first is the number of days with zero to 2 switching operations, the second is the number of days with 3 or 4 operations, the third is the number of days with 5 or more operations; all are in percentage on 365-day base.

Figures 5.10 and 5.11 show that most ESSs perform two switching operations per day or less for the larger part of the year (51.5%–59.5 % of 365 days). The only exception is wind farm WF14, where the associated ESS carries out two or less operations for 47.7% of the time. The 14 optimal ESSs perform 3 or 4 operations daily for 20.3%–32.6% of the time. The ESSs need to

carry out 5 or more operations for only 14.5%–26.8% of the time. Overall, the ESSs perform four or less switching operations daily for majority of the time (73.2%–85.5% of 365 days). On average, the ESSs carry out 2.5–3.1 operations per day (Table 5.7, Column 10). The results suggest that it is appropriate for the ESSs to operate according to the developed charge-discharge scheme and the desired output profile because they need to perform only a few switching operations per day. This is beneficial in preserving the equipment useful life.

#### 5.4.6 Increase in wind energy integration versus ESS optimal rating

An ESS impact on wind power integration is measured by the annual energy amount discharged by the ESS. This is the additional energy amount which would not be integrated if there is no ESS. The technique for calculating the ESS discharged energy is similar to the one presented in Section 4.3.4.1. The difference is that, for each wind farm, the discharged energy amount is calculated for the respective ESS optimal rating only. The results are presented in Table 5.6, Fig. 5.12 and Fig. 5.13.

Table 5.6 Increase in wind energy integration by ESS

Wind farm name	Wind farm rating, MW	Capacity factor, CF	ESS optimal rating		Discharged energy, MWh	Integrated energy, MWh	Increase in wind energy integration, %
			MW	hour			
1	2	3	4	5	6	7	8
WF1	28.5	0.2670	2.5	3.0	1,606	38,133	4.2
WF2	80.0	0.2418	5.5	4.0	4,329	103,377	4.2
WF3	82.5	0.2654	5.0	3.0	3,219	115,319	2.8
WF4	91.5	0.4130	10.5	4.0	8,152	213,779	3.8
WF5	100.0	0.1930	3.5	3.0	2,194	106,605	2.1
WF6	114.0	0.4090	15.5	4.5	13,326	265,143	5.0
WF7	120.6	0.3499	13.0	4.5	11,076	234,973	4.7
WF8	142.0	0.4078	16.0	4.5	13,385	310,348	4.3
WF9	150.0	0.3788	17.5	4.5	14,805	307,592	4.8
WF10	159.7	0.2372	5.5	3.0	3,311	196,535	1.7
WF11	160.0	0.3352	16.5	4.0	12,991	278,953	4.7
WF12	160.5	0.2810	7.0	3.0	4,320	251,423	1.7
WF13	210.0	0.3673	19.0	4.5	16,305	361,188	4.5
WF14	278.2	0.2782	30.5	4.5	28,096	351,177	8.0

In Table 5.6, the discharged energy shown in Column 6 is the annual energy amount discharged by each ESS. The integrated energy in Column 7 is the annual energy channeled into the grid freely without the aid of the ESS and with economic value (i.e. with payment). The surplus wind power which cannot be stored by the ESS is channeled into the grid without

payment. Therefore, it does not count towards the integrated energy. The percent-increase in wind energy integration in Column 8 is calculated by comparing the discharged energy and the integrated energy. For example, for wind farm WF1, the annual discharged energy amount is 1,606 MWh and the corresponding integrated energy amount is 38,133 MWh. The percent-increase in energy integration is calculated as  $100 * (1,606 / 38,133) / 38,133 = 4.2\%$ .

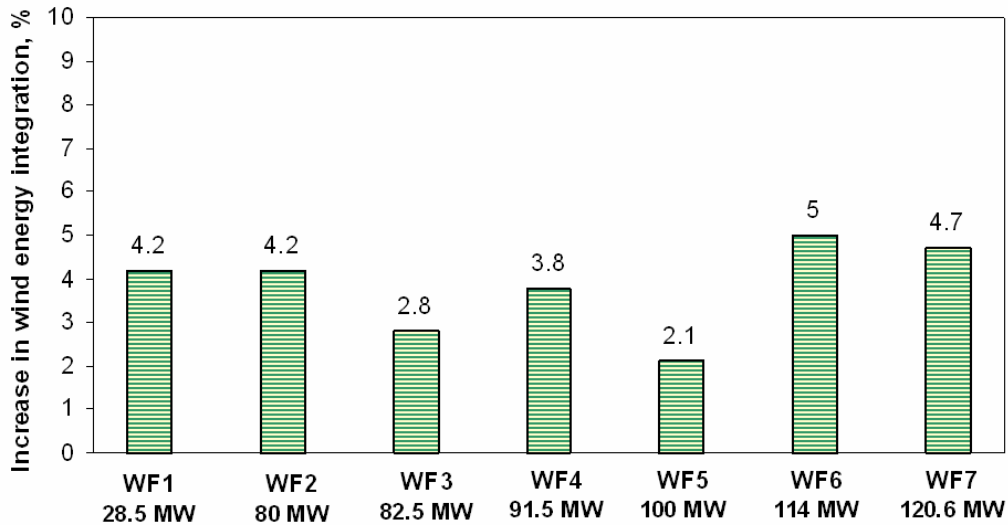


Fig. 5.12 Increase in wind energy integration for wind farms 1–7

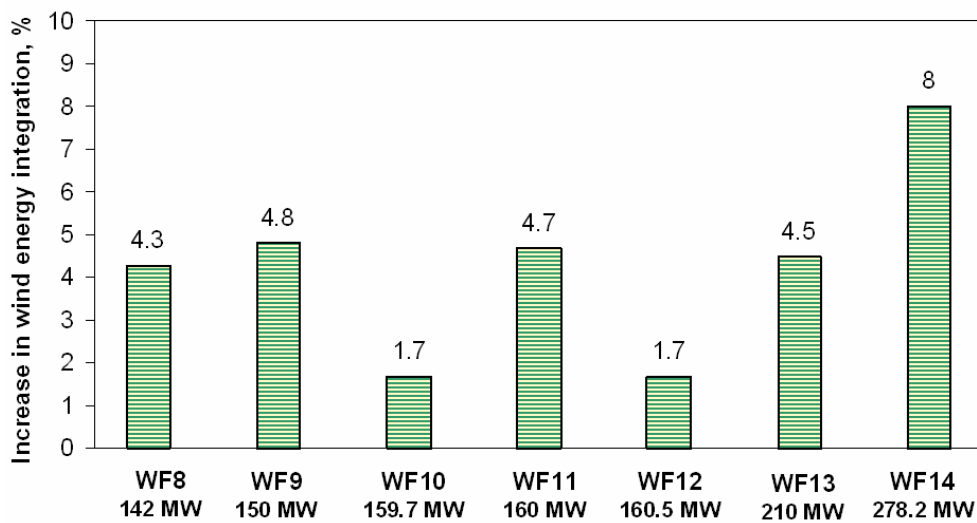


Fig. 5.13 Increase in wind energy integration for wind farms 8–14

Table 5.6, Fig. 5.12, and Fig. 5.13 show that the use of ESS increases wind power integration. Of the 14 wind farms under consideration, 9 wind farms obtain an increase in wind energy sale between 4.2% and 8%. The wind farms are shaded in Table 5.6. Overall, the increase

in wind energy integration is between 1.7% and 8%. Recall from Section 5.4.3 that this additional energy generates 39.8%–50.3% of the total revenue for the ESS projects. The result further emphasizes the ESS benefit in improving wind power integration.

#### 5.4.7 Voltage stability improvement versus ESS optimal rating

The net improvement in grid steady-state voltage stability is calculated using the technique presented in Section 4.3.4.2, where voltage stability is measured using eigenvalues. The only difference is that the improvement in stability is quantified for ESS optimal ratings only. The results are presented in Table 5.7, Fig. 5.14 and Fig. 5.15.

Table 5.7 Net increase in voltage stability by ESS

Wind farm name	Wind farm rating, MW	Capacity factor, CF	ESS optimal rating		Net increase in stability %
			MW	hour	
1	2	3	4	5	6
WF1	28.5	0.2670	2.5	3.0	0
WF2	80.0	0.2418	5.5	4.0	18.3
WF3	82.5	0.2654	5.0	3.0	13.9
WF4	91.5	0.4130	10.5	4.0	11.2
WF5	100.0	0.1930	3.5	3.0	13.6
WF6	114.0	0.4090	15.5	4.5	11.9
WF7	120.6	0.3499	13.0	4.5	13.3
WF8	142.0	0.4078	16.0	4.5	10.7
WF9	150.0	0.3788	17.5	4.5	12.7
WF10	159.7	0.2372	5.5	3.0	8.5
WF11	160.0	0.3352	16.5	4.0	13.2
WF12	160.5	0.2810	7.0	3.0	8.3
WF13	210.0	0.3673	19.0	4.5	10.8
WF14	278.2	0.2782	30.5	4.5	13.3

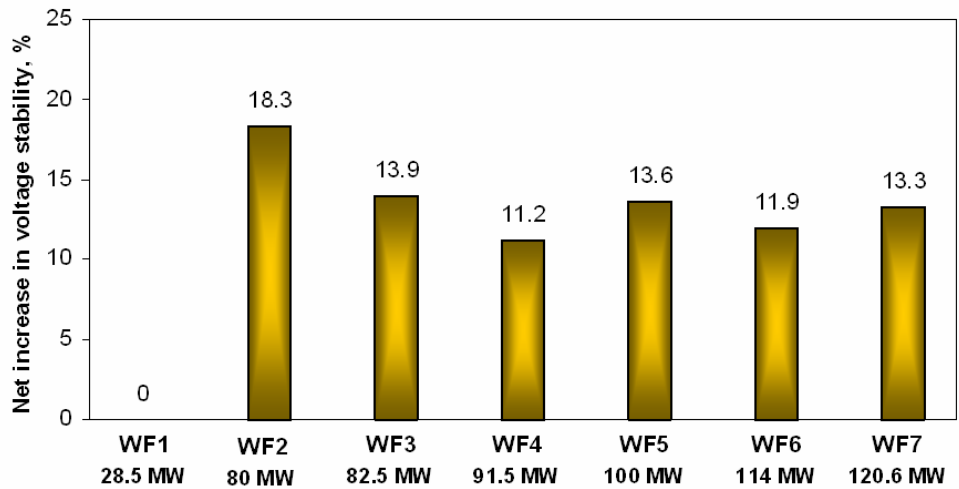


Fig. 5.14 Net increase in voltage stability for wind farms 1–7

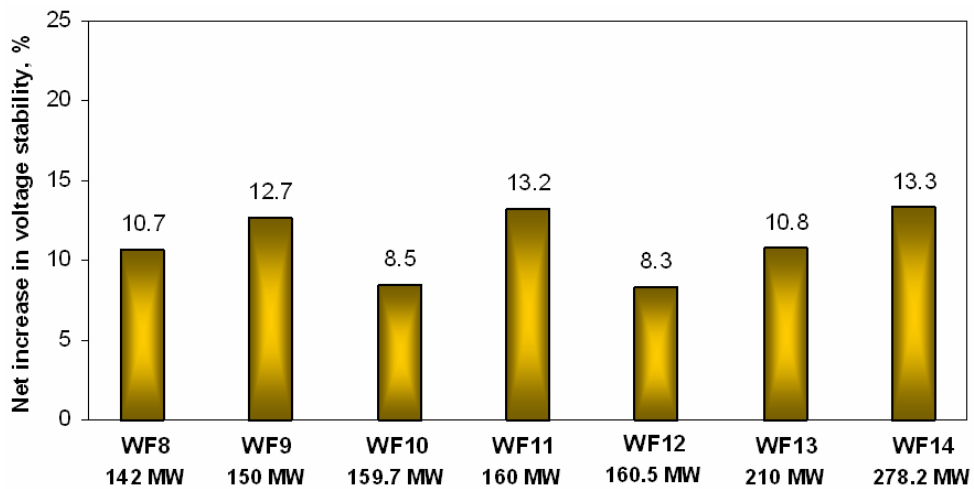


Fig. 5.15 Net increase in voltage stability for wind farms 8–14

Based on Table 5.7, Fig. 5.14 and 5.15, the grid voltage stability condition is improved significantly. A net increase in voltage stability between 10.7% and 18.3% is obtained for majority of wind farms (11 of 14 farms, shaded in Table 5.7). The only exception is wind farm WF1, for which the stability condition does not change (zero-increase) with the use of the ESS. The result is not a surprise because this wind farm is very small (28.5 MW). Its full output accounts for just 2.5% of the grid peak load (1148.6 MVA). It is likely that the grid can accommodate this wind farm so regulating its output does not improve the stability condition. Overall, a net increase in stability between 8.3% and 18.3% is achieved by 13 of 14 evaluated ESSs.

#### 5.4.8 Existence and uniqueness of solution to ESS-sizing problem

Recall that the ESS-sizing problem solution optimizes the ESS rating for maximizing its net profit. The net profit results from subtracting the ESS financial requirement (i.e. ESS costs) from the total revenue. The total revenue results from the ESS benefits, such as increased wind power integration, increased voltage stability, and so on. From optimization viewpoint, the obtained relation between the discharge duration and profit is of good-shape (Figure 5.7 and 5.8). The figures show that each curve has a unique maximum, meaning that, for each ESS, there is a unique discharge duration where the profit peaks. The finding suggests that the solution to the ESS unit-sizing problem in (5.3), if exists, is unique. The solution exists if the total revenue is larger than the ESS total cost i.e. the profit is positive. If negative profit is allowed, a solution may still be found. It shows how much loss one would suffer for each ESS project. Differently speaking, one can learn from this solution (i.e. with negative profit) how close an ESS project is to being profitable.

### 5.5 CHAPTER CONCLUDING REMARKS

In this chapter, a formulation and a solution to the ESS unit-sizing problem are presented. The solution method employs formulation of a cost-based objective function, discretization of this function, and exhaustive search of the function values to find the ESS optimal rating. The method efficacy is demonstrated via a case study with a large data set consisting of annual measured outputs of 14 wind farms, and a 27-bus real-world transmission grid with an annual measured load profile. The considered ESS technology is compressed-air energy storage system (CAES). The results and analyses lead to the following conclusion:

- (i) **General finding:** Large wind farms tend to require larger storage systems than smaller wind farms. Depending on particular wind farm rating and output pattern, the optimal ESS power rating varies from 2.5 MW to 30.5 MW. The optimal discharge duration ranges from 3 to 4.5 hours. The ratio between ESS power rating and wind farm nameplate rating is 3.4%–13.6%.
- (ii) **ESS optimal rating versus wind farm rating:** For wind farms with capacity of 91.5–210 MW and capacity factor of around 33% or better, the ESS optimal power rating is 10.5–19 MW, or 9%–14% of the farm rating. For these farms, the optimal discharge duration is between 4 and 4.5 hours. Using the same cost and

benefit values, this finding is recommended for use as empirical estimation of CAES optimal rating for similar wind farms.

- (iii) ***Profitability of ESS projects:*** For the considered 14 wind farms, the revenue from discharged energy accounts for 39.8%–50.3% of the ESS total revenue. All ESS projects can be profitable with annual return rates of 4.2%–11.5%. The results are based on the assumption that, apart from discharged energy, combination of four other ESS benefit factors is worth \$45.5/kW-year. If the four benefits cannot be claimed (i.e. unpaid), the storage energy cost is \$89–121 per MWh.
- (iv) ***ESS impacts on wind power integration:*** The use of ESS improves wind power integration. Of the 14 wind farms under consideration, 9 wind farms obtain an increase in wind energy sale between 4.2%–8%. Overall, the enhancement in wind energy integration is 1.7%–8%.
- (v) ***ESS impact on grid steady-state voltage stability:*** The grid stability condition is improved significantly thanks to the ESS operation. A net increase in voltage stability between 10.7%–18.3% is obtained for majority of the 14 wind farms (11 of 14). The only exception is the case of the small 28.5-MW wind farm, where the grid stability condition does not change with the use of the ESS. Overall, a net increase in stability of 8.3%–18.3% is achieved by 13 of the 14 evaluated ESSs.
- (vi) ***ESS switching operation:*** The 14 optimal ESSs perform four or less switching operations daily most of the time (73.2%–85.5% of 365 days). On average, the ESSs carry out 2.5–3.1 switching operations per day. The results suggest that the developed charge-discharge scheme and the desired output calculation technique are appropriate for ESS operation.
- (vii) ***Existence and uniqueness of solution to ESS unit-sizing problem:*** The solution to the ESS-sizing problem exists if the total revenue is higher than the total cost i.e. the profit is positive. In this case the solution is unique i.e. there is a unique ESS rating that maximizes the profit for each wind farm. The study results

show that the developed optimization-based method (the direct-calculation method) is effective for solving the ESS unit-sizing problem.

This study completes the design of the ESS-based application for regulating wind farm power output variation and improving grid small-disturbance voltage stability. In the following Chapter 6, a new scheme is proposed to operate ESS so as to increase wind farm transient stability performance.

## Chapter 6

### **Improving wind farm transient stability using synchronous-machine-based ESS**

#### **6.1 INTRODUCTION**

In Chapter 4 and 5, a complete design of the application using energy storage systems (ESS) is presented. Two performed studies show that the ESS-based application is efficient in reducing wind farm output variation and increasing grid small-disturbance (steady-state) voltage stability. Using the developed optimization-based method, an ESS optimal rating can be found for any wind farm with a high degree of accuracy.

This chapter study investigates a technique to stabilize a wind farm after being subjected to large disturbances, such as faults near the farm or on the host grid. Being induction generators, the farm wind turbines must remain in synchronism with the grid to stay connected. Disconnection of wind turbines due to disturbances is not desired because it affects both the grid and the wind farm. For the grid, loss of considerable wind generation capacity reduces its ability to supply loads, leading to stability and reliability problems. For the wind farm, disconnection means loss of wind energy sale. Therefore, it is essential that the wind farm maintains its stability after experiencing disturbances. Based on the discussion, the study goals are defined as follows.

- (i) To develop a scheme using an energy storage system for improving wind farm transient stability.
- (ii) To validate the scheme efficacy using voltage stability criteria, namely, critical clearing time, voltage recovery and voltage sag.

The proposed scheme exploits a synchronous-machine-based ESS as a synchronous condenser to stabilize a wind farm by dynamic reactive power supply during faults. The approach, to the best knowledge of the author, is new and has never been proposed for use with wind farms.

The scheme efficacy is assessed by experiments with the modified 6-bus power system (Section 3.1.1 and Appendix A2), a 60-MW wind farm, and two most popular types of wind turbines, namely, stall-controlled wind turbine and DFIG (doubly-fed induction-generator based wind turbine). Matlab Simulink SimPowerSystems is used for simulation.

The results show that, apart from its ability to regulate a wind farm real power output, the SM-based ESS can also be used to provide dynamic reactive support to wind farms. For DFIG, using the ESS as a reactive compensation device is not efficient because these wind turbines have the ability to regulate their own reactive power. The ESS just has a slight benefit in reducing voltage sag. However, the ESS is particularly effective for use with the wind farm consisting of stall-regulated wind turbines. The ESS increases the farm critical clearing time (CCT) by 1 cycle for worst-case bolted three-phase-to-ground (3P2G) faults. For bolted single-phase-to-ground faults (1P2G), the CCT is improved by 23.1%–52.2%, depending on the fault location. The ESS helps reduce the voltage sag severity and shorten the post-fault voltage recovery duration by up to 54.5%. The ESS performance is better than a static var compensator (SVC) of comparable capacitive rating in most situations investigated. The finding suggests a new technique to operate the ESS so as to maximize its efficiency and value.

**Publication:** The work reported in this chapter has been published in *IEEE Power & Energy Society General Meeting 2010* with the title "Increasing Wind Farm Transient Stability by Dynamic Reactive Compensation: Synchronous-Machine-based ESS versus SVC" [37].

## 6.2 PROPOSED SCHEME BACKGROUND

The subject of using ESS to improve wind farm transient stability has gained increasing attention during the past few years. The ESS technologies that draw considerable research interest include battery energy storage systems (BESS) [70, 71], super-capacitor [72-74], and superconducting magnetic energy storage systems (SMES) [75-77].

This study proposes using different ESS technology for enhancing wind farm transient stability. They are bulk ESS technologies that have received less research attention so far, namely, pumped-hydro electric storage (PHES), compressed-air energy storage (CAES), or a thermal unit with a storage in general. These storage systems can also be called synchronous-machine-based ESS because their core energy converter element is a synchronous machine.

Using the ESS for wind-power applications offers several advantages. First, they are bulk storage systems with MW-range ratings, which can meet the storage requirement of large wind farms with high output fluctuation. Second, they are mature technologies with units operational in the field. Third, PHES and CAES have the least life-cycle cost compared to most batteries [28, 65].

Furthermore, it is envisioned that wind power plants can be integrated with concentrating solar power plants where they compensate each other to produce a stable output. Utilities are

increasingly interested in concentrating solar power plants because of abundant solar resource in the U.S. Southwest [78, 79]. Potential sites for CAES are available, for instance, near the panhandle areas of Texas and Oklahoma [80]. In short, there are opportunities and advantages for using the synchronous-machine-based (SM-based) ESS for wind power plants.

The new scheme proposes using ESS as dynamic reactive compensation devices to improve wind farm transient stability. An SM-based ESS is mostly run in two modes: motor mode for charging and generator mode for discharging. The ESS can supply reactive power when operating in generator mode. This scheme makes use of the third mode for reactive supply, which is running the ESS as a synchronous condenser. There are times when the ESS energy storage unit is empty so exploiting it as a synchronous condenser is useful because it would sit idle otherwise.

Synchronous condensers have been used as excellent reactive supply devices for transmission and distribution for years [11, 81]. However, to the best knowledge of the author, they have never been proposed for supporting wind farms.

The ESS operation scheme is tested with two types of wind turbines, namely, stall-regulated induction-generator based wind turbines and doubly-fed induction-generator based wind turbines (DFIG). The stall-regulated wind turbines represent the worst-case scenario for reactive compensation and DFIG represent the best-case scenario. The scheme is also validated by comparing its efficacy with that of a static var compensator (SVC).

## **6.3 MODELING OF WIND TURBINES AND POWER SYSTEM COMPONENTS**

### **6.3.1 Modeling of stall-controlled wind turbine**

The modeling and testing of stall-regulated(fixed-speed) wind turbine are presented in detail in Chapter 2 and [33], where the induction generator modeling is based on [47]. For brevity, the modeling is not repeated here.

### **6.3.2 Modeling of DFIG**

The DFIG model used in this study is a build-in model by Matlab [30]. The DFIG consists of a wound rotor induction generator and an AC/DC/AC IGBT-based PWM converter. It is also equipped with a pitch control system and is built based on [82-84].

The AC/DC/AC converter consists of two components: the rotor-side converter and the grid-side converter. A capacitor coupling the two converters acts as the DC voltage source. The rotor-side converter is used to control the wind turbine output power and the voltage (or reactive

power) measured at the grid terminals. The turbine output power is controlled to achieve a pre-defined power-speed characteristic. The grid-side converter is used to regulate the DC-bus voltage. The model allows using the grid-side converter to generate or absorb reactive power [30].

The 3-phase rotor winding is connected to the grid through the rotor-side converter by slip rings and brushes. The stator winding is connected to the grid through a coupling inductor. The DFIG model can generate positive and negative-sequence currents, but no zero-sequence current. It is deemed suitable for transient stability studies with long simulation duration. For more details, refer to [30].

### 6.3.3 Validation of stall-regulated wind turbine and DFIG models

The stall-regulated wind turbine model is validated using its power generation behavior and torque-speed characteristics under normal and fault conditions. For brevity, only the power curve is presented here. The detailed testing of the stall-regulated wind turbine model is presented in Chapter 2 and [33]. The power curve for the Matlab built-in DFIG model is obtained by running the model under wind speeds of 5–25 m/s. The power curves generated by the two wind turbine models are plotted in Fig. 6.1, together with the measured power curve of a 1.5-MW real-world variable-speed wind turbine.

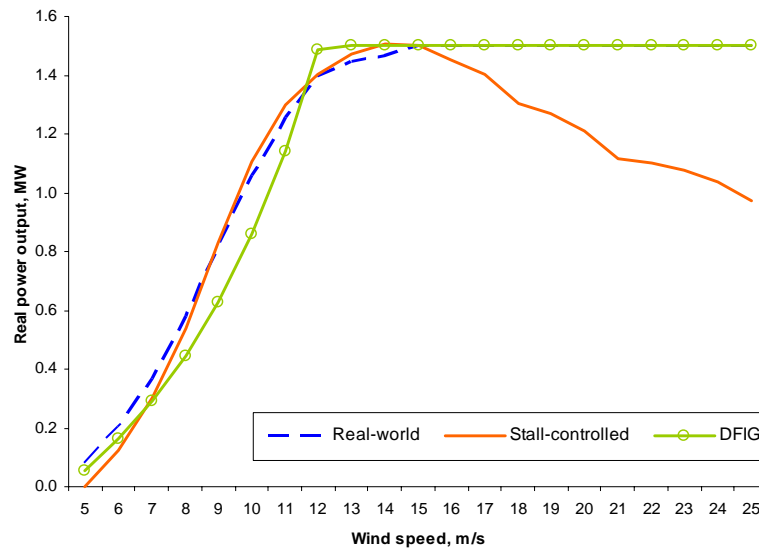


Fig. 6.1 Power curves of stall-regulated wind turbine and DFIG

Figure 6.1 shows that the power curve of the stall-regulated wind turbine model follows the curve of the real-world variable-speed wind turbine closely, up to the rated wind speed of 15 m/s. Its output then falls, which is also a correct behavior of a fixed-speed wind turbine. The DFIG power curve differs from the other two since the wound-rotor induction generator has different torque-speed characteristics. Though, the DFIG model achieves stable rated output of 1.5 MW at 13 m/s and beyond, nearly like the real-world variable-speed wind turbine. When its var-regulation mode is set to “on”, the DFIG model can control its reactive power such that no reactive power is drawn from the grid.

As explained in Section 6.4 and 6.5, the testing of the proposed ESS operation scheme is carried out under the scenarios where all wind turbines encounter the rated wind speed of 15 m/s. These are worst-case scenarios for reactive compensation because wind turbines consume most reactive power at the rated wind speed (i.e. when their power outputs peak). Since only the full power output region (15 m/s) is used for the study, the difference in the DFIG power output behavior for wind speeds of around 7–13 m/s will not affect the results.

### 6.3.4 Modeling of power system components

#### 6.3.4.1 Power system for analysis

The power system used in this study is a 5-bus system (Fig. 6.2), a modified version of the 6-bus 138-kV grid where the Swing generator is modeled as a 5500-MVA equivalent source. The 6-bus system is described in Section 3.1.1. The data for the 5-bus system is provided in Appendix A2. For reader convenience, a brief description of the system is provided here.

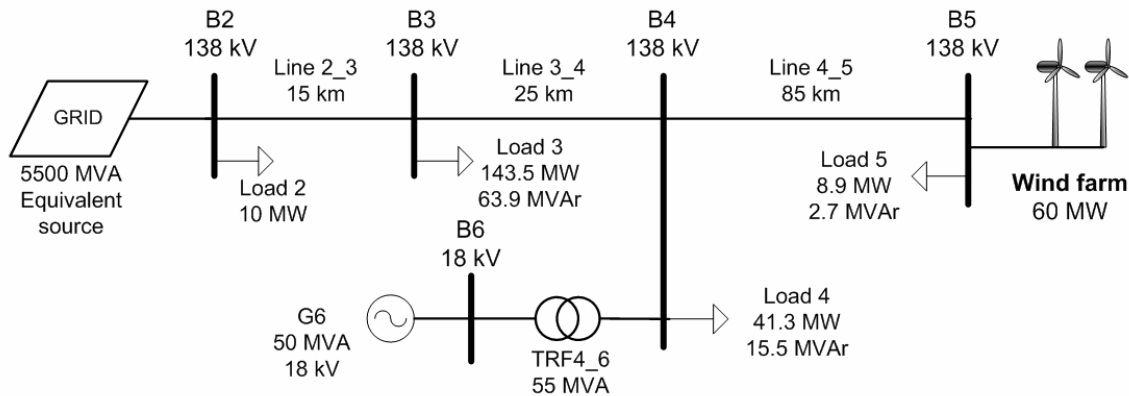


Fig. 6.2 Schematic diagram of 5-bus power system with 60-MW wind farm

The 5-bus system is derived from the 27-bus system, which is a regional network of a large power utility (Section 4.3.1 and Appendix A3). There are four load points totaling 203 MW and 82.1 MVAR (219 MVA). The total power factor is 0.93 lagging. A 50-MVA synchronous generator  $G6$  (PV generator,  $P_{ref} = 43$  MW) is connected at bus  $B6$ . A wind farm with the nameplate rating of 60 MW is connected to the grid at bus  $B5$  through two step-up transformers. When being considered, either an ESS or an SVC is connected at bus  $B5$ , which is the point of connection of the wind farm with the grid.

The 5-bus system is connected to a larger grid at bus  $B2$  through a bus tie. The larger grid is modeled as an equivalent source consisting of a 138-kV 3-phase voltage source in series with an RL-impedance and having the short-circuit capacity of 5500 MVA. Synchronous generator  $G6$ , a round-rotor type machine, is modeled in detail with its steam turbine, governor and excitation systems. All transmission lines are modeled using pi-model. Under normal operating conditions (with the wind farm online), the system is a healthy grid with voltage profiles within the permissible limits of  $\pm 5\%$  of the nominal values.

The 60-MW wind farm consists of 40 1.5-MW wind turbines (either all stall-regulated or all DFIG). It is modeled as three groups of wind turbines. Group 1 is largest with 20 wind turbines (30 MW), followed by Group 2 (12 wind turbines, 18 MW). Group 3 is smallest with 8 wind turbines (12 MW). Depending on the considered scenario, three groups of wind turbines may experience identical or different wind speed profiles.

#### **6.3.4.2 Modeling of ESS**

As said in Section 6.1, the storage technologies being considered in this study are synchronous-machine-based ESS, such as PHES, CAES or a thermal unit with any type of energy storage. Since the ESS (to be connected at bus  $B5$ , Fig. 6.2) is to be used to supply solely reactive power, it is modeled as a synchronous machine with an excitation system. The excitation system [30] consists of an IEEE type I synchronous machine voltage regulator and an exciter.

The SM-based ESS is rated based on a previous work on estimating ESS economic rating (Chapter 5 and [36]). An optimal rating for ESS is around 13% of the wind farm rating, or 7.8 MVA for the 60-MW wind farm. The reactive demand of 1.5-MW stall-regulated wind turbine at the rated output is 0.605 MVAR (Chapter 2, Section 2.3.3.1). Therefore, the wind farm reactive demand at its peak output is 24.2 MVAR (40 turbines  $\times$  0.605). Combining the economic rating and the peak reactive demand, the ESS (named  $E7$ ) rating is set at 10 MVA. At full output, the ESS could supply around 41% of the wind farm reactive demand at the rated output.

### **6.3.4.3 Modeling of SVC**

The SVC is a built-in component by Matlab. It is modeled using two current sources. It can generate positive and negative currents, but no zero-current. Two control modes are possible: voltage control and var regulation. The SVC susceptance is hold constant for var regulation mode [30]. To facilitate comparison with the ESS, the SVC capacitive rating is set equal to the ESS i.e. +10/-5 MVAR. The allowed voltage droop is 1%.

### **6.3.4.4 Data and simulation package**

The data for the stall-regulated wind turbine, DFIG, ESS, and the 5-bus power system are provided in Appendix A2. The power system is built and simulated using Matlab Simulink SimPowerSystems [30].

## **6.4 EXPERIMENT WITH STALL-REGULATED WIND TURBINE**

In this section, the efficacy of the SM-based ESS is examined with stall-regulated wind turbines. Three performance criteria are used, namely, (i) Wind farm voltage recovery after a remote fault, (ii) Critical clearing time, and (iii) Voltage sag at the wind farm terminals under nearby faults. The results are compared with those of SVC and Base case A.

### ***Base case A:***

The 60-MW wind farm with all stall-regulated wind turbines is online and outputs the rated power. All wind turbines encounter the same wind speed of 15 m/s. This is to create the worst-case situation of reactive consumption by the wind farm. Three capacitor banks are placed next to the three groups of wind turbines to provide full reactive supply to the farm at the rated output. All protection systems are disabled to allow complete recording of the desired quantities.

### **6.4.1 Wind farm voltage recovery after a remote fault**

#### ***Scenario 1:***

The ESS  $E7$  is connected at bus  $B5$  under Base case A condition. A remote 3-phase-to-ground (3P2G) fault with fault impedance  $Z_f = 3.3$  ohms occurs at bus  $B3$  at  $t = 15$ s and lasts 30 cycles (0.5s). The voltage at the induction generator terminal (i.e. 690-V bus) is recorded. The ESS is later disconnected and the SVC is connected to the same bus  $B5$  and the same fault condition is repeated. Before the fault occurs, although the ESS or the SVC is online, they output no reactive power. This is done by setting the voltage reference for the excitation system (ESS) and for the SVC control system equal to the grid normal voltage at the point of connection (0.971

pu). In this way the prefault voltage condition of the network is kept to be identical to that of Base case A, despite the presence of the ESS or the SVC. The ESS or the SVC is controlled to provide dynamic reactive support only for some short duration during and after the fault is cleared (i.e. the voltage recovery period).

### Results

Figure 6.3 shows the wind farm terminal voltage before, during and after the fault for Base case A (no ESS or SVC), and the situations with the ESS or the SVC online. The ESS and SVC reactive output behavior is shown in Fig. 6.4.

It can be seen from Fig. 6.3 that both the ESS and SVC help the wind farm voltage recover effectively. Notably, the ESS performance is better than the SVC. For Base case A, the voltage recovery duration, which is measured from the time the fault is cleared at  $t = 15.5\text{s}$  to the time the voltage resumes its prefault value (0.9538 pu), is 5.376s. The recovery duration is 3.764s (improved by 30%) with the support of the SVC and 2.446s (improved by 54.5%) with the ESS. The magnitude of the voltage sag is smallest for the ESS, followed by the SVC and Base case A.

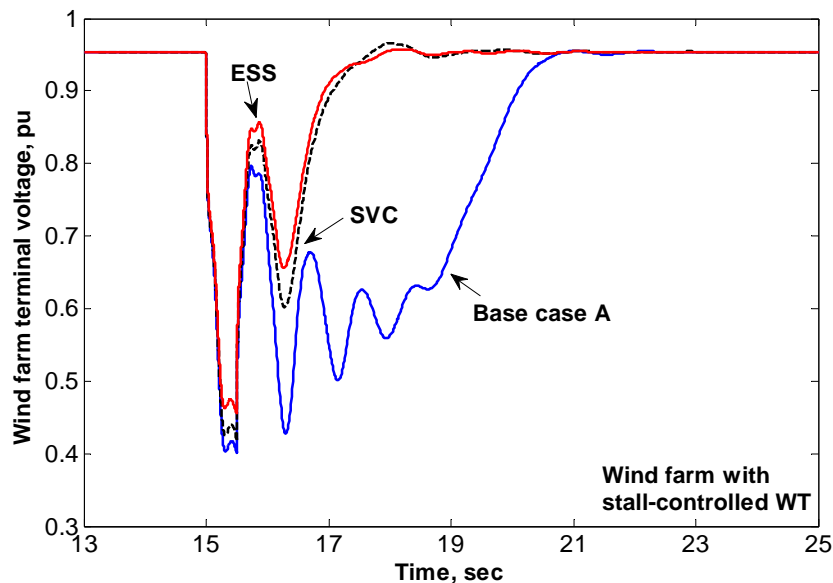


Fig. 6.3 Wind farm voltage profile under 30-cycle remote 3P2G fault

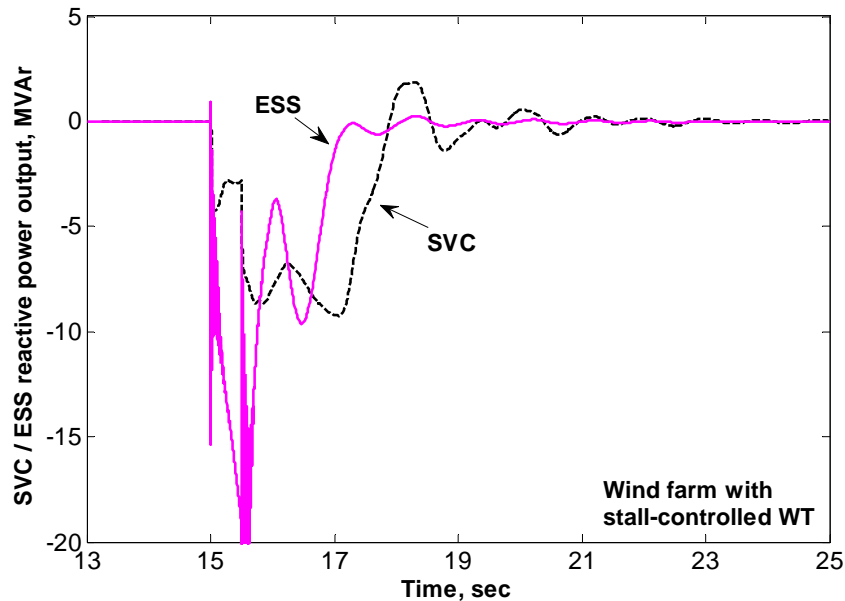


Fig. 6.4 ESS and SVC reactive output

By visual inspection of Fig. 6.4, the ESS and the SVC post-fault dynamics are similar. After the wind farm voltage recovers, the ESS output subsides to zero faster than the SVC. Being a synchronous machine, the ESS can boost its reactive output up to the value approximately twice its continuous rating (10 MVA) for a short duration. It is visible from Fig. 6.4 that the ESS output jumps to around -20 MVAR during the fault. The observation suggests that rapid reactive supply help reduce the wind farm voltage sag during the fault.

## 6.4.2 Critical clearing time for wind farm

### *Scenario 2:*

The ESS or the SVC is online under Base case A condition. Under grid normal conditions, they do not supply reactive power as explained in Scenario 1. A bolted 3-phase-to-ground (3P2G) fault is applied at bus  $B5$  (the point of wind farm connection with the grid) and bus  $B4$  (the point of connection of generator  $G6$  with the grid). Then, the same experiment is repeated with a bolted single-phase-to-ground (1P2G) fault. The fault duration is gradually increased until an induction generator reaches its critical speed (i.e. the speed that the generator must not exceed to be able to return to synchronism after the fault clearance). The fault duration corresponding to the critical speed is the critical clearing time for the wind farm.

### *Results*

The obtained critical clearing time (CCT) for the 60-MW wind farm is presented in Table 6.1 and Fig. 6.5. For 3P2G fault (Table 6.1), the CCT is not improved significantly with the aid of the ESS or the SVC. Though, the ESS and the SVC bring some benefit by raising the wind farm CCT from 4–5 cycles (Base case A) to 5–6 cycles. It usually takes a circuit breaker 5 or 6 cycles to operate to clear a fault [85]. Hence, without the SVC or the ESS, the wind farm would pull out of synchronism before the breaker operation (with the base-case CCT = 4 cycles). With the aid of the ESS or the SVC, the wind farm can withstand the bolted 3P2G faults for 5-6 cycles. Then, the breaker would operate to clear the faults so the wind farm stays in synchronism.

Table 6.1 Critical clearing time for 60-MW wind farm

	Critical clearing time, cycle			Critical clearing time, second		
	Base case A	SVC	ESS	Base case A	SVC	ESS
<b>3-phase to ground fault, <math>Z_f = 0</math></b>						
<b>Fault at B5</b>	4	5	5	0.0667	0.0833	0.0833
<b>Fault at B4</b>	5	5	6	0.0833	0.0833	0.1000
<b>1-phase to ground fault, <math>Z_f = 0</math></b>						
<b>Fault at B5</b>	26	29	32	0.4333	0.4833	0.5333
<b>Fault at B4</b>	67	79	102	1.1167	1.3167	1.7000

For 1P2G fault, the impact of the ESS and the SVC is more visible (Fig. 6.5). They both raise the CCT compared to that of Base case A, but the ESS is more efficient than the SVC. For example, under the 1P2G fault at bus *B5*, the ESS increases the CCT to 0.5333s, a 23.1-percent improvement compared to that for Base case A (0.4333s). The SVC, on the other hand, raises the CCT only by 11.5% (0.4833s). For the 1P2G at bus *B4*, the improvement is 52.2% for the ESS and 17.9% for the SVC.

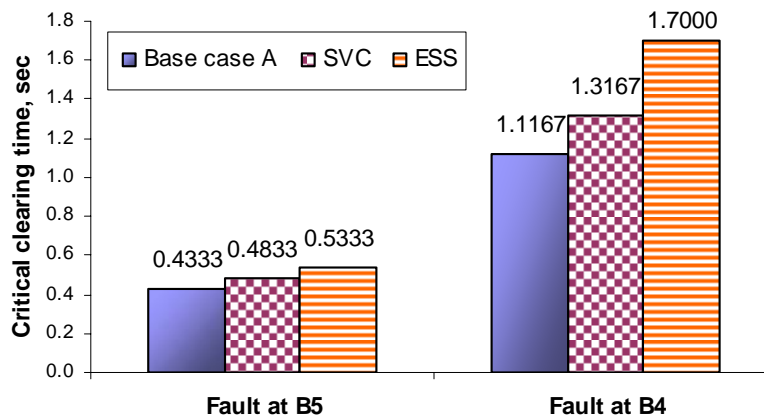


Fig. 6.5 Critical clearing time under bolted 1P2G fault

### 6.4.3 Voltage sag at the wind farm terminals under nearby faults

#### *Scenario 3:*

Similar to Scenario 2. The difference is that the faults are now limited in duration to facilitate observance of voltage sag. The bolted 3P2G fault lasts 4 cycles and the bolted 1P2G fault lasts 26 cycles. Note that the fault durations are the critical durations for Base case A when the faults occur at bus *B5* (Table 6.1). However, the durations are not critical for other situations, such as when the faults occur at bus *B4*, or when the ESS or SVC is present on the system.

#### *Results*

Table 6.2 shows the magnitudes of the voltage at the wind farm terminal. The sag durations are plotted in Fig. 6.6. In Fig. 6.6, for each group of three columns, the first is for Base case A, the second is for the SVC, and the third is for the ESS.

Table 6.2 Magnitude of voltage at wind farm terminal

Wind farm terminal voltage, pu			
	Base case A	SVC	ESS
<b>Bolted 4-cycle 3-phase-to-ground fault</b>			
<b>Fault at B5</b>	0.3610	0.3610	0.3610
<b>Fault at B4</b>	0.4897	0.4991	0.5072
<b>Bolted 26-cycle 1-phase-to-ground fault</b>			
<b>Fault at B5</b>	0.3690	0.3826	0.3979
<b>Fault at B4</b>	0.7020	0.7268	0.7435

The voltage magnitude (Table 6.2) tends to be higher for the ESS, followed by the SVC and Base case A. In other words, the voltage sag is most severe for Base case A, followed by that for the SVC. The sag is least severe for the ESS. For example, when the 1P2G fault occurs at bus *B5*, the wind farm experiences a sag of 29.8% under Base case A condition. With the SVC support, the sag is just 27.3%. It is further reduced to 25.7% with the ESS support.

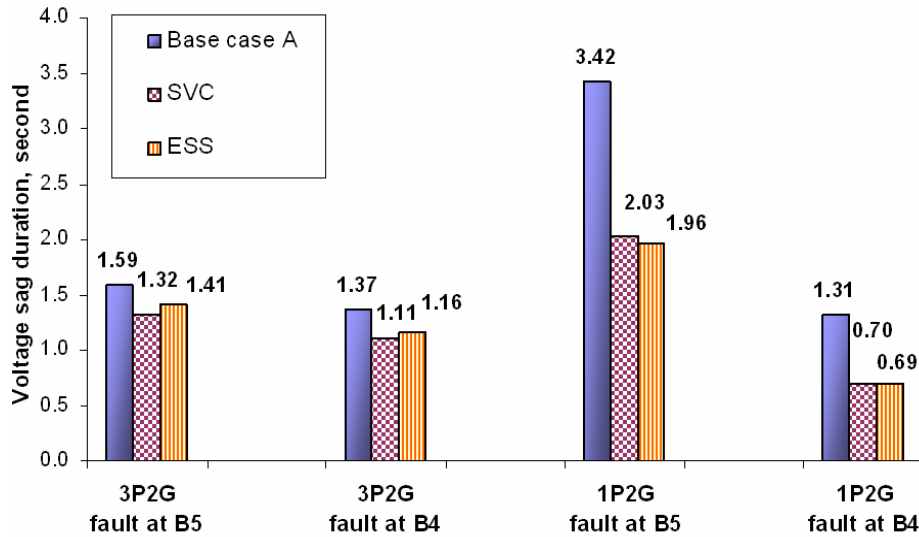


Fig. 6.6 Voltage sag duration under 4-cyc 3P2G and 26-cyc 1P2G faults

The voltage sag duration (Fig. 6.6) is shortened compared to that of Base case A with either SVC or ESS operational. In most cases, the sag duration for the SVC is similar to that for the ESS.

The ESS or the SVC brings certain benefit in terms of low-voltage ride-through capability of the wind farm. For example, a grid code [86] requires that wind farms stay connected when their terminal voltage drops below 0.75 pu for 1.0s. In the event of the 1P2G fault at bus B4 (Fig. 6.6), with the aid of the ESS or the SVC, the voltage is below 0.75 pu for only around 0.7s and the wind farm remains in synchronism. Therefore, the wind farm can stay connected as the code requires. Without the ESS or the SVC, the wind farm voltage is below 0.75 pu for 1.31s so the wind farm would likely trip.

## 6.5 EXPERIMENT WITH DFIG

In this section, the efficacy of the SM-based ESS is validated with doubly-fed induction-generator-based wind turbine (DFIG). Two performance criteria are used, namely, (i) Wind farm voltage recovery after a remote fault, and (ii) Voltage sag at the wind farm terminals under nearby faults. The results are compared with those of SVC and Base case B. The critical clearing time is not used because it is hard to determine the critical speed for DFIG.

### ***Base case B:***

Base case B is similar to Base case A (Section 6.4), except for two differences. One is that the 60-MW wind farm consists of all DFIG. The other is that no capacitor bank is connected at

the wind farm bus. Instead, all DFIG is operated in var-regulation mode so that no reactive power is drawn from the grid.

### 6.5.1 Wind farm voltage recovery after a remote fault

**Scenario:** Repeating Scenario 1 (Section 6.4.1).

#### **Results**

Figure 6.7 shows the wind farm terminal voltage before, during and after the remote 30-cycle bolted 3P2G fault (with  $Z_f = 3.3$  ohms) occurs at bus  $B3$ . The voltage profiles for Base case B, the SVC and the ESS are similar. Since DFIG wind turbines can control their reactive power, the ESS or the SVC do not have considerable impact on voltage recovery. Their only noticeable benefit is that the voltage sag during the fault is milder compared to Base case B.

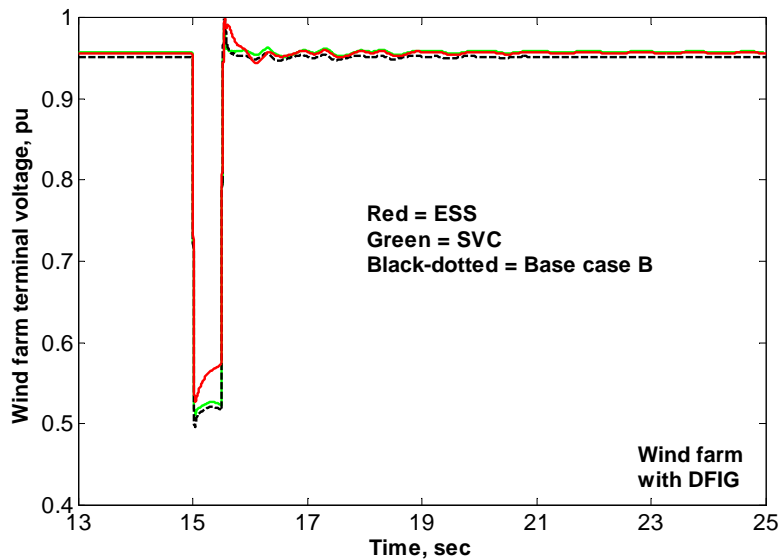


Fig. 6.7 Voltage profile at the wind farm terminal under 30-cyc 3P2G fault

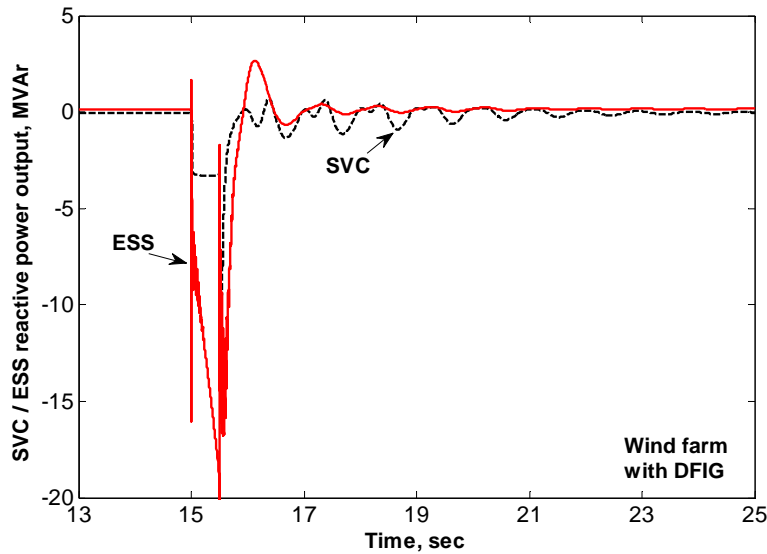


Fig. 6.8 SVC and ESS reactive output (3P2G fault with DFIG)

Like its behavior with stall-regulated wind turbines (Section 6.4), the ESS boosts its reactive output temporarily to around twice its continuous rating during the fault (red curve, Fig. 6.8). Visual inspection of Fig. 6.8 shows that the ESS reactive output rapidly increases and reaches a value of around -20 MVAR during the fault. Thanks to its rapid reactive ramping ability, the ESS helps lower the sag severity compared to the SVC. It is also noted that the postfault response of the ESS is smoother than that of the SVC.

### 6.5.2 Voltage sag at the wind farm terminals under nearby faults

**Scenario:** Repeating Scenario 3 (Section 6.4.3).

#### Results

Table 6.3 shows the magnitudes of the voltage at the wind farm terminal. The sag durations are shown graphically in Fig. 6.9.

Table 6.3 Magnitude of voltage at wind farm terminal (DFIG)

Wind farm (with DFIG) terminal voltage, pu			
	Base case B	SVC	ESS
<b>Bolted 4-cycle 3-phase-to-ground fault</b>			
Fault at B5	0.0146	0.0372	0.0109
Fault at B4	0.0643	0.0323	0.0430
<b>Bolted 26-cycle 1-phase-to-ground fault</b>			
Fault at B5	0.4803	0.4890	0.4997
Fault at B4	0.6841	0.7025	0.7123

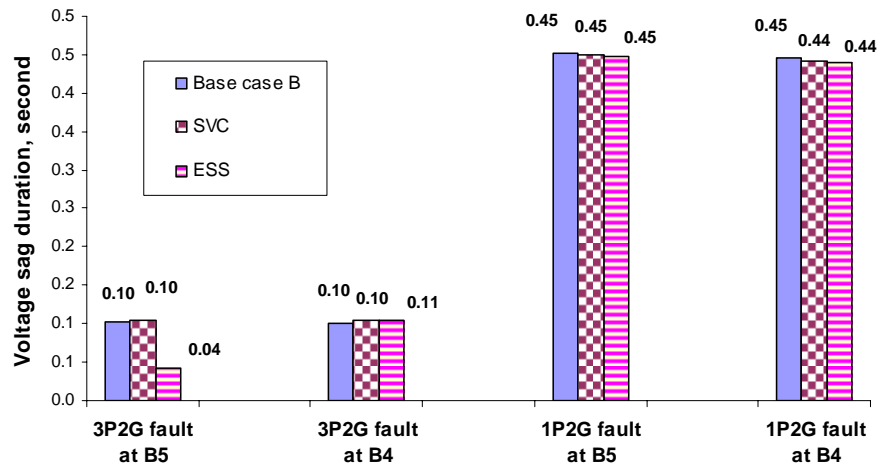


Fig. 6.9 Voltage sag duration under 4-cyc 3P2G and 26-cyc 1P2G faults (DFIG)

The results show that, for the 4-cycle 3P2G fault, the sag magnitudes are much larger for DFIG compared to the stall-regulated wind turbines (see Table 6.2, Section 6.4.3). During the fault, the wind farm terminal voltage is reduced to some near-zero value but the sag duration is short (6-8 cycles, Fig. 6.9). For the 26-cycle 1P2G fault, the sag magnitude is nearly similar to that for stall-regulated wind turbines but the duration is shorter. The impact of the SVC and the ESS on reducing voltage sag is not significant. However, under 1P2G faults, the sag magnitude tends to be less with the SVC or the ESS support. Notably again, the ESS performance is better than the SVC (Table 6.3).

## 6.6 CHAPTER CONCLUDING REMARKS

This chapter presents an investigation into the efficacy of a novel ESS operation scheme in increasing wind farm transient stability. The scheme employs synchronous-machine-based ESSs (e.g. PHES, CAES) to supply reactive power dynamically to wind farms during faults. The validation experiment is carried out with a 60-MW wind farm and two popular types of wind turbines, namely, stall-regulated and DFIG. Furthermore, the ESS effectiveness is compared with that of an SVC. The results have led to the following conclusion:

- (i) **General finding:** Apart from their ability to regulate wind farm real power output, the SM-based ESSs can also be used to provide dynamic reactive support to wind farms so as to increase the farms transient stability condition.

- (ii) **ESS and DFIG:** The investigated SM-based ESS is not an efficient device if used for supplying reactive power to DFIG because these wind turbines have the ability to regulate their own reactive power. The ESS has some benefit in reducing the voltage sag but the benefit is insignificant.
- (iii) **ESS and stall-regulated wind turbine:** The ESS is particularly effective if used for the wind farm with stall-regulated wind turbines. The ESS can increase the farm critical clearing time by 1 cycle for worst-case bolted 3P2G faults. For bolted 1P2G faults, the CCT is improved by 23.1%–52.2%, depending on the fault location. The ESS helps reduce the voltage sag severity and shorten the post-fault voltage recovery duration by up to 54.5%.
- (iv) **ESS versus SVC:** The ESS performance is better than that for the SVC of comparable capacitive rating in most considered situations. For example, under bolted 1P2G faults, the ESS increases the wind farm CCT by 23.1%–52.2% while the SVC achieves 11.5%–17.9%. Therefore, an SM-based ESS can successfully substitute an SVC for providing dynamic reactive support for wind farms.
- (v) **ESS mode of operation:** The results suggest that the SM-based ESS should be operated in three modes instead of the two usual modes, namely, (i) Motor mode for charging, (ii) Generator mode for discharging (with lagging or unity power factor), and (iii) Synchronous-condenser mode for reactive supply. The last mode is particularly useful when the ESS is fully discharged (i.e. the energy storage is empty). In this way the ESS can be fully exploited to maximize its efficiency and value.

## Chapter 7

### Conclusion and future work

#### 7.1 RESEARCH SUMMARY

This section provides a summary of the research motivation, objectives, approach, and major results. Based on these results, further study is proposed to improve the current research.

##### 7.1.1 Research motivation and objectives

The research was motivated by the necessity to solve two main problems which hinder wind power integration. They are: how to reduce wind power fluctuation and how to ensure stability of the farm and host grid. It is envisaged that wind farm output fluctuation can be reduced by using a specific type of buffer, such as an energy storage system (ESS), to absorb its negative impact. An energy storage systems can be used to store unwanted wind power from time to time and appropriately re-dispatch it later. An ESS can also be used to stabilize a farm by dynamic reactive power supply during faults. It is proposed, therefore, to use energy storage systems to solve the wind-farm-related problems.

The overall research goal is to *“Increase both wind power penetration and voltage stability limits using energy storage systems”*. The term “wind power penetration” is defined as the amount of wind power channeled into the grid. The term “voltage stability” includes two types; steady-state (small-disturbance) voltage stability and transient (large-disturbance) stability.

Specifically, the research aims to design an application, based on an energy storage system, to regulate the output from a wind farm in order to meet the overall research goal. Conceptually, the design consists of a wind farm and an ESS, defined as an “aggregate system”. The system may also include several wind farms and one ESS. The expanded research objectives are:

- (i) To develop a wind turbine model suitable for voltage stability studies.
- (ii) To define a framework for the ESS-based application by specifying the sequence (steps) to be followed when designing an ESS for use with a wind farm.
- (iii) To develop a unique method for estimating the optimal ESS rating, a technique for determining a reference power profile, and an ESS charge-discharge scheme, based on the farm rating and other characteristics such as capacity factor and power output profile.

- (iv) To use the wind turbine model, the ESS-application framework, and the optimal-sizing method to construct a unique strategy for the operation of an ESS which meets the overall research goal of increasing wind power integration and grid voltage stability.

### 7.1.2 Research approach

The wind-farm related problems are solved using current engineering theories and quantitative validation. The overall research is broken down into a set of sub-problems which are solved one step at a time. For each sub-problem, an analytical solution or procedure is developed based on power system voltage stability criteria, optimization, and general science. The solution or procedure is then quantitatively validated or tested using realistic power systems and wind farm data.

The specific approach for each objective is as follows.

- (i) **Objective 1:** In developing a wind turbine model, wind turbine, electric machine, and modeling theories are used. The wind turbine model is connected to a power system and comprehensively tested to ensure accuracy. The validation criteria are wind turbine power generation behavior and torque-speed characteristics under normal and fault conditions.
- (ii) **Objective 2:** In defining the framework for an ESS-based application, existing knowledge of power system operations and wind farms are utilized together with engineering design concepts. The framework efficacy is evaluated using the case study of a 183 MW wind farm connected to 27-bus power system. The evaluation criteria include voltage stability, ESS impact on wind power integration, and the ability of an ESS to reduce mismatch between wind farm output and grid demand.
- (iii) **Objective 3:** For the development of a reference power profile (desired output profile), an ESS charge-discharge scheme, and a new method of determining ESS optimal rating, optimization theory is applied. The aim of this stage is to increase wind power integration and grid steady-state voltage stability. The outcomes are validated using both technical and economic criteria, and a large data set. The data set includes 17 wind farms with diverse characteristics, a wide range of ESS ratings (0.5–165 MW and 0.5–8 hours) and 27-bus grid realistic load conditions. The ESS technology under consideration is compressed-air energy storage (CAES).

- (iv) **Objective 4:** A new ESS operation scheme for increasing wind farm transient stability is proposed. The scheme efficacy is assessed using a case study with a 60 MW wind farm, a 5-bus power system, and two types of popular wind turbines (stall-regulated and DFIG). The stability criteria for evaluation are critical clearing time, voltage recovery, and voltage sag.

Four computation and simulation packages are used for all of the studies. They are PSCAD/EMTDC [29], Matlab [30], Neplan [31], and Matpower [32]. Software results are either validated by analytical calculation or cross-checked with a comparable package to ensure accuracy. All codes used for computation are written in Matlab.

### 7.1.3 Research main results

- (i) ***Development of a wind turbine model suitable for stability studies:*** This objective is met with the development of a stall-regulated wind turbine model which is one of the most popular types of wind turbines in use today. Detailed testing shows that the developed model is accurate. Given that dynamic wind turbine models are in a developmental stage, this model contributes to the area of wind turbine modeling.
- (ii) ***Design of a framework for an ESS-based application:*** The proposed framework includes a new technique for calculating the reference power profile (the desired output profile), an ESS charge-discharge scheme, and a unique optimization-based (direct-calculation) method for determining an optimal ESS rating.
- (iii) ***Technique for calculating desired output profile:*** The proposed technique uses optimal power flow to determine the best output profile achievable by the aggregate system for the benefit of the grid. The term “benefit” is defined as “minimizing the total cost of grid generated power”. Regulating the wind farm output according to the desired profile causes the farm to behave like a dispatchable power source while taking into account the cost of system generation. This technique, to the best knowledge of the author, has never been proposed and, therefore, is a completely new approach.
- (iv) ***ESS charge-discharge scheme and switching operation:*** The designed ESS charge-discharge scheme, used in conjunction with the desired output profile, directs the ESS to store and re-dispatch wind energy as necessary. Analysis with 14 wind farms shows that the developed charge-discharge scheme and the desired output calculation technique are appropriate for ESS operation. While regulating

output variation from the 14 wind farms, the optimal ESS perform 4 or less switching operations daily for 73.2%–85.5% of the year. On average, the ESS carry out 2.5–3.1 switching operations per day.

- (v) **Optimization-based method for determining ESS optimal rating:** The unique method developed in this research is based on the formulation of a cost-based objective function, discretization of this function, and an exhaustive search of the function values to determine an optimal ESS rating. Using this method, an optimal ESS rating can be calculated for any wind farm with a high degree of accuracy. Analysis with a compressed-air energy storage system (CAES) and 14 wind farms shows a significant trend. For wind farms with ratings of 91.5–210 MW and a capacity factor of 33% or better, the ESS optimal power rating is between 9% and 14% of the wind farm nameplate capacity. The optimal ESS energy rating is 4–4.5 hours. Using the same cost and benefit values, this finding is recommended for the empirical estimation of an CAES rating for similar wind farms. The result is based on the ESS operating under the developed charge-discharge scheme and being able to discharge 100% of accumulated energy. Overall, the proposed method is efficient for solving the ESS sizing problem. It has a considerable advantage over traditional differential-based methods because it does not require knowledge of the analytical form of the objective function. Hence, it is very suitable for the ESS sizing problem where the analytical form of the objective function is hard to determine. Using discretization and exhaustive search, the proposed method is capable of finding a global optimum for the problem, if such an optimum exists.
- (vi) **Wind power integration and small-disturbance stability:** From the case study with the 183-MW wind farm connected to the 27-bus transmission grid, the ESS can increase the grid steady-state voltage stability, measured using the smallest eigenvalues, by a net amount between 2.7% and 22.3%, compared to the case where the wind farm output variability is completely unregulated. For ESS rating of 1–183 MW and 0.5–8 hours, the mismatch between the wind farm output and the grid load-demand can be reduced by 0.1%–77.7%. The analysis with the 14 wind farms shows that, for optimal ESSs rating, the overall enhancement in wind energy integration is between 1.7% and 8%. In addition, a net increase in steady-

state voltage stability of 8.3%–18.3% is achieved for the 27-bus grid by 13 of the 14 evaluated ESSs.

- (vii) ***ESS operation scheme for increasing wind farm transient stability:*** The unique scheme exploits the use of a synchronous-machine-based ESS as a synchronous condenser to stabilize wind farms by dynamic reactive power supply during faults. Analysis with an ESS and a 60 MW wind farm consisting of stall-regulated wind turbines shows that the ESS increases the farm critical clearing time (CCT) by 1 cycle for worst-case bolted three-phase-to-ground faults. For bolted single-phase-to-ground faults, the CCT is improved by 23.1%–52.2%. The ESS helps mitigate the voltage sag severity and reduce the post-fault voltage recovery duration by up to 54.5%. In most of the situations investigated, the performance of the ESS is better than that for a static var compensator (SVC) of comparable capacitive rating. This leads to a new technique for operating a synchronous-machine-based ESS so as to increase its efficiency and value.

## 7.2 FUTURE WORK

The future research, which is proposed to improve the current completed work, includes two main tasks.

Task 1: **To optimize the ESS charge-discharge scheme**

Task 2: **To enhance the optimization-based method for determining the optimal ESS rating.**

### ***Rationale for Task 1***

The current ESS charge-discharge scheme is designed on the rule to “discharge whenever there is a wind power deficit and aim at compensating for 100% of the deficit amount”. While this approach proves to be helpful in achieving the completed research goal, it may not be the best approach based on a consideration of voltage stability and an economic viewpoint.

With respect to voltage stability, the energy available in the ESS can be distributed in a specific optimal manner to maximize grid stability. For example, using a wind power forecast tool, it is possible to predict the wind farm output for 30 minutes, for an hour, or for a longer period in advance. Then, based on this forecast, the accumulated wind energy in the ESS can be appropriately dispatched to achieve the highest possible stability.

For the economic consideration, in addition to using the wind power forecast, the real-time electricity market price information can be included in the design of the ESS charge-discharge scheme. The goal is two-fold; ensuring stability and selling the wind energy at the highest possible price to maximize economic benefit.

### ***Rationale for Task 2***

As discussed in Chapter 5 and Section 7.1.3, the optimization-based method developed in the research has a significant advantage when used to solve the ESS sizing problem in which the analytical form of the objective function is unknown. By employing discretization coupled with exhaustive search, the method is shown to be capable of finding the global optimum for the problem, provided the optimum exists. Given the method efficacy, it is desirable for it to be improved for better performance.

The key to enhancing this method is based on developing techniques for defining the benefit terms included in the objective function. The current objective function includes five benefit factors: (i) revenue from discharged energy, (ii) revenue from wind farm capacity firming, (iii) revenue from improved voltage stability, (iv) revenue from improved reliability, and (v) revenue from environmental considerations.

In the study presented for validating the method in Chapter 5, an assumption is made to implement a staged solution. This is because the benefit terms (iii) to (v) above cannot be expressed as functions of an ESS rating. As a consequence, they have to be combined with benefit term (ii) to form a single term which then enables the staged solution. If a benefit term, such as revenue from improved voltage stability, can be expressed as a function of the ESS rating, it will be accounted for in a more accurate manner during the optimization process. It then follows that the solution (ESS optimal rating) is also likely to be more accurate.

In summary, the overall research goal – to increase wind power penetration and voltage stability limits – has been achieved. The developed techniques for application-design, sizing, and operation of energy storage systems may be used for other applications with storage systems. Some examples include using energy storage systems for deferral of transmission and distribution upgrades, enhancement of power quality and reliability, demand response, and frequency control.

## Appendix A1

### Publication record

1. Ha Thu Le and T. K. Saha, "Investigation of power loss and voltage stability limits for large wind farm connections to a subtransmission network," in *Power Engineering Society General Meeting*, 2004. IEEE, 2004, pp. 2251-2256 Vol.2.
2. S. Santoso and Ha Thu Le, "Fundamental time-domain wind turbine models for wind power studies," *Renewable Energy* journal, vol. 32, pp. 2436-2452, 2006.
3. Ha Thu Le and S. Santoso, "Analysis of Voltage Stability and Optimal Wind Power Penetration Limits for a Non-radial Network with an Energy Storage System," in *Power Engineering Society General Meeting*, 2007. IEEE, 2007, pp. 1-8.
4. Ha Thu Le and Thang Quang Nguyen, "Sizing energy storage systems for wind power firming: An analytical approach and a cost-benefit analysis," in *Power and Energy Society General Meeting - Conversion and Delivery of Electrical Energy in the 21st Century*, 2008 IEEE, 2008, pp. 1-8.
5. Ha Thu Le, S. Santoso, and W. M. Grady, "Development and analysis of an ESS-based application for regulating wind farm power output variation," in *Power & Energy Society General Meeting*, 2009. PES '09. IEEE, 2009, pp. 1-8.
6. Ha Thu Le and S. Santoso, "Increasing Wind Farm Transient Stability by Dynamic Reactive Compensation: Synchronous-Machine-Based ESS versus SVC," in *Power & Energy Society General Meeting*, 2010, IEEE, 2010, pp. 1-8.

## Appendix A2 Power system, wind turbine, and ESS data

Table A2.1 Stall-regulated wind turbine data [33, 47]

Notation	Parameter	Value	Unit
Aerodynamic block and Shaft			
$J_T$	Rotor moment of inertia	995.8	kgmm
$R_T$	Rotor radius	35	m
GR	Gear ratio	70	
D	Equivalent damping	30.3	Nms/rad
K	Equivalent stiffness	19720	Nm/rad
$V_{wind\_rated}$	Rated wind speed	15	m/s
	Cut-in / Cut-out wind speed	5 / 25	m/s
Induction generator (a)			
S	Generator apparent power	1667	kVA
P	Generator rated real power	1500	kW
$V_{rated}$	Generator rated voltage	690	V
$I_{rated}$	Generator rated current	1395	A
Poles	Number of poles	6	
$f_n$	Nominal frequency	60	Hz
$r_s$	Stator resistance	0.0092	pu
$X_{ls}$	Stator leakage reactance	0.0717	pu
$X_M$	Magnetizing reactance	4.1376	pu
$r_r$	Rotor resistance	0.007	pu
$X_{lr}$	Rotor leakage reactance	0.0717	pu
$J_G$	Generator moment of inertia	63.87	kgmm
Slip	Slip at rated power	0.67	%

**Note:** (a) Induction generator data are in per unit on its own base.

Table A2.2 DFIG data [30, 82-84]

Notation	Parameter	Value	Unit
Turbine data			
Nominal mechanical power (b)		1500	kW
Tracking characteristic speed		[0.7 0.71 1.2 1.21]	pu
Power at point C (pu/ mechanical power)		0.99	
Wind speed at point C		12	m/s
Pitch angle controller gain (Kp)		500	
Maximum pitch angle		45	deg
Maximum rate of change of pitch angle		2	deg/s
Wound-rotor generator (c)			
S	Generator apparent power	1670	kVA
P	Generator rated real power	1500	kW
$V_{rated}$	Generator rated voltage	575	V
Poles	Number of poles	6	
$f_n$	Nominal frequency	60	Hz
$r_s$	Stator resistance	0.00706	pu
$X_{ls}$	Stator leakage reactance	0.171	pu
$X_M$	Magnetizing reactance	2.9	pu
$r_r$	Rotor resistance	0.005	pu
$X_{lr}$	Rotor leakage reactance	0.156	pu
$H_G$	Generator inertia constant	5.04	s

Table A2.2 DFIG data (continued)

Converter data		
Converter maximum power	0.5	pu
Grid-side coupling inductor L/R	0.15 / 0.0015	pu
Coupling inductor initial current mag/phase	0 / 90	pu / deg
Nominal DC bus voltage	1200	V
DC bus capacitor	0.01	F

**Note:** (b) Mechanical power is adjusted to  $1500 \times 1.025$  kW to achieve the real power output of 1.5 MW at 15 m/s.

(c) Wound-rotor generator data are in per unit on its own base.

Table A2.3 5-bus power system data

Notation	Parameter	Value	Unit
Equivalent source (5500 MVA 138 kV) X / R =		15	
Equivalent source X0 / X1 =		3	
Line data			
Line 2_3	Line R1 / X1	0.0409132 / 0.375125	Ohm/km
Line 3_4	Line R1 / X1	0.0409132 / 0.375125	Ohm/km
Line 4_5	Line R1 / X1	0.135343 / 0.483124	Ohm/km
Generator G6 data (d)			
S	Generator apparent power	50	MVA
$V_{rated}$	Generator rated voltage	18	kV
$f_n$	Nominal frequency	60	Hz
Poles	Number of poles	2	
Reactances $X_d / X_d' / X_d''$		2 / 0.3 / 0.266	pu
Reactances $X_q / X_q' / X_q''$		2 / 0.3 / 0.266	pu
$R_s$	Stator resistance	0.0016	pu
$X_l$	Stator leakage reactance	0.133	pu
$H_G$	Inertia constant	5	s
Time constants $T_{do}' / T_{do}''$		6.666667 / 0.056391	s
Time constants $T_{qo}' / T_{qo}''$		1e-6 / 0.37594	s
Time constants $T_d' / T_d''$		1 / 0.05	s
Time constants $T_q' / T_q''$		1e-6 / 0.05	s
Transformer data (e)			
TRF4_6	18/138 kV, 55 MVA, Y-Y, R / X =	0.0031 / 0.105	pu
TRF5_1	34.5/138 kV, 70 MVA, Yg-D, R / X =	0.0015 / 0.060304	pu
TRF6_1	690V/34.5 kV, 35 MVA, Yg-Y, R/ X=	8.333e-7 / 0.06	pu
TRF6_2	690V/34.5 kV, 25 MVA, Yg-Y, R/ X=	Same as TRF6_1	pu
TRF6_3	690V/34.5 kV, 20 MVA, Yg-Y, R/ X=	Same as TRF6_1	pu
TRF7_1	575V/34.5 kV, 35 MVA, Yg-Y, R/ X=	8.333e-7 / 0.0575	pu
TRF7_2	575V/34.5 kV, 25 MVA, Yg-Y, R/ X=	Same as TRF7_1	pu
TRF7_3	575V/34.5 kV, 20 MVA, Yg-Y, R/ X=	Same as TRF7_1	pu

**Note:** (d) Generator G6 data are in per unit on its own base.

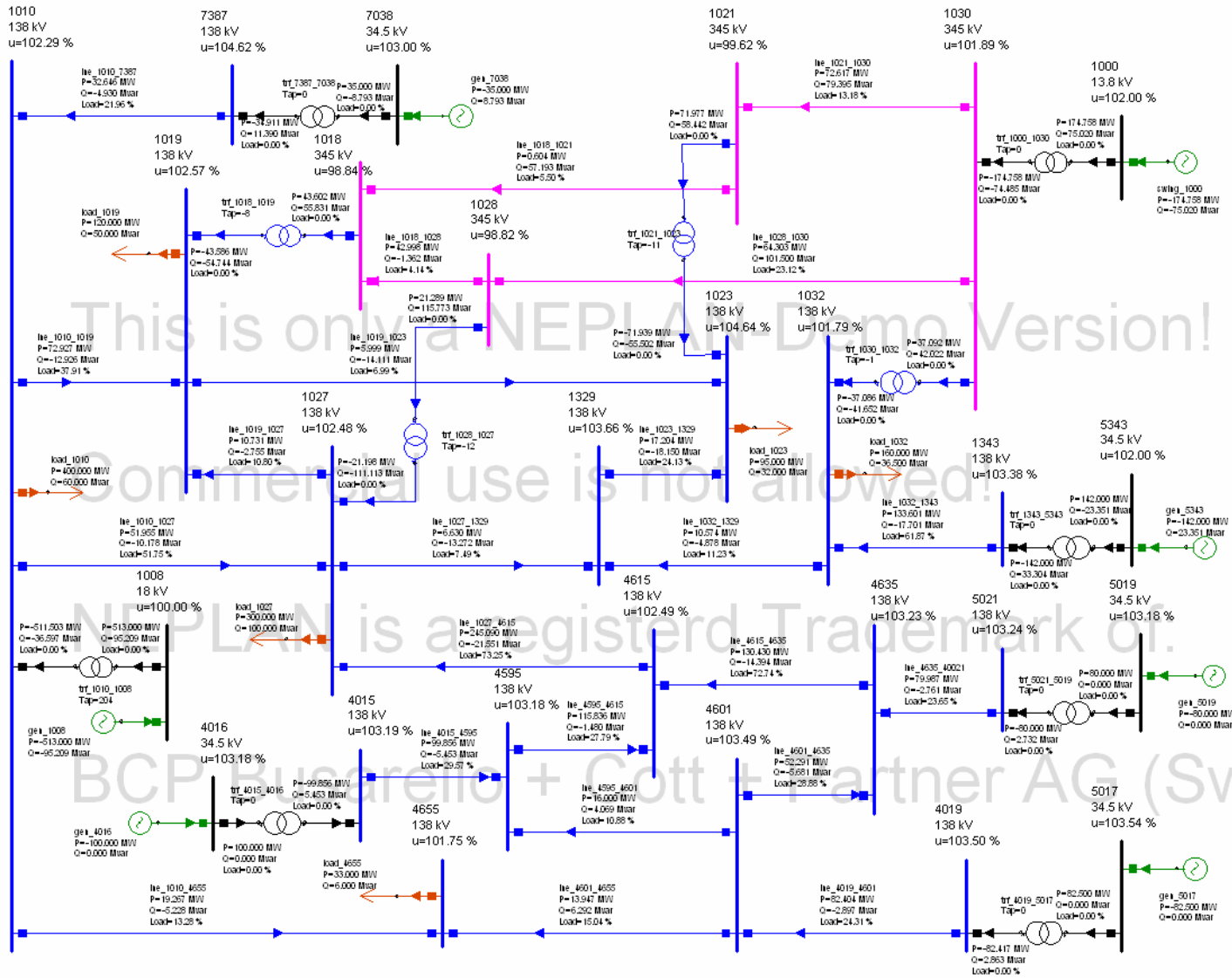
(e) Transformers TRF6\_1, TRF6\_2, TRF6\_3 are used to connect Group 1, Group 2 and Group 3 of stall-regulated wind turbines to TRF5\_1, in the stated order. Similarly, transformers TRF7\_1, TRF7\_2, TRF7\_3 are used to connect Group 1, Group 2 and Group 3 of DFIG to TRF5\_1. TRF5\_1 is connected to the grid at bus B5.

Table A2.4 Synchronous-machine-based ESS data

Notation	Parameter	Value	Unit
S	Apparent power (f)	10	MVA
$V_{\text{rated}}$	Rated voltage	13.8	kV
$f_n$	Nominal frequency	60	Hz
Poles	Number of poles	6	
Reactances $X_d / X_d' / X_d''$		2 / 0.3 / 0.215	pu
Reactances $X_q / X_q''$		2 / 0.215	pu
$R_s$	Stator resistance	0.0019	pu
$X_l$	Stator leakage reactance	0.1075	pu
$H_G$	Inertia constant	5	s
Time constants $T_{do}' / T_{do}''$		6.65578 / 0.069767	s
Time constant $T_{qo}''$		0.465116	s
Time constants $T_d' / T_d''$		1 / 0.05	s
Time constant $T_q''$		0.05	s

**Note:** (f) SM-based ESS data are in per unit on its own base.

## Appendix A3 One-line diagram of 27-bus grid with peak-load power flow



## Appendix A4

### Validation of Matpower optimal power flow solution

This appendix presents a test on compatibility between Matpower optimal power flow (OPF) solution and an analytical solution. First, the analytical solution is obtained for a custom-designed 6-bus power system using the theory on optimal dispatch of generation in [53]. Then, Matpower is run to find the OPF solution for the same 6-bus system. The two solutions are compared to learn if they are compatible. The purpose is to verify the validity of Matpower OPF solution before using it for other calculations. The analytical calculation is performed with the aid of Matlab.

The 6-bus power system is described in Section 3.1.1 (Chapter 3). Its oneline diagram and data are reproduced here for viewing convenience.

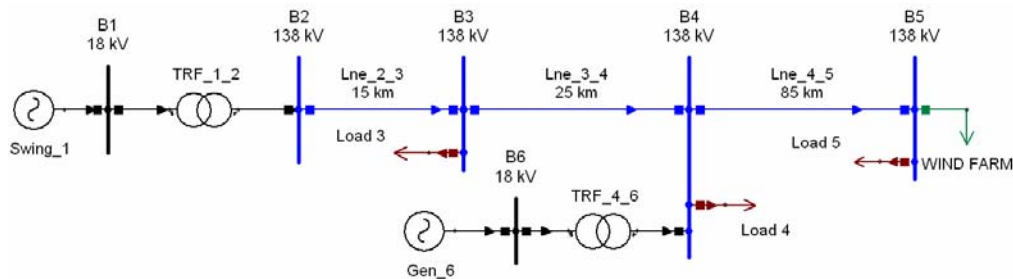


Fig. A4.1 Schematic diagram of 6-bus power system

#### *Power system data*

Generator Swing1:	220 MVA, 18 kV, $R=0.0008713 \Omega$ , $X_d=2$ pu
Generator Gen6:	50 MVA, 18 kV, $R=0.000052 \Omega$ , $X_d=2$ pu
Transformer TRF12:	300 MVA, 18 kV/138 kV, GY-GY, $R=0.154\%$ , $X=6.0304\%$
Transformer TRF46:	55 MVA, 18 kV/138 kV, GY-GY, $R=0.3\%$ , $X=10.05\%$
Line 23:	15 km, $R=0.0409132 \Omega/\text{km}$ , $X=0.375125 \Omega/\text{km}$ , $B=4.43$ microS/km
Line 34:	25 km, $R=0.0409132 \Omega/\text{km}$ , $X=0.375125 \Omega/\text{km}$ , $B=4.43$ microS/km
Line 45:	85 km, $R=0.135343 \Omega/\text{km}$ , $X=0.483124 \Omega/\text{km}$ , $B=3.425$ microS/km
Load 3:	$153.5 + j63.9$ MVA, PF= 0.923 lagging
Load 4:	$41.3 + j15.5$ MVA, PF = 0.936 lagging
Load 5:	$8.9 + j2.7$ MVA, PF = 0.957 lagging
Wind farm:	140 MW, PF=1.0

The test is to find the optimal economic dispatch for the system generators under the maximum load condition as shown in the “Power system data” section above. The wind farm is assumed to be replaced by a conventional generator which has comparable power cost and is operated at unity power factor. For convenience, the system generators are renamed as follows:

Swing\_1 = Generator 1, Gen\_6=Generator 3, and assumed generator (i.e. the replacement for wind farm at Bus 5) = Generator 2. The generators' fuel cost expressions, developed based on [53, 59, 60], and their operation limits are provided in Table A4.1.

Table A4.1 Data for 6-bus power system generators

Generator name	Coefficients of cost functions			Pmax, MW	Pmin, MW	Qmax, MVAR	Qmin, MVAR
	$\gamma$	$\beta$	$\alpha$				
Generator 1	0.0849	5.9	117	200	10	88	-11
Generator 2	0.2500	5.5	152	25	10	1E-7	-1E-7
Generator 3	0.0809	5.6	111	43	10	25	-25

The cost function of generator  $i$  is of the form  $C_i = \gamma_i P_i^2 + \beta_i P_i + \alpha_i$  where  $P$  is the generator output in MW. The generator limits are of the form  $P_{i(\min)} \leq P_i \leq P_{i(\max)}$  and  $Q_{i(\min)} \leq Q_i \leq Q_{i(\max)}$ . The upper P-limit for Generator 2 is set at 25 MW although the wind farm capacity is 140 MW. This is simply to imitate the case where the wind farm outputs up to 25 MW into the system.

The economic dispatch power for the system generators can be found using conventional optimization method with Lagrangian multiplier and KKT conditions. The solution steps, developed based on [53], are as follows. The goal of economic dispatching is to minimize the system total generated power cost  $C_t$  which is the summation of the costs of individual generators, i.e.

$$C_t = \sum_{i=1}^{n_g} C_i = \sum_{i=1}^{n_g} \gamma_i P_i^2 + \beta_i P_i + \alpha_i \quad (\text{A4.1})$$

subject to the equality and inequality constraints

$$\sum_{i=1}^{n_g} P_i = P_D + P_L \quad (\text{A4.2})$$

$$P_{i(\min)} \leq P_i \leq P_{i(\max)} \quad i = 1, 2, \dots, n_g \quad (\text{A4.3})$$

The equality constraint requires that total generation be equal total demand  $P_D$  plus total power loss  $P_L$ . The inequality constraint requires that the generator real power limits be observed. In (A4.1) through (A4.3),  $n_g$  is the number of generators. In this problem, the total power loss  $P_L$  is found using Kron's loss formula [53] and approximated by a quadratic function to facilitate hand-calculation as follows.

$$\begin{aligned}
P_L &= B_{11}P_1^2 + B_{22}P_2^2 + B_{33}P_3^2 \\
&= 0.000053P_1^2 + 0.000632P_2^2 + 0.000106P_3^2 \quad (MW)
\end{aligned} \tag{A4.4}$$

The Lagrangian with added terms to include the inequality constraint is

$$L = C_i + \lambda(P_D + P_L - \sum_{i=1}^{n_g} P_i) + \sum_{i=1}^{n_g} \mu_{i(\max)} (P_i - P_{i(\max)}) + \sum_{i=1}^{n_g} \mu_{i(\min)} (P_i - P_{i(\min)}) \tag{A4.5}$$

The minimum to this unconstrained function is found at the point where the following optimality conditions are satisfied, i.e.

$$\begin{aligned}
1) \quad \frac{\partial L}{\partial P_i} &= 0 & 2) \quad \frac{\partial L}{\partial \lambda} &= 0 \\
3) \quad \frac{\partial L}{\partial \mu_{i(\max)}} &= P_i - P_{i(\max)} = 0 & 4) \quad \frac{\partial L}{\partial \mu_{i(\min)}} &= P_i - P_{i(\min)} = 0
\end{aligned} \tag{A4.6}$$

When the P-limits are not violated, the associated values  $\mu_i$  in (A4.5) are zero (i.e. the constraint is inactive) and only the first two conditions in (A4.6) must be met. In the context of this problem,  $\lambda$  is the incremental cost of delivered power, measured in \$/MWh. Without going further into derivation details, the solution starts by assuming a value for the Lagrangian multiplier  $\lambda$ . Then, the estimates for the generators' real power outputs are found using

$$P_i^{(k)} = \frac{\lambda^{(k)} - \beta_i}{2(\gamma_i + \lambda^{(k)} B_{ii})} \tag{A4.7}$$

In (A4.7)  $B_{ii}$  is the power loss coefficient in (A4.4). The mismatch between the total estimated generation obtained from (A4.7) and total demand (plus estimated power loss) is calculated by

$$\Delta P^{(k)} = P_D + P_L^{(k)} - \sum_{i=1}^{n_g} P_i^{(k)} \tag{A4.8}$$

The error for the Lagrangian multiplier  $\lambda$  is found by

$$\Delta \lambda^{(k)} = \frac{\Delta P^{(k)}}{\sum_{i=1}^{n_g} (\partial P_i / \partial \lambda)^{(k)}} = \frac{\Delta P^{(k)}}{\sum_{i=1}^{n_g} \frac{\gamma_i + B_{ii} \beta_i}{2(\gamma_i + \lambda^{(k)} B_{ii})^2}} \tag{A4.9}$$

The new value for  $\lambda$  is obtained by

$$\lambda^{(k+1)} = \lambda^{(k)} + \Delta \lambda^{(k)} \tag{A4.10}$$

The iteration continues until the error for  $\lambda$  becomes very small. Then, the generator outputs computed using the final  $\lambda$  and (A4.7) are the optimal outputs for the generators. The optimal total cost of generated power is obtained using (A4.1).

Following the steps defined above, assuming that  $\lambda^{(1)} = 12$ , the first estimates of dispatch power for the 6-bus system generators are found using (A4.7)

$$P_1^{(1)} = \frac{12 - 5.9}{2(0.0849 + 12(0.000053))} = 35.6575 \text{ MW}$$

$$P_2^{(1)} = \frac{12 - 5.5}{2(0.25 + 12(0.000632))} = 12.6172 \text{ MW}$$

$$P_3^{(1)} = \frac{12 - 5.6}{2(0.0809 + 12(0.000106))} = 38.9427 \text{ MW}$$

Checking the real power estimates against the P-limits in Table A4.1, there is no violation so calculation can continue without any adjustment. The total real power loss is computed using (A4.4). For convenience, the units are omitted. The interested reader can easily verify the consistency of the units.

$$P_L^{(1)} = 0.000053(35.6575)^2 + 0.000632(12.6172)^2 + 0.000106(38.9427)^2 = 0.3288$$

The mismatch between total generation and demand plus loss is

$$\Delta P^{(1)} = 203.7 + 0.3288 - (35.6575 + 12.6172 + 38.9427) = 116.8113$$

The denominator of (A4.9) is found by

$$\begin{aligned} \sum_{i=1}^3 (\partial P_i / \partial \lambda)^{(k)} &= \frac{0.0849 + 0.000053(5.9)}{2(0.0849 + 12(0.000053))^2} + \frac{0.25 + 0.000632(5.5)}{2(0.25 + 12(0.000632))^2} + \frac{0.0809 + 0.000106(5.6)}{2(0.0809 + 12(0.000106))^2} \\ &= 13.7681 \end{aligned}$$

The error for  $\lambda$  is computed using (A4.9). The updated value of  $\lambda$  is computed using (A4.10) for the second iteration.

$$\Delta \lambda^{(1)} = \frac{116.8113}{13.7681} = 8.4842$$

$$\lambda^{(2)} = 12 + 8.4842 = 20.4842$$

For the second iteration using  $\lambda^{(2)}$ , the dispatch power values of the generators are

$$P_1^{(2)} = 84.8059$$

$$P_2^{(2)} = 28.4929$$

$$P_3^{(2)} = 89.5868$$

It is observed that the upper limits for Generator 2 and 3 are violated. Therefore, the generator outputs are fixed at the respective maximum values (25 and 43 MW). It follows that the estimates of the generators' output for the second iteration are

$$P_1^{(2)} = 84.8059$$

$$P_2^{(2)} = 25$$

$$P_3^{(2)} = 43$$

Using these estimates, the calculation continues as in the first iteration to give

$$P_L^{(2)} = 0.9722$$

$$\Delta P^{(2)} = 51.8662$$

$$\sum_{i=1}^3 (\partial P_i / \partial \lambda)^{(2)} = 13.5003$$

$$\Delta \lambda^{(2)} = 3.8419$$

$$\lambda^{(3)} = 24.3260$$

The OPF iteration converges after 18 iterations with  $\Delta \lambda^{(18)} = 0.00057$  which is sufficiently small ( $\lambda^{(18)} = 29.6419$ ). The corresponding power outputs for the generators are the optimal dispatch values and total power cost of the system is calculated using (A4.1). The result is compared with Matpower OPF solution in Table A4.2.

Table A4.2 Analytical OPF solution versus Matpower OPF solution

Item	Analytical	Matpower	Difference, %
Generator 1 output, MW	137.283	136.780	-0.36734
Generator 2 output, MW	25.000	25.000	0
Generator 3 output, MW	43.000	43.000	0
System total output, MW	205.283	204.780	-0.2454
Total generated power cost, \$/h	3474.200	3459.460	-0.4261

Table A4.2 shows that the analytical OPF solution and Matpower OPF solution differ from each other only by a fraction of a percent. The reason is likely to be the slight difference when determining the system power loss. Note that the total power loss is approximated by a quadratic polynomial for obtaining the analytical solution while exact calculation is employed by Matpower. Despite this, the two solutions are equivalent.

## References

- [1] "Wind Energy - The Facts - Executive Summary," Global Wind Energy Council (GWEC), 2009. [http://www.wind-energy-the-facts.org/pdf/1565\\_ExSum\\_ENG.pdf](http://www.wind-energy-the-facts.org/pdf/1565_ExSum_ENG.pdf), 15 December 2009.
- [2] "Interactive world map", Global Wind Energy Council (GWEC), <http://www.gwec.net/index.php?id=126>, 15 December 2009.
- [3] "Annual-Wind-Report 2009," American Wind Energy Association (AWEA) 15 Dec 2009, 2009, <http://www.awea.org/publications/reports/AWEA-Annual-Wind-Report-2009.pdf>.
- [4] GWEC, "GWEC Global Wind 2005 Report", Global Wind Energy Council, [http://www.gwec.net/fileadmin/documents/Publications/GWEC-Global\\_Wind\\_05\\_Report\\_low\\_res\\_01.pdf](http://www.gwec.net/fileadmin/documents/Publications/GWEC-Global_Wind_05_Report_low_res_01.pdf), 25 Sept 2005.
- [5] "AWEA projects", American Wind Energy Association (AWEA), <http://www.awea.org/projects/>, 15 December 2009.
- [6] AWEA, "AWEA Year End 2009 Market Report " American Wind Energy Association (AWEA) 27 February 2010, 2010, <http://www.awea.org/publications/reports/4Q09.pdf>.
- [7] GWEC, "Global Wind Energy Outlook 2006", Global Wind Energy Council, [http://www.gwec.net/fileadmin/documents/Publications/Global\\_Wind\\_Energy\\_Outlook\\_2006.pdf](http://www.gwec.net/fileadmin/documents/Publications/Global_Wind_Energy_Outlook_2006.pdf), Sept. 27, 2006.
- [8] "Renewable Portfolio Standards - RPS Map", Database of State Incentives for Renewables and Efficiency (DSIRE), [www.dsireusa.org/documents/summarymaps/RPS\\_map.ppt](http://www.dsireusa.org/documents/summarymaps/RPS_map.ppt), 17 Dec 2009.
- [9] "2003 State of the Market Report for the ERCOT Wholesale Electricity Market," Potomac Economics, Ltd, 2004.
- [10] "Grid information", The Electric Reliability Council of Texas (ERCOT), <http://www.ercot.com/gridinfo/load/ltdf/>, 22 December 2009.
- [11] P. Kundur, *Power System Stability and Control*. New York: McGraw-Hill, Inc., 1994.
- [12] S. Heier, *Grid Integration of Wind Energy Conversion Systems*. Chichester: John Wiley & Sons Ltd., 1998.
- [13] T. Ackermann (Ed), *Wind Power in Power Systems*. Chichester: John Wiley and Sons, Ltd., 2005.
- [14] M. Bruntt, J. Havsager, and H. Knudsen, "Incorporation of wind power in the east Danish power system," in *International Conference on Electric Power Engineering (PowerTech)*, Budapest, 1999.
- [15] P. Fairley, "Steady as She Blows," *IEEE Spectrum*, vol. 40, No 8, pp. 35-39, Aug 2003 2003.
- [16] K. Burges and J. Twele, "Power systems operation with high penetration of renewable energy - the German case," 2005.

- [17] I. Erlich and U. Bachmann, "Grid code requirements concerning connection and operation of wind turbines in Germany," in *IEEE Power Engineering Society General Meeting*, 2005, pp. 1253-1257 Vol. 2.
- [18] N. Jenkins and G. Strbac, "Impact of embedded generation on distribution system voltage stability (Digest No: 1997/101)," in *IEEE Colloquium on Voltage Collapse*, 1997.
- [19] J. Usaola and P. Ledesma, "Dynamic incidence of wind turbines in networks with high wind penetration," in *IEEE Power Engineering Society Summer Meeting*, 2001.
- [20] L. Holdsworth, N. Jenkins, and G. Strbac, "Electrical stability of large, offshore wind farms," in *Seventh International Conference on AC-DC Power Transmission*, 2001.
- [21] M. P. Palsson, T. Toftevaag, K. Uhlen, and J. O. G. Tande, "Large-scale Wind Power Integration and Voltage Stability Limits in Regional Networks," in *IEEE Power Engineering Society Summer Meeting*, 2002.
- [22] J. M. Rodriguez, J. L. Fernandez, D. Beato, R. Iturbe, J. Usaola, P. Ledesma, and J. R. Wilhelmi, "Incidence on power system dynamics of high penetration of fixed speed and doubly fed wind energy systems: study of the Spanish case," *IEEE Transactions on Power Systems*, vol. 17, pp. 1089-1095, 2002.
- [23] T. Gjengedal, "Integration of wind power and the impact on power system operation," in *IEEE Power Engineering Society Conference on Large Engineering Systems*, 2003.
- [24] F. W. Koch, I. Erlich, F. Shewarega, and U. Bachmann, "Dynamic interaction of large offshore wind farms with the electric power system," in *IEEE Bologna Power Tech Conference 2003*.
- [25] B. Roberts and J. McDowall, "Commercial Successes in Power Storage," *IEEE Power and Energy Magazine*, vol. 3, 2, pp. 24-30, 2005.
- [26] I. Guyk, P. Kulkarni, J. H. Sayer, J. D. Boyes, and G. H. Peek, "The United States of Storage," *IEEE Power and Energy Magazine*, vol. 3, 2, pp. 31-39, 2005.
- [27] A. Nourai, B. P. Martin, and D. R. Fitchett, "Testing the limits," *IEEE Power and Energy Magazine*, vol. 3, 2, pp. 40-46, 2005.
- [28] S. M. Schoenung, "Characteristics and Technologies for Long- vs. Short-Term Energy Storage," Sandia National Laboratories, Albuquerque, SAND2001-0765, 2001.
- [29] "PSCAD(R)", Manitoba HVDC Research Centre, <https://pscad.com/index.cfm?>,
- [30] "Matlab," The MathWorks, Inc., <http://www.mathworks.com/>.
- [31] "NEPLAN - Electricity", Busarello+Cott+Partner Inc. (BCP), [www.neplan.ch](http://www.neplan.ch), 5 November 2003.
- [32] "Matpower," Cornell University, 2007. <http://www.pserc.cornell.edu/matpower/>, 15 February 2007.
- [33] S. Santoso and Ha Thu Le, "Fundamental time-domain wind turbine models for wind power studies," *Renewable Energy journal*, vol. 32, 14, pp. 2436-2452, 2006, doi 10.1016/j.renene.2006.12.008.
- [34] Ha Thu Le and S. Santoso, "Analysis of Voltage Stability and Optimal Wind Power Penetration Limits for a Non-radial Network with an Energy Storage System," in *Power Engineering Society General Meeting, 2007. IEEE*, 2007, pp. 1-8.

- [35] Ha Thu Le, S. Santoso, and W. M. Grady, "Development and analysis of an ESS-based application for regulating wind farm power output variation," in *Power & Energy Society General Meeting, 2009. PES '09. IEEE*, 2009, pp. 1-8.
- [36] Ha Thu Le and Thang Quang Nguyen, "Sizing energy storage systems for wind power firming: An analytical approach and a cost-benefit analysis," in *Power and Energy Society General Meeting - Conversion and Delivery of Electrical Energy in the 21st Century, 2008 IEEE*, 2008, pp. 1-8.
- [37] Ha Thu Le and S. Santoso, "Increasing Wind Farm Transient Stability by Dynamic Reactive Compensation: Synchronous-Machine-Based ESS versus SVC," in *Power & Energy Society General Meeting 2010, IEEE*, 2010, pp. 1-8.
- [38] D. A. Spera (Ed), *Wind Turbine Technology*. New York: The American Society of Mechanical Engineers Press, 1994.
- [39] M. R. Patel, *Wind and Solar Systems*. Boca Raton, Florida: CRC Press, 1999.
- [40] P. W. Carlin, A. S. Laxson, and E. B. Muljadi, "The History and State of the Art of Variable-Speed Wind Turbine," National Renewable Energy Laboratory, Golden, Colorado, NREL/TP-500-28607, 2001.
- [41] P. B. Eriksen, T. Ackermann, H. Abildgaard, P. Smith, W. Winter, and J. M. Rodriguez Garcia, "System operation with high wind penetration," *Power and Energy Magazine, IEEE*, vol. 3, 6, pp. 65-74, 2005, doi
- [42] J. F. Manwell, J. G. McGowan, and A. L. Rogers, *Wind energy explained : theory, design and application*. Chichester: John Wiley & Sons, Ltd. (UK), 2002.
- [43] E. Hau, *Windturbines: Fundamentals, Technologies, Application and Economics*. Verlag Telos: Springer, 2000.
- [44] B. C. Kuo and F. Golnaraghi, *Automatic Control Systems*, 8th ed. Hoboken, New Jersey: John Wiley and Sons, Inc., 2003.
- [45] N. S. Nise, *Control Systems Engineering*, 3 ed. New York: John Wiley & Sons, Inc., 2000.
- [46] A. D. Hansen, P. Sorensen, F. Blaabjerg, and J. Becho, "Dynamic modelling of wind farm grid interaction," *Wind Engineering*, vol. 26, pp. 191-210, 2002.
- [47] P. C. Krause, *Analysis of Electric Machinery*: McGraw-Hill, Inc., 1986.
- [48] J. G. Sloopweg, H. Polinder, and W. L. Kling, "Dynamic modelling of a wind turbine with doubly fed induction generator," in *Power Engineering Society Summer Meeting, 2001. IEEE*, 2001, pp. 644-649 vol.1.
- [49] M. Y. Uctug, I. Eskandarzadeh, and H. Ince, "Modelling and output power optimisation of a wind turbine driven double output induction generator," *Electric Power Applications, IEE Proceedings-*, vol. 141, 2, pp. 33-38, 1994.
- [50] Seul-Ki Kim, Eung-Sang Kim, Jae-Young Yoon, and Ho-Yong Kim, "PSCAD/EMTDC based dynamic modeling and analysis of a variable speed wind turbine," in *Power Engineering Society General Meeting, 2004. IEEE*, 2004, pp. 1735-1741 Vol.2.
- [51] S. K. Salman and A. L. J. Teo, "Investigation into the estimation of the critical clearing time of a grid connected wind power based embedded generator," in *Transmission and*

- Distribution Conference and Exhibition 2002: Asia Pacific. IEEE/PES, 2002, pp. 975-980 vol.2.*
- [52] Ha Thu Le and T. K. Saha, "Investigation of power loss and voltage stability limits for large wind farm connections to a subtransmission network," in *Power Engineering Society General Meeting, 2004. IEEE, 2004, pp. 2251-2256 Vol.2.*
  - [53] H. Saadat, *Power System Analysis*. Singapore: WCB/McGraw-Hill, Inc., 1999.
  - [54] C. Abbey and G. Joos, "A doubly-fed induction machine and energy storage system for wind power generation," in *Canadian Conference on Electrical and Computer Engineering, 2004, pp. 1059-1062.*
  - [55] C. Abbey and G. Joos, "Integration of energy storage with a doubly-fed induction machine for wind power applications," in *IEEE 35th Annual Power Electronics Specialists Conference, 2004, pp. 1964-1968.*
  - [56] F. Zhou, G. Joos, C. Abbey, L. Jiao, and B. T. Ooi, "Use of large capacity SMES to improve the power quality and stability of wind farms," in *2004 IEEE Power Engineering Society General Meeting, 2004, pp. 2025-2030.*
  - [57] J. D. Boyes, "Energy Storage Systems Program Report for FY99," Sandia National Laboratories, Albuquerque, SAND2000-1317, 2000, <http://www.prod.sandia.gov/cgi-bin/techlib/access-control.pl/2000/001317.pdf>.
  - [58] S. M. Schoenung, "Characteristics and Technologies for Long- vs Short-Term Energy Storage," Sandia National Laboratories, Albuquerque, New Mexico, SAND2001-0765, 2001.
  - [59] "Estimated Average Engine Performance " University of Texas at Austin Utilities and Energy Management - Power Plant, Austin, 2005.
  - [60] "Costs by Generation Technologies (Report)," Department of Energy - Energy Information Administration, DOE/EIA-0554(2007), 2007.
  - [61] J. D. McCalley, "Modeling of Cost-Rate Curves", [www.ee.iastate.edu/~jdm/EE457/CostRateCurves.doc](http://www.ee.iastate.edu/~jdm/EE457/CostRateCurves.doc), 28 Mar 2008.
  - [62] W. H. Greene, *Econometric Analysis*, 5th ed. New Jersey: Prentice Hall, 2003.
  - [63] M. Korpaas, A. T. Holen, and R. Hildrum, "Operation and sizing of energy storage for wind power plants in a market system," *Electric Power and Energy Systems*, vol. 25, pp. 599-606, doi 10.1016/S0142-0615(03)00016-4.
  - [64] J. Eyer, J. Iannucci, and P. C. Butler, "Estimating Electricity Storage Power Rating and Discharge Duration for Utility Transmission and Distribution Deferral," Sandia National Laboratories, Albuquerque, SAND2005-7069, 2005.
  - [65] J. Eyer, J. J. Iannucci, and G. P. Corey, "Energy Storage Benefits and Market Analysis Handbook," Sandia National Laboratories, Albuquerque SAND2004-6177, 2004.
  - [66] S. M. Schoenung and W. V. Hassenzahl, "Long- vs. Short-Term Energy Storage Technologies Analysis - A Life-Cycle Cost Study," Sandia National Laboratories, Albuquerque, SAND2003-2783, 2003.
  - [67] "Information obtained from private communication with some power engineering professionals. ," 2008.

- [68] AWEA, "What is "capacity factor"?", American Wind Energy Association [http://www.awea.org/faq/wwt\\_basics.html](http://www.awea.org/faq/wwt_basics.html), Oct. 10, 2006.
- [69] D. Brooks, T. Key, and L. Felton, "Increasing the value of wind generation through integration with hydroelectric generation," in *IEEE Power Engineering Society General Meeting*, 2005, pp. 1923-1925.
- [70] R. S. Bhatia, S. P. Jain, D. K. Jain, and B. Singh, "Battery Energy Storage System for Power Conditioning of Renewable Energy Sources," in *Power Electronics and Drives Systems, 2005. PEDS 2005. International Conference on*, 2005, pp. 501-506.
- [71] Z. Jie, Z. Buhan, M. Chengxiong, and W. Yunling, "Use of Battery Energy Storage System to Improve the Power Quality and Stability of Wind Farms," in *Power System Technology, 2006. PowerCon 2006. International Conference on*, 2006, pp. 1-6.
- [72] T. Kinjo, T. Senjyu, N. Urasaki, and H. Fujita, "Output levelling of renewable energy by electric double-layer capacitor applied for energy storage system," *Energy Conversion, IEEE Transactions on*, vol. 21, 1, pp. 221-227, 2006.
- [73] Abbey C. and Joos G., "Integration of energy storage with a doubly-fed induction machine for wind power applications," in *Power Electronics Specialists Conference, 2004. PESC 04. 2004 IEEE 35th Annual*, 2004, pp. 1964-1968 Vol.3.
- [74] S. M. Muyeen, R. Takahashi, M. H. Ali, T. Murata, and J. Tamura, "Transient Stability Augmentation of Power System Including Wind Farms by Using ECS," *Power Systems, IEEE Transactions on*, vol. 23, 3, pp. 1179-1187, 2008.
- [75] Zhou F., Joos G., Abbey C., Jiao L., and Ooi B.T., "Use of large capacity SMES to improve the power quality and stability of wind farms," in *Power Engineering Society General Meeting, 2004. IEEE*, 2004, pp. 2025-2030 Vol.2.
- [76] Senjyu T., Kinjo T., Uezato K., and Fujita H., "Analysis of terminal voltage and output power control of wind turbine generator by series and parallel compensation using SMES," in *Power Electronics Specialists Conference, 2004. PESC 04. 2004 IEEE 35th Annual*, 2004, pp. 4278-4284 Vol.6.
- [77] T. Senjyu, T. Kinjo, K. Uezato, and H. Fujita, "Analysis of terminal voltage and output power control of wind turbine generator by series and parallel compensation using SMES," in *Power Electronics Specialists Conference, 2004. PESC 04. 2004 IEEE 35th Annual*, 2004, pp. 4278-4284 Vol.6.
- [78] "Concentrating Solar Power Commercial Application Study: Reducing Water Consumption of Concentrating Solar Power Electricity Generation (Report to U.S. Congress)," U.S. Department of Energy Accessed 23 Nov 2009, <http://www.nrel.gov/csp/publications.html>.
- [79] L. Stoddard, J. Abiecunas, and R. O'Connell, "Economic, Energy, and Environmental Benefits of Concentrating Solar Power in California," National Renewable Energy Laboratory (NREL), Overland Park, Kansas, NREL/SR-550-39291, 2006.
- [80] "The Economic Impact of CAES on Wind in TX, OK, and NM," Ridge Energy Storage & Grid Services L.P., 2005, [http://www.seco.cpa.state.tx.us/zzz\\_re/re\\_wind\\_projects-compressed2005.pdf](http://www.seco.cpa.state.tx.us/zzz_re/re_wind_projects-compressed2005.pdf), 23 Nov 2009.
- [81] C. W. Taylor, *Power System Voltage Stability*. New York: McGraw-Hill, Inc., 1993.

- [82] R. Pena, J. C. Clare, and G. M. Asher, "Doubly fed induction generator using back-to-back PWM converters and its application to variable-speed wind-energy generation," *Electric Power Applications, IEE Proceedings -*, vol. 143, 3, pp. 231-241, 1996.
- [83] V. Akhmatov, "Variable-Speed Wind Turbines with Doubly-Fed Induction Generators, Part I: Modelling in Dynamic Simulation Tools," *Wind Engineering*, vol. 26, No. 2, 2002.
- [84] N. W. Miller, J. J. Sanchez-Gasca, W. W. Price, and R. W. Delmerico, "Dynamic modeling of GE 1.5 and 3.6 MW wind turbine generators for stability simulations," GE Power Systems Energy Consulting, IEEE WTG Modeling Panel, Session July 2003, 2003.
- [85] Dugan R.C., McGranaghan M.F., and Beaty H.W., *Electrical Power Systems Quality*. New York: McGraw-Hill, 1996.
- [86] G. Joos, "Wind turbine generator low voltage ride through requirements and solutions," in *Power and Energy Society General Meeting - Conversion and Delivery of Electrical Energy in the 21st Century, 2008 IEEE*, 2008, pp. 1-7.

## Vita

Ha Thu Le earned her BSEE from Odessa College (Odessa city, Ukraine), MEEE from the University of Queensland (Brisbane city, Australia), and Ph.D. degree from the University of Texas at Austin (Texas, USA). Her Ph.D. research focused on large-scale wind power integration, wind farm and grid stability, and energy storage systems. Part of her work has been published in the *Renewable Energy* journal and *IEEE Power & Energy Society* conference proceedings. Before going back to graduate study, she worked as a consultant in Hanoi, Vietnam, her home country, for seven years. She provided technical service in the field of automatic identification to businesses for article tracking, supply chain management and related applications. She was employed as a teaching and research assistant by the Department of Electrical and Computer Engineering, University of Texas at Austin, for over 2.5 years. In summer 2006, she worked as a student intern at the Electric Power Research Institute (EPRI). Her research interests include renewable energy, large-scale wind power integration, energy storage systems, applied optimization in engineering, power system simulation, power quality, and realization of Smart-Grid concepts. She is a member of the Institute of Electrical and Electronics Engineers, Inc. (IEEE) since 2003. She was a recipient of Australian Development Scholarship (AusAID) for Master study and the Vietnam Education Foundation fellowship for Ph.D. study. Her dissertation wind project was funded by the U.S. National Science Foundation. Ha was born to Vietnamese parents, Mr. Hoa, a college lecturer, and Mrs. Thin, a high school teacher. She is happily married to her loving husband Thang, a Ph.D. in Economics from the University of Texas at Austin. They have a cute, bright, and lively little son Wing.

Permanent address: Nha 39, Ngo 12, Me Linh Street, Vinh Yen, Vinh Phuc, Vietnam

This manuscript was typed by the author.